DESIGN AND SYNTHESIS OF SOME NOVEL SQUARAINE BASED NEAR INFRARED SENSITIZERS AND PROBES

THESIS SUBMITTED TO
THE UNIVERSITY OF KERALA
FOR THE DEGREE OF
DOCTOR OF PHILOSOPHY
IN CHEMISTRY
UNDER THE FACULTY OF SCIENCE

By

M. C. BASHEER

PHOTOSCIENCES AND PHOTONICS
CHEMICAL SCIENCES AND TECHNOLOGY DIVISION
NATIONAL INSTITUTE FOR INTERDISCIPLINARY SCIENCE & TECHNOLOGY,
CSIR, TRIVANDRUM - 695 019, KERALA, INDIA

SEPTEMBER 2007

Dedicated to

My parents and family members……
……for their love and care

My mentors……
……for their invaluable advice

STATEMENT

I hereby declare that the matter embodied in the thesis entitled: ***"Design and Synthesis of Some Novel Squaraine Based Near Infrared Sensitizers and Probes"*** is the result of the investigations carried out by me at the Photosciences and Photonics Section, Chemical Sciences and Technology Division, National Institute for Interdisciplinary Science and Technology (Formerly, Regional Research Laboratory), CSIR Trivandrum, under the supervision of Dr. Suresh Das and the same has not been submitted elsewhere for a degree.

In keeping with the general practice of reporting scientific observations, due acknowledgement has been made wherever the work described is based on the findings of other investigators.

M. C. Basheer

National Institute for Interdisciplinary Science and Technology
(*formerly* Regional Research Laboratory, Trivandrum)

Council of Scientific and Industrial Research (CSIR)
Industrial Estate P.O.,Trivandrum 695 019
Kerala, INDIA
http://www.niist.res.in

ISO 9001 REGISTERED
DNV Certification B.V., The Netherlands

Suresh Das, F. A. Sc.
Scientist F & Head
Chemical Sciences and Technology Division
E-mail: sureshdas55@gmail.com

Tel.: +91-471-2515318
Fax: +91-471-2490186

24 September 2007

CERTIFICATE

This is to certify that the work embodied in the thesis entitled, ***"Design and Synthesis of Some Novel Squaraine Based Near Infrared Sensitizers and Probes"*** has been carried out by Mr. M. C. Basheer under my supervision and the same has not been submitted elsewhere for a degree.

Suresh Das
Thesis Supervisor

ACKNOWLEDGEMENTS

First and foremost, I have great pleasure in placing on record my deep sense of gratitude to Dr. Suresh Das, my thesis supervisor, for suggesting the research problem and for his guidance, support and encouragement, leading to the successful completion of this work.

I would like to express my sincere thanks to Professor M. V. George for his constant encouragement, inspiration and useful discussions during the tenure of this work.

I thank Professor T. K. Chandrashekar, Director, Dr. B. C. Pai, acting Director and Dr. G. Vijay Nair, former Director of the NIST, Trivandrum for providing the necessary facilities and infrastructure of the laboratory for carrying out the work.

I am also grateful to:

- *Dr. C. H. Suresh, Computational Modeling and Simulation Section, NIST, Trivandrum for discussions and help in carrying out the theoretical studies reported in the thesis.*
- *Dr. A. Ajayaghosh, Dr. K. R. Gopidas, Dr. D. Ramaiah, Dr. K. George Thomas and Dr. A. Sreenivasan Scientists of the Photosciences and Photonics Section for all the help and support extended to me.*
- *Mr. Robert Philip and Mrs. Sarada Nair for their help and cooperation, Mrs. Saumini Shoji for NMR spectra, Mrs. S. Viji for HRMS spectra and Miss Priya A. Nair for FTIR Spectra.*
- *All the members of the Photosciences and Photonics Section and in particular Dr. Saji Alex, Dr. Shibu Abraham, Mr. K. M. Shafeekh, Mr. N. S. Saleeshkumar, Mr. G. Ajayakumar, Mr. G. Narayan, Mr. K. V. Ratheesh, Mr. Shinto Varghese and Mr. Sajith Menon.*
- *All my friends in other sections of NIST, Trivandrum in particular Mr. V. Sreekumar, Mr. Jijoy Joseph and Dr. A. T. Biju for their help extended to me.*
- *CSIR, DST and Task Force for financial assistance.*

I am deeply grateful to my parents, brothers, sisters and other family members for their constant love and care which has motivated me greatly.

M. C. Basheer

CONTENTS

PREFACE

The chemistry of functional organic dyes has made significant contributions to photon-based technologies such as in optical data storage, imaging and communication including several biological applications such as in noninvasive imaging and photodynamic therapy. However, much less effort has been devoted towards the development of new dyes with strong emission in the near infrared (NIR) region especially in the 700-900 nm, for fluorescent imaging applications of biological systems. Cells excited at wavelengths below 500 nm produce considerable autofluorescence mainly from flavins, flavoproteins and NADH, which can very often swamp the probe fluorescence. This aspect combined with greater tissue penetration and reduced photochemical damage of cells at higher wavelengths makes fluorescence microscopy in the NIR region especially attractive for biomedical applications. Squaraines belong to an important class of organic functional dyes, having intense absorption and strong emission in the visible to NIR region. Their unique photochemical and photophysical properties make them useful in a variety of applications such as fluorescent probes for noninvasive imaging and sensing biologically relevant metal ions. The work described in this thesis is related to the design and synthesis of some novel squaraine based near infrared sensitizers and probes. The first Chapter of the thesis presents a general overview of squaraine based sensitizers and probes reported in the literature.

The design of molecular probes for sensing metal ions using the concept of photo-induced electron transfer (PET), host-guest chemistry or metal ion induced changes in aggregation behaviour has been attracting considerable

attention in recent years. Of particular interest is the detection of Hg^{2+} and Pb^{2+}, highly toxic environmental pollutants arising from both natural and industrial sources. In Chapter 2, we describe an unsymmetrical cationic squaraine dye, absorbing in the NIR region (600-850 nm). Its absorption spectra in the presence of various metal ions have been studied. Addition of micromolar amounts of Hg^{2+} and Pb^{2+} to solutions of dichloromethane brought about significant changes in its absorption spectrum, resulting in a change in colour of the solution from green to pink. The absorption spectrum of the dye was relatively insensitive to other environmentally relevant metal ions, making it possible to visually detect Hg^{2+} and Pb^{2+} in their presence. Molecular modeling of the complexes at the density functional theory (DFT) and semi empirical PM3 levels also indicated a high affinity of Hg^{2+} and Pb^{2+} towards the formation of 2:1 complexes, which is in good agreement with the experimental results.

In Chapter 3, we describe our work on the synthesis and study of a variety of dialkylanthracene containing squaraine dyes possessing intense absorption and emission in the NIR region. Replacement of dialkylaniline by dialkylanthracene provided a facile method for extending the absorption and emission of squaraine dyes far into the NIR region. The structural and electronic features of these dyes were investigated using DFT methods. The absence of fluorescence in aqueous media and enhanced fluorescence when encapsulated into hydrophobic domains makes this class of dyes especially useful as probes for mapping hydrophobic domains in biological systems. Since water compatibility is an important criterion for use of dyes in biological systems, one of the dyes was designed such that it would have improved water solubility.

The photophysical properties of two water compatible unsymmetrical squaraine dyes absorbing in the NIR region and possessing large Stokes' shift in emission (~100-140 nm), good quantum yields of fluorescence, high extinction coefficients in organic solvents and good photostability are discussed in Chapter 4. They also exhibited enhanced fluorescence efficiency and lifetimes in the presence of proteins such as bovine serum albumin (BSA), human serum albumin (HSA). One of the water compatible squaraines was observed to be capable of selectively detecting Hg^{2+} in the presence of other environmentally relevant metal ions in aqueous media. In this Chapter, we also describe the synthesis and study of a novel class of unsymmetrical squaraine dyes containing dialkylaminophenyl and N-heteroaromatic moieties as nucleophilic substituents on the central cyclobutane ring. Unlike conventional unsymmetrical squaraine dyes reported earlier, the nitrogen in the heteroaromatic ring of these dyes existed in its free base form, and the ability of this nitrogen atom to undergo protonation made them sensitive to pH and these aspects are also discussed.

CHAPTER 1

Squaraine Based Sensitizers and Probes - An Overview

1.1. Introduction

Squaraine dyes belong to an important class of organic functional dyes, possessing intense absorption and emission in the visible to near infrared (NIR) region. These properties combined with their photoconductive nature make them important for various technological applications such as in electrography,[1] xerography,[1] optical data storage,[2] nonlinear optics[3-6] and solar energy conversion.[7] The genesis of squaraines can be tracked back to more than 40 years, when Treibs and Jacob reported the preparation of a dye by the condensation of squaric acid with pyrrole.[8] In general, squaraines are prepared by the condensation between squaric acid and electron-rich aromatic, heteroaromatic, or olefinic compounds in a one-step reaction. Squaraines can be described as compounds containing two donor moieties (D) connected to a central C_4O_2 electron withdrawing group (A) forming a donor-acceptor-donor (D-A-D) arrangement. The donor molecules can be of the same or different type, giving rise to symmetrical and unsymmetrical dyes. Structure of a representative symmetrical

squaraine dye bis[4-(*N,N*-dimethylamino)phenyl]squaraine (**1**), is shown in Chart 1.1.

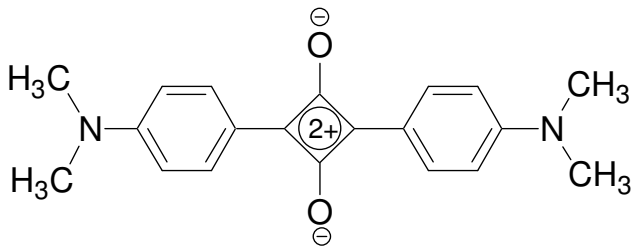

1

Chart 1.1

Squaraines are often classified as cyanine dyes because of the similarity in structure, but they also contain a central squarate bridge. It is possible to draw a localized electronic structure of their π-conjugated chromophore showing a zwitterionic donor-acceptor system linked by polymethine carbons. Such a unique electronic structure often affords a variety of interesting photochemical properties such as large light absorption in the visible or NIR region, which became broad and red shifted in the solid state due to the strong intermolecular donor-acceptor interactions. The squarate residue helps to shift the absorption and emission maxima to longer wavelengths relative to cyanine dyes, and also increases the photostability of the dyes.

Theoretical studies have suggested that the squaraine model exhibits a single/double bond length alternation. This was confirmed by single crystal X-ray crystallographic studies, which indicated that squaraines possess a quinoid like

structure. Using MNDO and CNDO semiempirical calculations, Bigelow and Freund[9] have shown that both the ground (S_0) and the excited (S_1) electronic states of squaraines are intramolecular D-A-D charge transfer (CT) states. The aniline moieties and oxygen atoms behave as electron donors and the central four membered ring as an electron acceptor. The S_0-S_1 electronic excitation involves a CT process, which is primarily confined to the central C_4O_2 ring (80%), *i.e.* from each oxygen atom to the four-membered ring with a small degree of CT from the aniline moiety to the C_4O_2 unit. The intramolecular CT character of this transition, combined with an extended conjugated π-electron donor network, gives rise to the observed sharp and intense bands in the visible to NIR region.

A brief description of some recent studies related to the use of squaraine dyes as sensitizers and probes for various applications are described below.

1.2. Sensitizers for Solar Energy Conversion

Dye-sensitized solar cells (DSSCs) are photoelectrochemical cells, which make use of transparent conducting electrodes coated with wide band-gap mesoporous oxide semiconductors, which are photosensitized by dyes. These cells were invented by Michael Grätzel[10] in 1991 and are often referred to as Grätzel cells. These cells are extremely promising, since they are made up of low-cost materials and do not need elaborate apparatus to manufacture. The cells have a simple structure consisting of two electrodes and an iodide-containing electrolyte.

One of the electrodes in the cell consists of a dye-absorbed highly porous nanocrystalline titanium dioxide (TiO_2) deposited on a transparent electrically conducting substrate, while the counter electrode consists of a plain transparent electrically conducting substrate (Scheme 1.1). The mode of action of these cells has been compared to photosynthesis since photoinduced electron transfer processes are involved. Although the energy conversion efficiency of the cells has only reached about 10%, it is expected that in future the energy conversion efficiency can match that of silicon solar cells and even rise to the theoretical level of 33% .

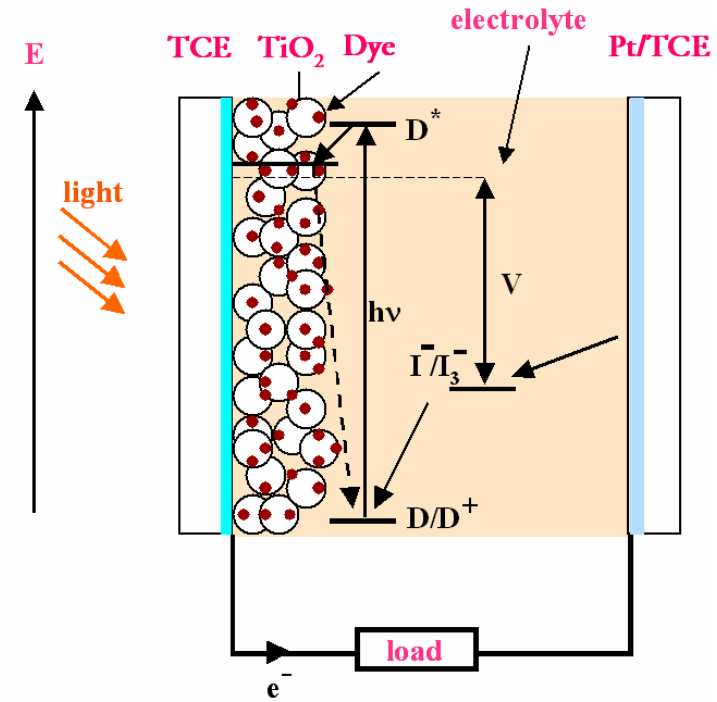

TCE - Transparent Conducting Electrode, D*- Excited state of dye, I^-/I_3^- - Iodide/triiodide

Scheme 1.1. Schematic representation of DSSC.

Among the various sensitizers investigated so far, polypyridyl complexes of ruthenium and osmium have been shown to have the best performance, both in terms of conversion efficiency and long-term stability.[11]

Currently, there is increasing interest in the use of organic dyes as sensitizers in DSSCs. Organic dyes possess several advantages such as ease of preparation, ability to modify their spectral response by bringing about suitable structural variations and low-cost of production. Several metal free organic dyes such as porphyrins, phthalocyanines, anthocyanines and perylene dyes have been investigated as sensitizers. However, their performance in DSSCs has been reported to be very poor. Squaraines are a class of highly stable dyes, which have been extensively investigated for their sensitization properties. The ability of squaraine dyes to sensitize large band-gap semiconductors has been well investigated. However, in view of the low efficiency of sensitization of large band-gap semiconductors by squaraines, with few exceptions, their use as sensitizers in DSSCs have not been well explored. Also most reported studies have utilized only symmetrical squaraines as sensitizers. Recently, Das and coworkers[12] have reported on the synthesis of a series of novel symmetrical and unsymmetrical squaraine dyes **2**–**8** (Chart 1.2) and the study of their comparative photocurrent generating efficiencies in DSSCs. They have shown that the sensitization efficiencies of unsymmetrical squaraines in DSSCs are significantly higher than those of symmetrical squaraines.

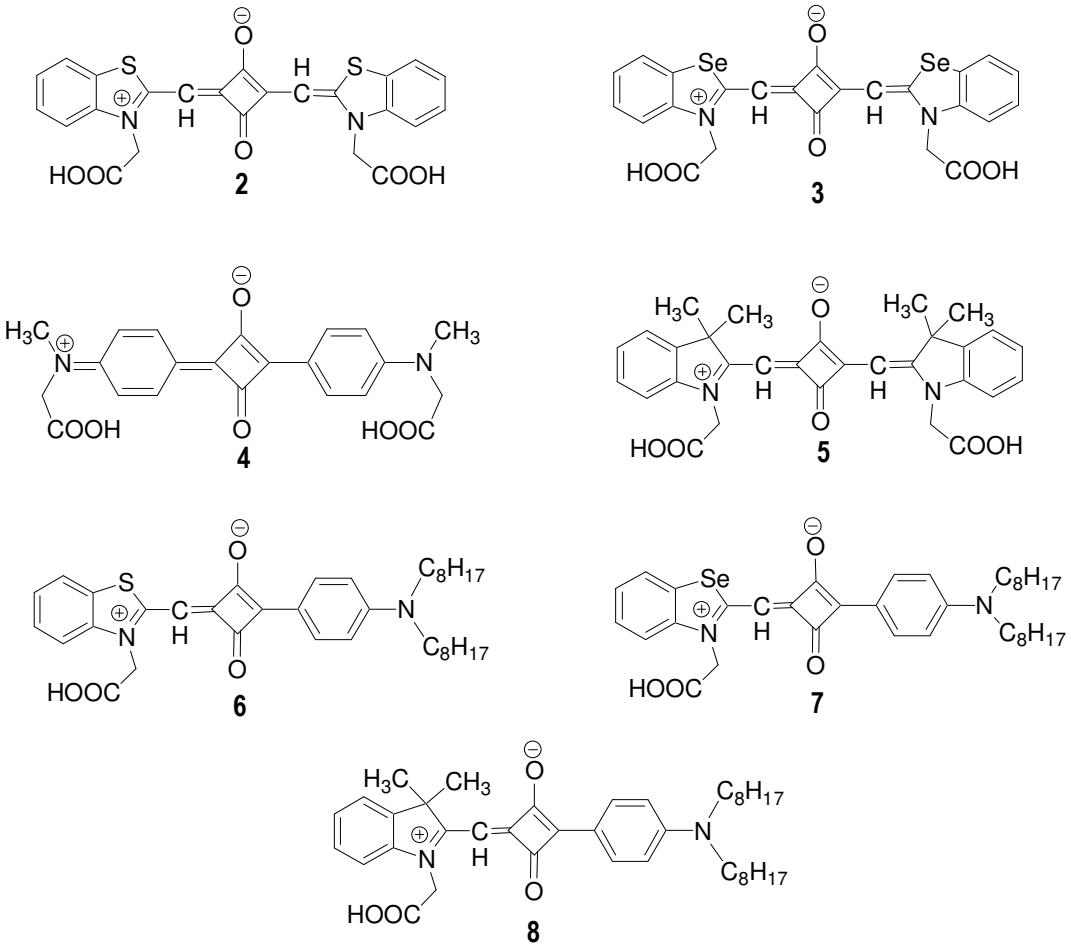

Chart 1.2

Molecular orbital calculations for these dyes indicated that excitation of the dye would result in a unidirectional flow of electrons towards the part of the molecule attached to TiO_2 whereas for symmetrical squaraines, increase in charge density towards the centre of the molecule would be expected. As a result, the charge separation from the excited state of the unsymmetrical squaraines to TiO_2 would be more efficient than that from the symmetrical squaraine dyes and an enhanced efficiency of sensitization of TiO_2 nanocrystalline electrodes could be

observed. Both the symmetrical and unsymmetrical dyes were observed to form aggregates on the TiO_2 surface. The sensitization efficiencies of the aggregates of the symmetrical dyes were observed to be very low whereas that of the unsymmetrical dyes were very high. In the case of the symmetrical dye **5** (Chart 1.2), it was found that aggregates were not formed on the TiO_2 surface, and this was attributed to the presence of the bulky dimethyl substituents on the benzindolenium moiety. As a result the DSSCs, employing this dye as sensitizer showed efficiencies comparable to that of the unsymmetrical dyes.

The ability of unsymmetrical squaraines to behave as efficient sensitizers in DSSCs has been subsequently reported by others.[13,14] Funabiki and coworkers[13] for example, have designed and synthesized unsymmetrical squaraine dyes as photosensitizers. The introduction of the dibutyl group into the benzindolenium moiety of **8** to enhance steric hindrance was effective for inhibiting H-aggregation to a higher degree than the dimethyl group. These dyes when used as sensitizers for ZnO based photoelectrodes, gave DSSCs with 1.5% solar-to electricity conversion efficiency (η), a short-circuit current density (J_{sc}) of 4.04 $mAcm^{-2}$, an open-circuit photovoltage (V_{oc}) of 0.61 V and a fill factor (ff) of 0.61 under standard AM 1.5 irradiation (100 $mWcm^{-2}$).

Very recently, Nazeeruddin and coworkers[14] have demonstrated that DSSCs utilizing the unsymmetrical squaraine sensitizer **9** (Chart 1.3), possess very high efficiency. Under sunlight an IPCE of 0.85 was observed for this cell, with a J_{sc} of

10.50 ± 0.20 $mAcm^{-2}$, an open circuit voltage of 603 ± 30 mV and a fill factor of 0.71 ± 0.03. This, corresponds to an overall conversion efficiency of 4.5% under standard AM 1.5 solar light. Cyclic voltammetry studies indicated oxidation and reduction potentials of 0.98 and -0.78 V respectively for this dye. The optical transition energy $E^{(0\text{-}0)}$ of the squaraine sensitizer which is at 1.92 eV, yielded an excited state reduction potential of -0.94 V *vs* NHE, which is negative enough to allow electron transfer into the TiO_2 conduction band. Excited state DFT/TDDFT calculations indicated a charge flow from the squaraine core to the outer molecular region involving the anchoring carboxylic group. This fact together with the high dye molar extinction coefficient was attributed to be responsible for the high photocurrent and overall photovoltaic efficiency observed for these cells.

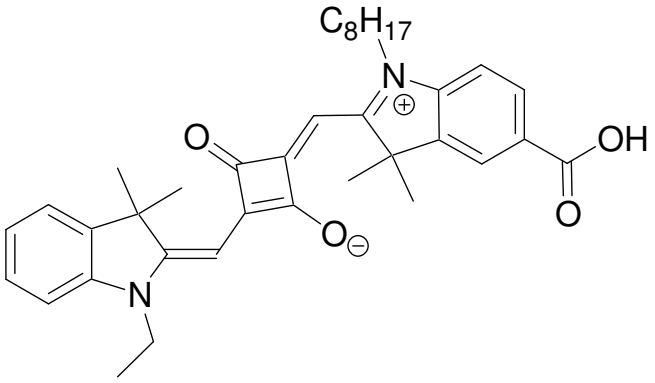

9

Chart 1.3

Chao *et al.*[15] have however reported that symmetrical squaraine dyes can also act as efficient sensitizer in DSSCs. They reported the use of four carboxyl-containing squaraines, **4** (Chart 1.2) and **10–12** (Chart 1.4) in DSSCs. The

similarity between the action spectra and the absorption spectra of these dyes coated on TiO_2 photoelectrodes indicated that the photocurrent originated from the excited squaraines including both their monomer and aggregate forms. According to the authors, the short carboxyl anchoring groups of **4** and **12** enhanced the interaction of dyes with TiO_2 by shortening the distance between them, and helped to promote electron injection. They also proposed that the presence of these groups helped to raise the oxidation potential of the dyes, which resulted in enlarging the energy gap between the oxidized **Sq** and I^-/I_3^- couples, thereby speeding up the reduction of oxidized **Sq** by I^- and restricting the recombination of injected electrons with oxidized dyes.

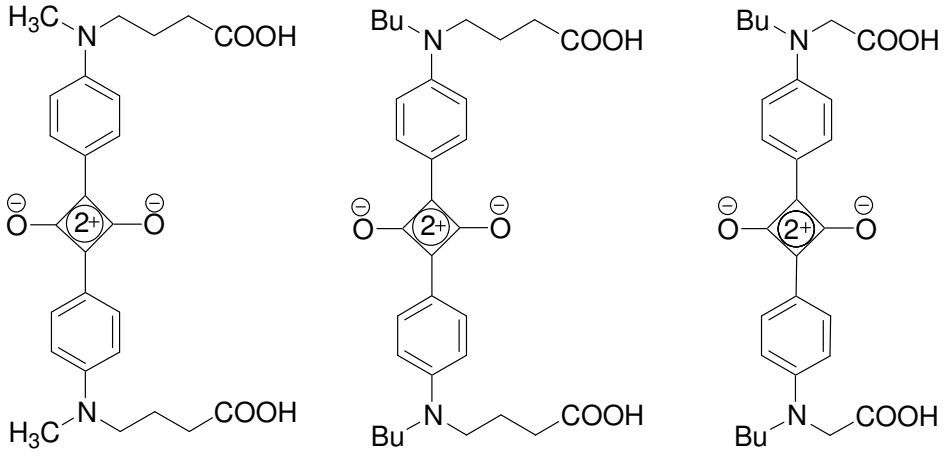

10 **11** **12**

Chart 1.4

Grätzel and coworkers[16] investigated the use of a squaraine dye with extended absorption in the NIR range as sensitizer for DSSCs. The blue coloured

dye with two carboxylic acid attaching groups (**13**, Chart 1.5) has been used successfully in both liquid and solid state solar cells. Despite the narrow absorption in the NIR region, the liquid cells gave a short circuit current density of 8.6 $mAcm^{-2}$, an open circuit voltage of 591 mV and a fill factor of 0.73, giving an overall efficiency of 3.7%. It has been shown that the value of IPCE of the solid state device is ~4 times less than that of the liquid device with the amorphous organic hole transporter 2,2',7,7'-tetrakis-(*N,N*-di-*p*-methoxyphenylamine)-9,9'-*spiro*-bifluorene (*spiro*-OMeTAD). The significant difference in the IPCE values seen here for the liquid and solid state devices can be explained by the rate of the back electron transfer (BET) process to the *spiro*-OMeTAD in solid state cells. The solid state cell gave a short circuit current density of 4.2 $mAcm^{-2}$, an open-circuit voltage of 681 mV and a fill factor of 0.53, leading to a respectable overall efficiency of 1.5%. One advantage of solid-state devices is the higher V_{oc} obtained, *i.e.* 681 *vs.* 591 mV in liquid electrolyte cells. This is not only due to the redox level of the hole conductor which is slightly more positive than the respective I^-/I_3^- couple used in the latter, but also due to the thinner TiO_2 films which help to increase charge collection efficiency. This increase in potential is generally very useful when dealing with purely organic dye sensitizers, as the dyes themselves tend to have a lower LUMO with respect to their ruthenium based organometallic counterparts.

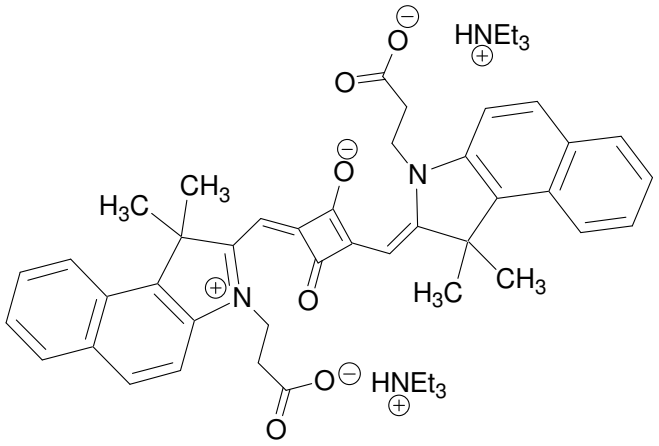

13

Chart 1.5

1.3. Photodynamic Therapy (PDT)

Squaraines have shown to be potentially useful for PDT applications because of their favourable absorption in the photodynamic window. The potential use of squaraine dyes substituted with heavy atoms such as bromine and iodine (**14**, **15**, Chart 1.6) as photosensitizers for PDT applications has been recently demonstrated.[17] Spin-orbit coupling induced by the presence of heavy atoms in these dyes resulted in enhancement of their intersystem crossing efficiencies causing their triplet yields to go up. These dyes have reasonably good water solubility and exist in various protonated forms, depending on the pH of the solution. Laser flash photolysis studies of these dyes indicated that the triplet excited states were the main transient intermediates involved. The singly deprotonated forms of **14** and **15** exhibited triplet lifetimes of 132 μs for **14** and 36 μs for **15** with the quantum yields of the triplet excited states being 0.22 for **14** and 0.50 for

15. The ability of these dyes to generate singlet oxygen with high efficiency was also demonstrated, with Φ ($^1O_2$) values of 0.13 and 0.47 for **14** and **15**, respectively.

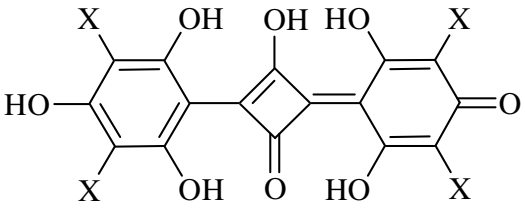

14) X = Br 15) X = I 16) X = H

Chart 1.6

The cytotoxicity and genotoxicity of the bromo derivative **14**, the iodo derivative **15** and the corresponding non-halogenated dye **16** in the absence and presence of visible light also have been investigated.[18] At concentrations of 1–2 μM, **14** and **15** reduced the cloning efficiency of AS52 Chinese hamster ovary cells to less than 1% under conditions that were well tolerated in the dark. Similarly, the proliferation of L5178Y mouse lymphoma cells was inhibited by photoexcited **14** and **15** with high selectivity, whereas the squaraine **16** was much less efficient. Both **14** and **15** induced only few mutations in the *gpt* locus of the AS52 cells in the presence of light and were not mutagenic in the dark. The mutagenicity with and without irradiation was not observed in *Salmonella typhimurium* TA100 and TA2638. However in the case of **14** and **15** the presence of light increased the frequency of micronuclei in AS52 cells. These results

indicated that the halogenated squaraines exhibit photobiological properties *in vitro* that are favourable for PDT applications.

To gain a better understanding of the mechanism of their photobiological activity, the DNA damage and the cytotoxicity induced by these photosensitizers in mammalian cells and cell-free systems in the presence and absence of various additives and scavengers have been studied.[19] Both photoactivated squaraines **14** and **15** were found to have similar efficiency in inducing single-strand breaks (SSB) in cell free DNA when compared with the cellular DNA. Superoxide dismutase and catalase did not show any influence. However, the presence of t-butanol and glutathione inhibited the formation of the DNA SSB, indicating an indirect (possibly squaraine radical mediated) mechanism under cell-free conditions. Replacing H_2O in the buffer by D_2O resulted in a five- to six-fold increase in the number of the SSB in cell-free DNA and a significant enhancement of the photocytotoxicity in mouse lymphoma cells. These results demonstrate that singlet oxygen is the major reactive species under cell-free and cellular conditions and confirm that squaraine based sensitizers **14** and **15** have potential for application in PDT.

Pagani *et al.* reported on some water soluble squaraines as singlet oxygen generators (**17**–**19**, Chart 1.7).[20] These dyes showed sharp and intense absorption spectrum, which are close to the biological window with remarkably high extinction coefficients. Their studies showed that all of the derivatives possessed

intrinsic triplet yield. In particular, the brominated compound **17d** proved to be the best.

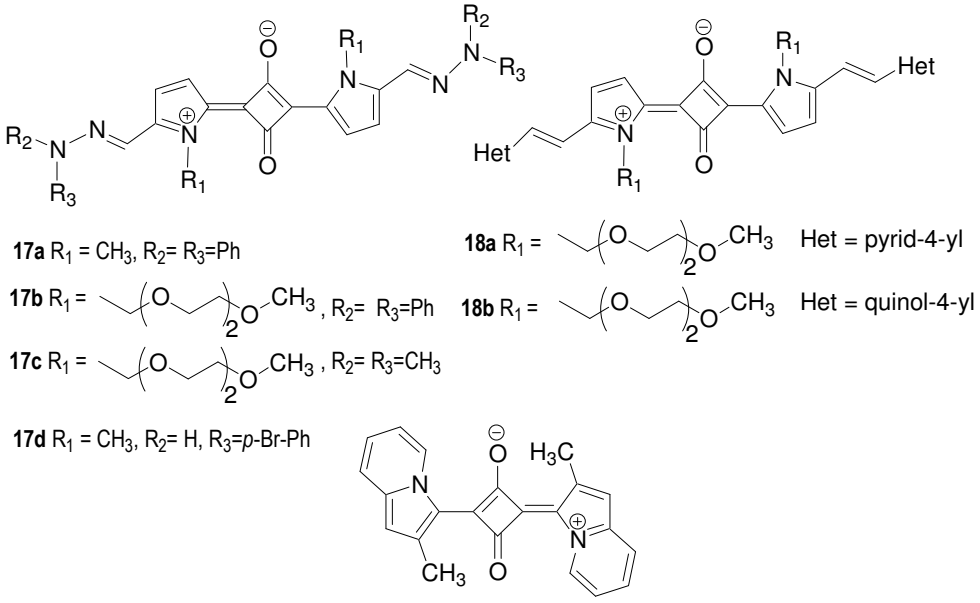

Chart 1.7

Santos and coworkers[21] have reported that the iodine substituted squaraine dyes derived from 1,3-benzothiazole were also potentially useful in PDT (**20**, **21**, Chart 1.8). Their ability to generate singlet oxygen was assessed by luminescence decay measurement in the NIR region.

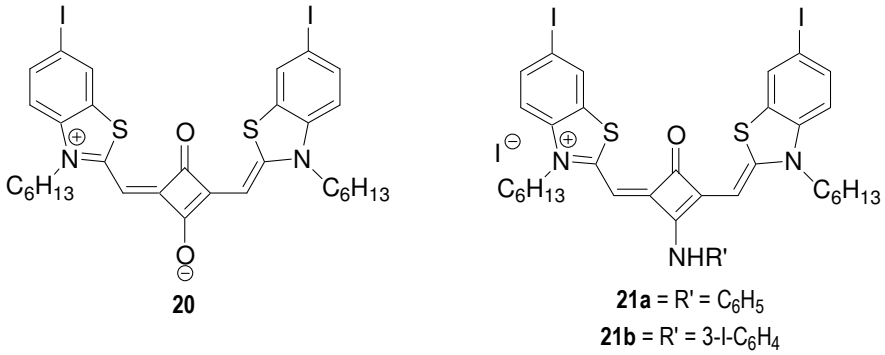

Chart 1.8

1.4. Metal Ion Sensors

Squaraines have also been shown to be ideal candidates for the design of metal ion sensors because of the favourable optical properties associated with their zwitterionic structure. The optical properties of squaraines are very sensitive to external effects such as the polarity of the medium, temperature, pH, and the presence of additives.[22-24] There are several reports in the literature, related to improvement of selectivity and sensitivity of squaraine based chemosensors, some of which are described below.

Monoaza crown ether bisphenylsquaraine dyes, **22a–c** (Chart 1.9) have been shown to be excellent candidates for alkali metal recognition.[25,26] These dyes possessed good solubility in both polar and non polar solvents, and their complexation with alkali metal ions such as Li^+, Na^+ and K^+ brought about significant changes in their fluorescence properties and oxidation potentials.

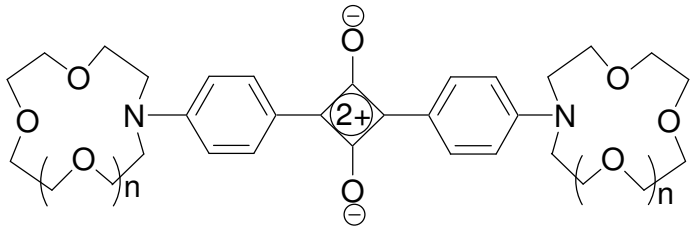

22a n = 1, b n = 2, c n = 3

Chart 1.9

The size of the crown ether group played an important role in determining the metal ion selectivity of these dyes. For example, the fluorescence of **22a** was

significantly more sensitive to the presence of lithium ions. Complexation of the cation by the crown ether moiety induces a reduction in the electron donating ability of the nitrogen atom thereby hindering its ability to contribute to the intramolecular charge transfer process.

Akkaya and coworkers[27] reported the design of a chemosensor, **23** (Chart 1.10) containing two highly calcium-selective BAPTA chelator units fused onto a squaryl moiety. This fluorescent chemosensor was very sensitive to micromolar concentrations of Ca^{2+}. In aqueous buffers with pH 7.2, the fluorescence intensity of this dye decreased with addition of Ca^{2+}, whereas the presence of large excess of Mg^{2+} ions had no effect on either the absorption or the emission spectrum. It was proposed that this chemosensor would be the prototype for a new generation of laser-diode excitable fluorescent chemosensors for Ca^{2+}.

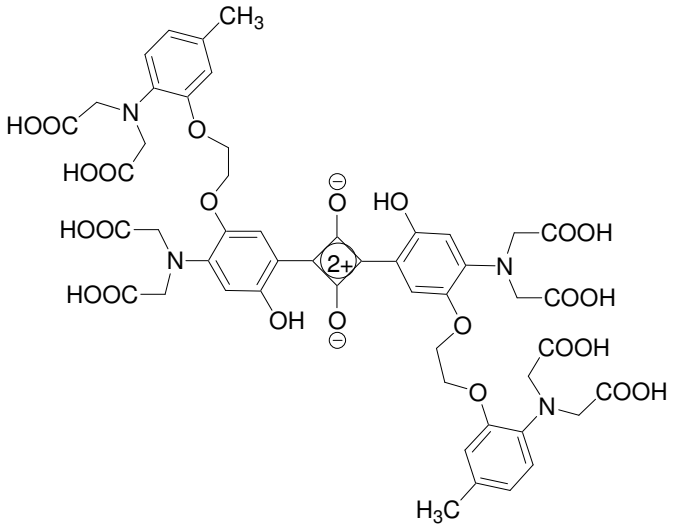

23

Chart 1.10

The same group reported a 2,3,3-trimethyl-3*H*-indole based squaraine dye, **24** (Chart 1.11), which exhibited metal ion concentration dependent changes in its fluorescence response in a 50% acetonitrile/n-butanol solvent mixture.[28] When excited at 600 nm, the emission maximum at 660 nm shifted to 665 nm, the fluorescence intensity went up on the addition of 1.0 μM Zn^{2+}. On further increase in the Zn^{2+} ion concentration, the emission intensity at 665 nm decreased, and as the Zn^{2+} concentration reached 0.025 M, the emission peak shifted to 650 nm. The fluorescence emission intensity of this dye at 640 nm first decreased three-fold at low concentrations and increased two-fold at high concentrations compared to that of the free squaraine ligand. Thus, the molecule offers three Zn^{2+} addressable states, providing an example of molecular ternary logic function.

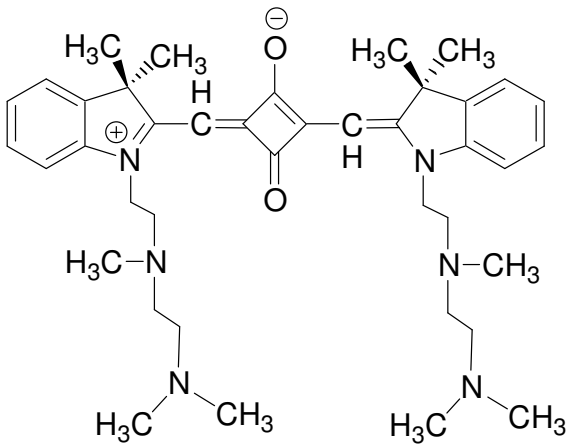

24

Chart 1.11

In addition to the numerous reports on single molecule based chemosensors that are capable of detecting analytes, considerable efforts have been directed

towards the design and synthesis of conjugated polymer based metal ion sensors. Pyrrole-derived squaraine polymeric sensors for lithium ions containing flexible oxymethylene side chains **25** (Chart 1.12) have been designed and were studied. [29] This molecular wire based fluorescent sensor exhibited enhanced sensitivity and specificity towards the Li^+ compared to Na^+ and K^+. An analogous simple squaraine dye could not sense any of the metal ions.

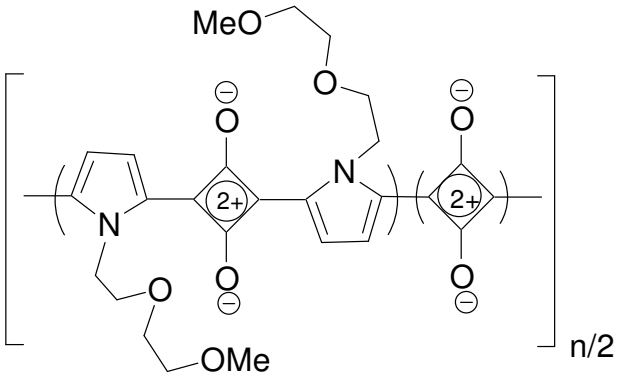

25

Chart 1.12

A supramolecular approach for the signaling of a specific cation binding, where the mode of complexation and chromophore interaction are controlled by the nature of the host and guest molecules was also reported recently.[30] The squaraine tethered bichromophoric podands **26a–c** with one, two, and three oxygen atoms in the podand (Chart 1.13), showed high selectivity towards the alkaline earth metal cations, particularly to Mg^{2+} and Ca^{2+} ions, whereas they were optically silent towards alkali metal ions.

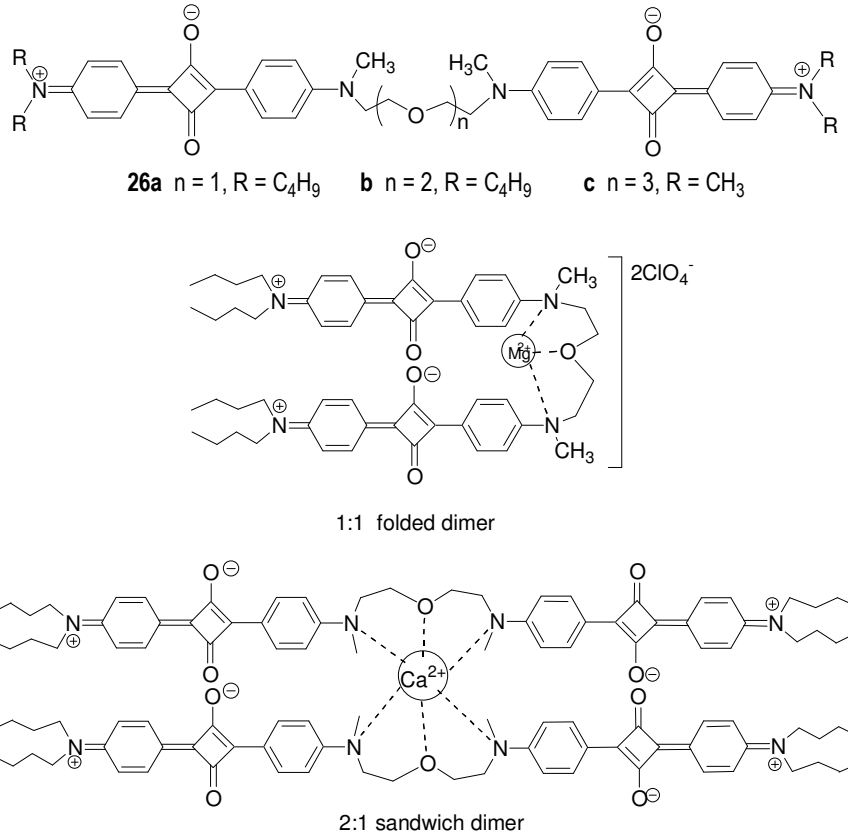

Chart 1.13

From the absorption and emission studies, it was clear that **26a** and **26b** bind with Mg^{2+} ion to form intramolecular 1:1 foldamers whereas Ca^{2+} ion preferred to bind in 1:2 stoichiometry leading to intermolecular sandwich dimers. However, the bichromophore **26c** formed 1:1 folded complexes with Mg^{2+} and Ca^{2+} ions. It was interesting to mention here that the cation-induced changes in the optical properties of **26a**–**c** are similar to those observed on the formation of H-aggregates of analogous squaraine dyes.[31-33] Addition of $LiClO_4$, $NaClO_4$, or $KClO_4$ did not bring any difference in the absorption or emission properties of these dyes, making them selective towards alkaline earth metal ions.

The synthesis of a new class of neutral methine-bridged bisquarylium NIR dye by the reaction of 4-(4-*N,N*-dialkylaminophenyl)-3-hydroxy-3-cyclobutene-1,2-dione with an excess amount of triethylorthoformate has been reported.[34] The X-ray crystallographic analysis of this dye confirmed that the bisquarylium dye consisted of two anilino substituted cyclobutene components which were bridged to each other by a methine carbon. The dye possessed a highly delocalized л-conjugated structure (**27**, Chart 1.14). It was also shown that the intense absorption band of the dye in the NIR region (815–828 nm in $CHCl_3$), underwent hypsochromic shifts of around 59–197 nm on complexation with transition metal cations such as Cr^{3+}, Mn^{2+}, Fe^{2+}, Co^{2+} and Cu^{2+}.

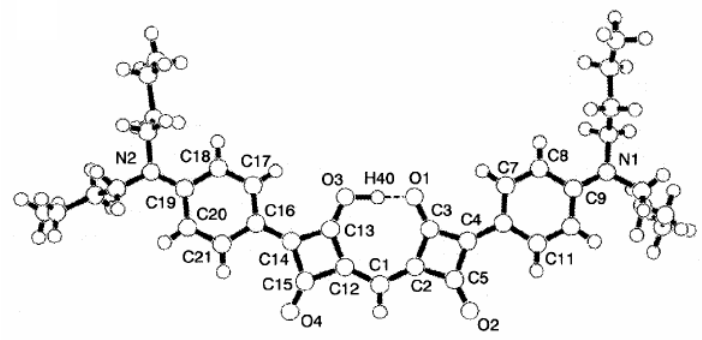

Chart 1.14. Molecular structure of the dye **27** (CHARON drawing).

Martínez-Máñez and coworkers[35] developed a chromogenic chemosensor for the detection of Hg^{2+} in aqueous media at the nanomolar level using a squaraine scaffold (**28**, Chart 1.15). The authors mentioned that their rational design relied upon the "binding site-signaling unit" approach, towards the development of colourimetric probes for Hg^{2+} cation sensing in mixed aqueous

media. The dithia-dioxa-aza crown $AT_2$15C5 was selected as the binding unit. This topological combination of sulfur, oxygen and nitrogen donor atoms anchored by ethylenic chains proved to be highly effective in forming Hg^{2+} complexes that facilitated efficient optical chemosensing.

The response of **28** toward Hg^{2+} as well as various other metal ions in CH_3CN/H_2O (20:80) solvent mixture was also investigated. On addition of Hg^{2+}, a complete bleaching of both the monomer and the aggregate bands was observed, which was fully reversible upon addition of excess of EDTA. Cations such as Li^+, Na^+, K^+, Mg^{2+}, Ca^{2+}, Ba^{2+}, Fe^{3+}, Ni^{2+}, Cu^{2+}, Zn^{2+} and Cd^{2+} did not lead to any noticeable change either in the monomer or in the aggregate band. Moreover, this monomer-to-aggregate "two-band" system was able to discriminate thiophilic cations. Hg^{2+} strongly diminished both bands at 647 and 560 nm, whereas Ag^+ induced disaggregation and a shift towards the formation of the monomer (Figure 1.1), and Pb^{2+} remained entirely silent, making this dye a remarkably selective chromogen for signaling the presence of Hg^{2+} in aqueous media at nanomolar levels.

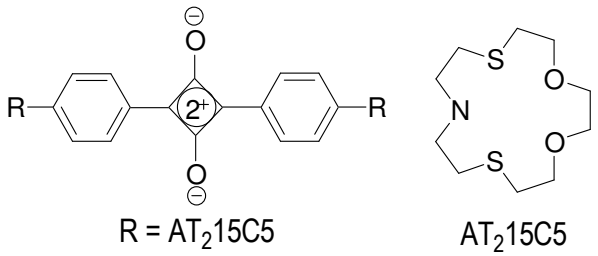

R = $AT_2$15C5 $AT_2$15C5

28

Chart 1.15

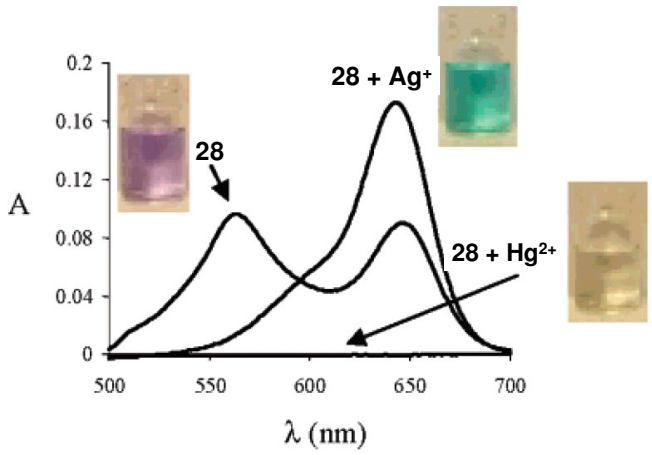

Figure 1.1. Absorption spectrum of **28** in 80:20 v/v H_2O/CH_3CN and in the presence of 5 equivalents of Hg^{2+} or Ag^{+}. The photographs show the colour of the three corresponding solutions (From ref 35).

The squaraine dye **29,** Chart 1.16, containing hydroxyl groups on the sites *ortho* to the squaric acid unit of the aromatic rings was observed to be a useful siderophore for the detection of Iron(III).[36] Deprotonation of a phenolic -OH with 1,8-diazobicyclo[5.4.0]undec-7-ene (DBU) produced a bidentate ligand between the two oxygen atoms, one from the deprotonated hydroxy group and the other from the negative charge on the carbonyl moiety of the cyclobutadiene ring. Chelation of Fe^{3+} was proposed to occur with the deprotonated hydroxyl group and the carbonyl group of the cyclobutadiene ring. The dye formed a 2:1 ligand:metal complex. Clear evidence for the coordination of the metal ion with the squaraine unit was obtained due to the formation of a new band in the 970 nm region. The crystal packing of the dye showed that each squaraine molecule stacked in such a way that the electron deficient squaraine ring was above the electron rich aromatic rings of an adjacent molecule. This stacking is in agreement

with the H-aggregates that are formed in solution, giving rise to the sharp bands observed at 650 nm. The optical response on addition of Fe^{3+} was observed at lower concentrations in comparison to other metal salts.

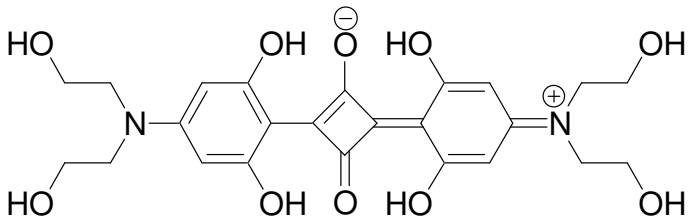

29

Chart 1.16

Kim and coworkers[37] investigated the use of squarylium dye **30** and dithiosquarylium dye **31** (Chart 1.17) for the detection of Cu^{2+} and Ag^{+} ions. The authors have investigated the metal sensing properties of these dyes in solution and in films. The changes in the absorption spectra of these dyes in the presence of Cu^{2+} was not observed on addition of metal ions such as Li^{+}, Na^{+}, Ca^{2+}, Mg^{2+} and K^{+}. They also demonstrated the development of ion sensing film optodes, which could easily determine metal ions such as Cu^{2+} and Ag^{+}. Using such disposable optodes, ions could be detected by immersing them into a glass cell filled with the sample solution, and measuring the absorbance change at the respective maximum absorption wavelength of the chromoionophore in the visible region. Highly selective ion sensing film optodes for determination of two kinds of ions, $Cu^{2+}$and Ag^{+} were prepared with plasticized PVC-PVAc-PVA membranes containing

either **30** or **31,** making them potentially suitable for the design of practical sensors.

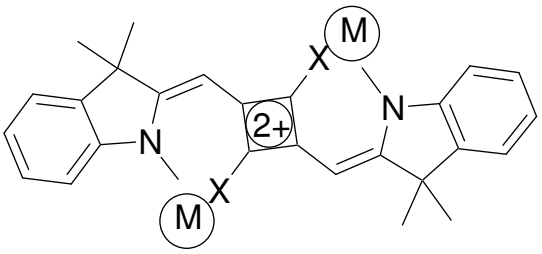

30 X = O, 31 X = S, M = Metals

Chart 1.17

1.5. Chemodosimeter

Martínez-Mańez and coworkers[38] reported a highly selective and sensitive regenerative molecular probe, **32T** (Chart 1.18) for the selective determination of mercuric ions by a "metal induced dye release" method, which involves the formation of a fluorescent or coloured product through a specific chemical reaction between the dosimeter molecule and target species.

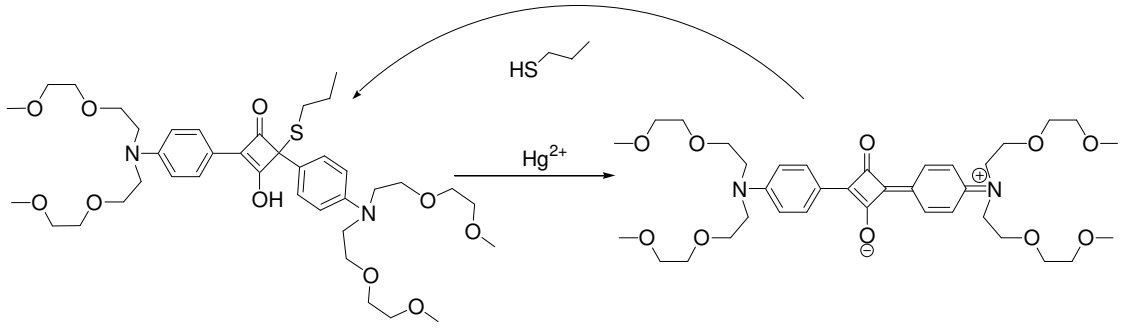

32T **32**

Chart 1.18. Chemodosimeter for Hg^{2+} ions.

In the present approach, **32** was first reacted with thiols, a spectroscopic inhibitor, which "switches OFF" the colour and fluorescence of the dye due to the formation of the derivative **32T**. This product is the chemodosimeter, which on reaction with the target ion, Hg^{2+}, liberates the dye causing "switching ON" of the colour and fluorescence. Whereas **32T** did not absorb above 400 nm, addition of Hg^{2+} ions led to the formation of an absorption band centered at 642 nm due to the release of the squaraine dye, causing a change from colourless to intense blue. This allowed the naked-eye detection of Hg^{2+} ion, since other metal ions such as Cu^{2+}, Fe^{3+}, Pb^{2+}, Ni^{2+}, Cd^{2+}, Zn^{2+}, Al^{3+} and Tl^{3+} did not react with the chemodosimeter, **32**.

It was also reported that **32** could be used as a selective chromogen for determination of cyanide in water.[39] This was the first report of squaraine being used for selective detection of anions. Initially, the chromogenic sensing ability was studied in acetonitrile in presence of the anions like F^-, Cl^-, Br^-, I^-, NO_3^-, $H_2PO_4^-$, HSO_4^-, Ac^-, Bz^-, CN^- and SCN^-. Among these, only cyanide was able to affect the band at 641 nm (Figure 1.2). In acetonitrile, on addition of CN^-, the decolouration process was not instantaneous but it increased with time and with the number of cyanide equivalents. The ^1H NMR data for **32** in acetonitrile upon cyanide addition was consistent with cyanide attack on a carbon of the four-atom squaraine ring next to the phenyl group. This led to a loss of the acceptor character of the ring as well as rupture of the electronic delocalization with the consequent

disappearance of the 641 nm CT band. Studies performed in buffered solutions of pH 9.5 (0.01 M of TRIS [tris(hydroxymethyl)aminomethane]) indicated that the cyanide ion could also be detected by this dye in aqueous media.

Figure 1.2. Acetonitrile solution of **31** [3.0 x 10^{-5} M] in the presence of 5 equivalents of anions, from left to right, F^-, Cl^-, Br^-, I^-, NO_3^-, $H_2PO_4^-$, HSO_4^-, Ac^-, Bz^-, SCN^-, CN^- and no anion.

1.6. Probes for Noncovalent Labeling

Serum albumin, often referred simply as albumin, is the most abundant plasma protein in human and other mammals. Albumin is essential for maintaining the osmotic pressure needed for proper distribution of body fluids between intravascular compartments and body tissues. It also acts as a plasma carrier by non-specifically binding several hydrophobic exogeneous and endogeneous ligand to specific targets.[40-42] The specific delivery of ligands by serum albumin is due to the presence of two major and structurally selective binding sites, namely, site I and site II, which are located in three homologous domains that form a heart-shaped protein.[43,44] The binding affinity offered by site I is mainly through hydrophobic interactions, whereas site II involves a combination of hydrophobic, hydrogen bonding and electrostatic interactions.[45,46] Human serum albumin (HSA)

is the most abundant protein in human blood. It is produced in the liver. Albumin comprises about half of the blood serum protein. Another important protein is bovine serum albumin (BSA).

The development of novel methods and new techniques for protein determination is vital in a number of areas, such as chemical and biochemical analysis, immunodiagnostics and biotechnology. Spectral methods are widely used due to their high sensitivity and selectivity. The labeling of biomolecules are of two types, covalent and noncovalent labeling. Most of the commercially available fluorescent probes are based on covalent labeling for proteins. Hence there is great demand for noncovalent labeling, which offers a simple and faster labeling procedure. Spectral methods are being widely used for noninvasive monitoring of diseased tissues.

Among the various probes used, long wavelength probes and labels are of special interest for several reasons. The advantages of NIR fluorescence are the following: (i) low levels of background interference, since few naturally occurring molecules can undergo electronic transitions in this low energy region of the electromagnetic spectrum, (ii) reduced scattering (Raman and Rayleigh) at higher wavelengths due to its dependence on the wavelength of detection by ¼, (iii) reduced photodecomposition on using longer excitation wavelengths, (iv) cheap, stable and compact diode lasers can be used for excitation resulting in increased

sensitivity and (v) effective penetration of NIR light through skin and overlaying tissue.

There have been considerable efforts devoted towards the design and synthesis of squaraine based fluorescent probes and labels. Lackowicz and co-workers[47-51] synthesized and studied the biological applications of the squaraine dyes **32** and **33** (Chart 1.19). The benzindolenium containing squaraines were found to be photostable and their short lifetimes and low quantum yields of fluorescence in water, increased significantly when bound to proteins such as BSA. The fluorescence quantum yield and lifetime of the squaraine-taurine derivatives were increased by 28-fold and 31-fold respectively, on binding with BSA. Also, their absorption maxima around 635 nm in water and 640 nm when bound to proteins allowed excitation with diode lasers, making these dyes highly suitable for applications as reactive fluorescent labels in immunochemical assays and in biophysical studies of proteins.

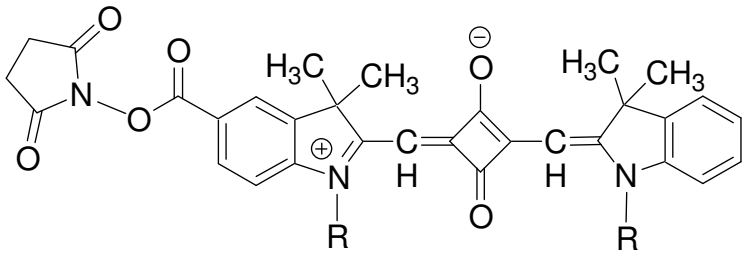

32 R = C_2H_5 **33** R = $(CH_2)_4SO_3^-$

Chart 1.19

Terpetschnig and coworkers[52] investigated the synthesis and spectral characterization of two reactive long wavelength fluorescence labels (**34** and **35**), possessing either one or two *N*-hydroxysuccinimidyl esters (Chart 1.20). They incorporated two sulfonic acid groups into the heterocyclic ring systems to improve water solubility and a reactive *N*-hydroxy-succinimide ester (NHS ester) for covalent attachment to proteins. The squaraine markers exhibited low quantum yields in water (0.15) and high quantum yields (0.6-0.7) when bound to proteins.

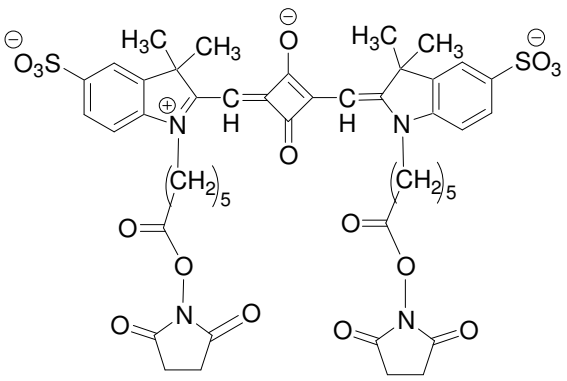

34

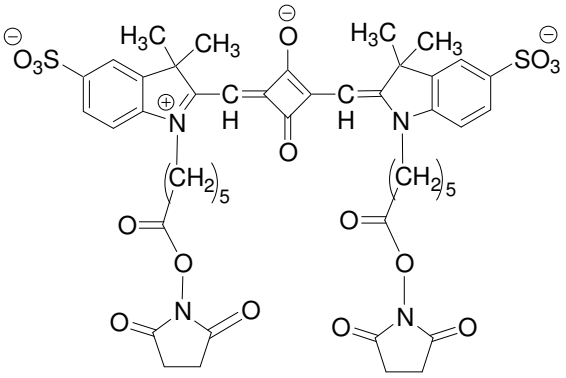

35

Chart 1.20

Nizomov *et al.*[53] investigated luminescent interactions of squaraine dyes **36**–**38** (Chart 1.21) with biological substances. It was observed that the addition of enzyme gialuronidaze (64 units) to water solution of the dye **36**, at constant concentration (2×10^{-6} M) of the dye, led to the drop of absorptive and fluorescent abilities of solution and to the broadening of the absorption spectrum. The addition of this enzyme to water solution of the dye **37** led to the appearance of a new

emission band at a λ_{max} of 702 nm in fluorescence spectrum and the fluorescence intensity increased with further increase in enzyme concentration.

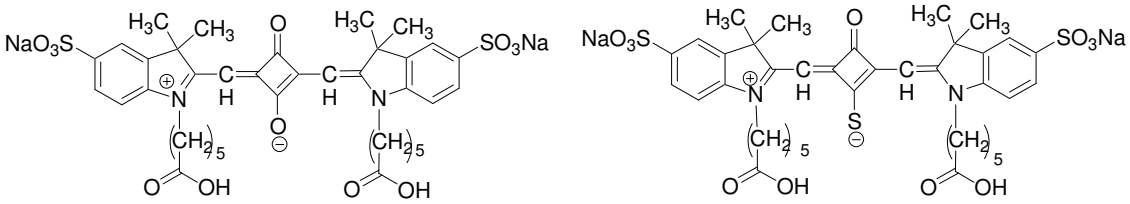

36 **37**

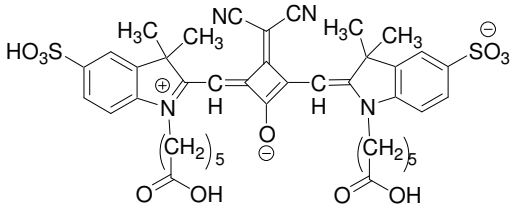

38

Chart 1.21

Nakazumi *et al.*[54] investigated some squaraine based fluorophores **39**–**41** (Chart 1.22), which exhibited a significant enhancement in fluorescence and increased quantum yield (maximum 97%) on formation of 1:1 dye–protein complexes. A large increase in fluorescence quantum yield was observed for **39** on complexation with HSA. Similarly, the fact that squarylium dyes **39c** and **41**, which displayed increase in fluorescence quantum yields upon binding to HSA could be especially advantageous for application as probes because, the emission was predominantly due to the HSA-bound species, with little emission arising from the free dye.

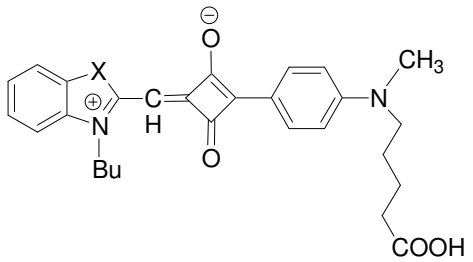

X

39 a = S
b = O
c = $C(CH_3)_2$
d = - CH=CH-

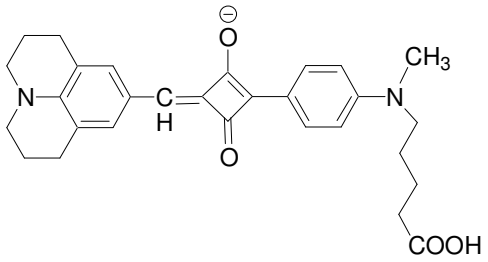

40

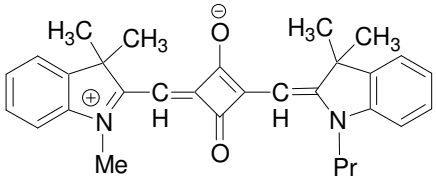

41

Chart 1.22

It was also reported that bis-squaraine dyes (**42**–**44**, Chart 1.23)[55] possessing fluorescence in the NIR region could be used for noncovalent labeling of proteins such as BSA and HSA. This bis-squaraine dye linked by a thiophene or pyrene spacer, having a terminal carboxyl group exhibited an enhancement in fluorescence in the NIR region in trizma buffer containing HSA and BSA. The Job's plot of the dye with HSA or BSA indicated a 1:1 stoichiometry. The stability constant for these complexes was calculated to be in the range of 10^6.

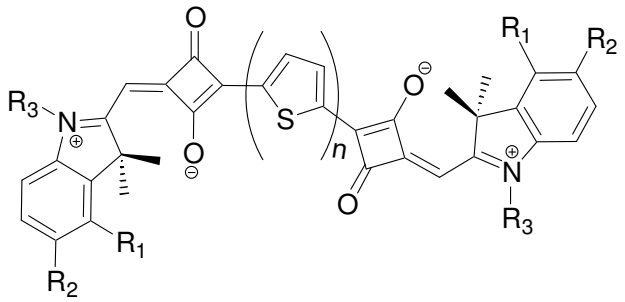

42a n=1, R_1=R_2=H, R_3=Bu, **42b** n=1, R_1=R_2=H, R_3=C_2H_4COOH,
42c n=1, R_1=R_2 = -(CH=CH)-, R_3=Bu, **42d** n=1, R_1=R_2 = -(CH=CH)-, R_3= C_2H_4COO
43a n=2, R_1=R_2=H, R_3=Bu, **43b** n=3, R_1=R_2=H, R_3=Bu

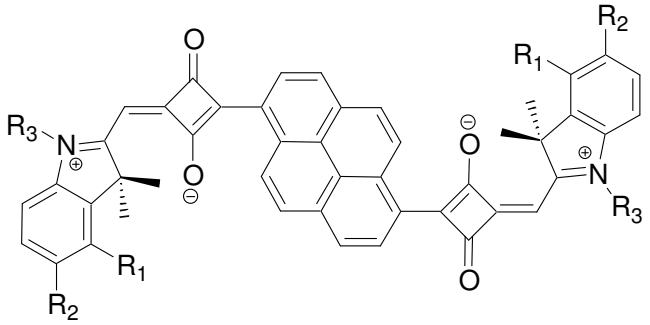

44a n=1, R_1=R_2=H, R_3=C_2H_4COOH, **44b** n=1, R_1=R_2 = -(CH=CH)-, R_3= C_2H_4COO

Chart 1.23

Recently Ramaiah and coworkers[56] reported the use of squaraine dyes for site-selective binding and dual mode recognition of serum albumin. The interactions of the squaraine dye **16**, (Chart 1.6), possessing polyhydroxyl groups with BSA was investigated. The initial addition of BSA (up to 1.5 μM) led to a decrease in the absorbance at 584 nm, corresponding to the squaraine chromophore. However, subsequent additions resulted in a gradual increase in the absorbance, but with the formation of a new band at 610 nm. Formation of the

bathochromically-shifted band resulted in a visual colour change from pinkish red (without protein) to bluish in the presence of BSA. Analysis of the absorption data indicated a 1:1 stoichiometry for the complex between squaraine and BSA, with an association constant of $(1.4 \pm 0.1) \times 10^6$ M^{-1} and change in free energy of −35 kJ mol^{-1}. Addition of BSA initially resulted in a gradual enhancement in fluorescence intensity, with a bathochromic shift in emission from 600 to 620 nm. However, subsequent additions led to significantly higher changes, until ca. 80-fold enhancement in fluorescence quantum yield was observed at 7 μM of BSA.

The authors have demonstrated the site-selective binding of the dye with BSA, by ligand displacement using known site selective binding ligands, such as dansylamide (DNSA, for site I) and dansylproline (DP, for site II). The significant increase in the absorbance and fluorescence yields of the dye at and above 1.5 μM concentrations of BSA could be attributed to the binding of **16** at site II with a relatively larger cavity size of 2.6 Å and involving a combination of hydrophobic, hydrogen bonding and electrostatic interactions. The absence of tryptophan residue in the hydrophobic cavity of site II and the formation of a relatively loose complex at this site led to the observation of significant bathochromic shifts in absorption and fluorescence emission.

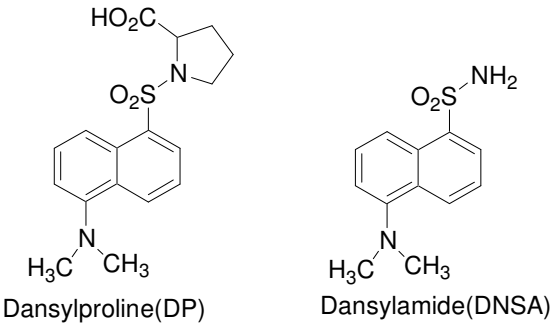

Chart 1.24

Very recently Yokoyama *et al.*[57] reported the use of squaraine for selective detection of a protein and demonstrated its application on a gel following electrophoresis using 1D SDS-PAGE minigel. The squaraine dye, which bears a hydroxy group **45** (Chart 1.25), underwent a colour change from pink to deep purple solution on binding with proteins BSA (Figure 1.3).

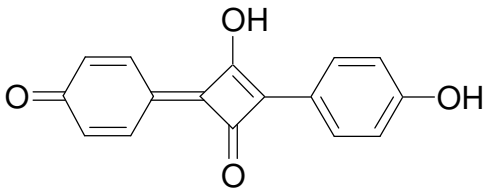

45

Chart 1.25

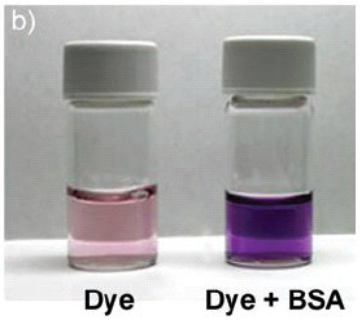

Figure 1.3. Photographs of solutions of compound **45** in the absence and presence of BSA.

This obvious colour change was due to the formation of dye-BSA complex and corresponded to a dramatic increase in the absorbance at around 600 nm. The proteins in the gel obtained after the electrophoresis using 1D SDSPAGE minigels were stained by compound **45**. After fixation of the proteins, the gels were incubated in the staining solution and washed with a solution of H_2O/MeOH/AcOH 87:10:3 v/v. The experimental results clearly showed that the squaraine dye had excellent protein sensitivity, was easy to handle, had a short reaction time, and could be used for protein staining in the gel after SDS-PAGE.

1.7. Nanocrystalline pH Sensor

Bawendi and coworkers[58] have designed a reversible nanocrystal (NC) based fluorescent sensor by attaching a dye possessing an equilibrium response to an analyte, to the surface of a CdSe/ZnS nanocrystal (Scheme 1.2). The authors demonstrated that energy transfer between the NC and dye could be used as a means for detecting analytes with high precision, irrespective of changes in excitation intensity, wavelength, or collection efficiency. Thus, it could remove several difficulties encountered with simple dye based ratiometric sensors.

The sensing action of the NC-squaraine conjugate is illustrated by modulation of the FRET efficiency arising from the overlap of the absorption spectrum of the pH-sensitive dye with that of the pH insensitive quantum dot emission. Owing to the pH dependence of the absorption spectrum of the dye, the

spectral overlap between the dye absorption and the NC emission increases as the pH is lowered. It was observed that the dye absorption band was suppressed under basic conditions for the free dye in homogeneous solution. Hence, energy transfer from the NC to the dye was not sufficient, and that of the NC at 613 nm dominated the emission spectrum. As the pH was lowered, the absorption cross section of the dye increased, and FRET from the NC to the dye became more efficient and the emission from the NC-dye conjugate was dominated by that of the dye at 650 nm. The major changes occurred near the p*K*a of the dye. The modulation of the FRET efficiency by pH resulted in emission dependence between the NC and dye that is naturally ratiometric. Thus, the solution pH can be read out precisely by taking the ratio of each emission peak intensity (NC and dye) to the intensity at the isosbestic point, which functions as an internal reference. This ratiometric approach is powerful when compared to typical chemo and biosensors that display a single intensity based response to analytes (*i.e.*, either brightening or darkening) because the ratiometric construction is not sensitive to fluctuations of light excitation or collection efficiency as sensing is self-referencing. Taken together with the broad excitation spectrum and photostability conferred by NCs, this reversible and ratiometric approach makes NCs versatile agents for chemical and biological sensing.

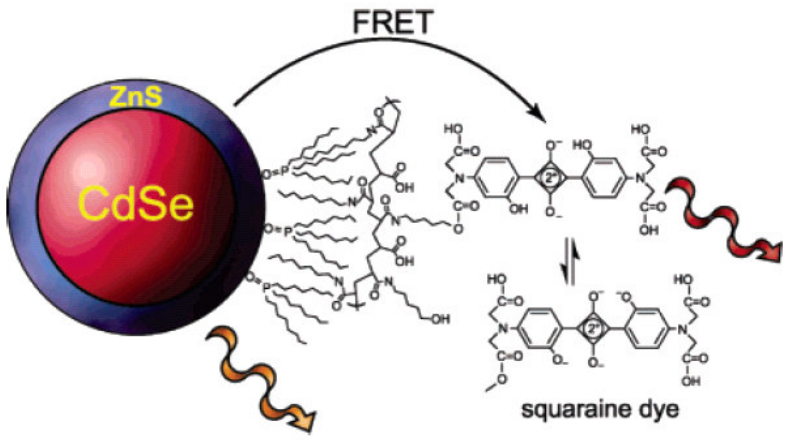

Scheme 1.2

1.8. Objectives of the Present Investigation

The main objective of the present work was to develop novel squaraine based NIR dyes possessing improved absorption and emission in the NIR region, in view of the potential application of such dyes as fluorescent probes in various biological applications, and to study their photophysical and metal ion sensing properties.

1.9. References

1. Law, K.-Y. *Chem. Rev.* **1993**, *93*, 449-486.
2. Emmelius, M.; Pawlowski, G.; Vollmann, H. W. *Angew. Chem., Int. Ed. Engl.* **1989**, *28*, 1445-1471.
3. Andrews, J. H.; Khagdarov, J. D. V.; Singer, K. D.; Hull, D. L.; Chuang, K. C. *Nonlinear Opt.* **1995**, *10*, 227.

4. Ashwell, G. J.; Jefferies, G.; Hamilton, D. G.; Lynch, D. E.; Robers, M. P. S.; Bahra, G. S.; Brown, C. R. *Nature* **1995**, *375*, 385-388.

5. Chen, C.-T.; Marder, S. R.; Cheng, L.-T. *J. Am. Chem. Soc.* **1994**, *116*, 3117-3118.

6. Chen, C.-T.; Marder, S. R.; Cheng, L.-T. *J. Chem. Soc. Chem. Commun.* **1994**, 259-260.

7. Loutfy, R. O.; Hsiao, C. K.; Kazmaier, P. M. *Photogr. Sci. Eng.* **1983**, *27*, 5-9.

8. Triebs, A.; Jacob, K. *Angew. Chem., Int. Ed. Engl.* **1965**, *4*, 694.

9. Bigelow, R. W.; Freund, H. *J. Chem. Phys.* **1986**, *107*, 159-174.

10. Regan, O.; Grätzel, M. *Nature* **1991**, *353*, 737-740.

11. Amirnasr, M.; Nazeeruddin, M. K.; Grätzel, M. *Thermochim. Acta* **2000**, *348*, 105.

12. Alex, S.; Santhosh, U.; Das, S. *J. Photochem. Photobiol., A* **2005**, *172*, 63-71.

13. Otsuka, A. Funabiki, K.; Sugiyama, N.; Yoshida, T.; Minoura, H.; Matsui, M. *Chem. Lett.* **2006**, *35*, 666-667.

14. Yum, J.-H.; Walter, P.; Huber, S.; Rentsch, D.; Geiger, T.; Nüesch, F.; Angelis, F. D.; Grätzel, M.; Nazeeruddin, M. K. *J. Am. Chem. Soc.* **2007**, *129*, 10320-10321.

15. Li, C.; Wang, W.; Wang, X.; Zhang, B.; Chao, Y. *Chem. Lett.* **2005**, *34*, 554-555.

16. Burke, A.; Schmidt-Mende, L.; Ito, S.; Grätzel, M. *Chem. Commun.* **2007**, 234-236.

17. Ramaiah, D.; Joy, A.; Chandrasekhar, N.; Eldho, N. V.; Das, S.; George, M. V. *Photochem. Photobiol*. **1997**, *65*, 783-790.

18. Ramaiah, D.; Eckert, I.; Arun, K. T.; Weidenfeller, L.; Epe, B. *Photochem. Photobiol.* **2002**, *76*, 672-677.

19. Ramaiah, D.; Eckert, I.; Arun, K. T.; Weidenfeller, L.; Epe, B. *Photochem. Photobiol.* **2004**, *79*, 99-104.

20. Beverina, L.; Abbotto, A.; Landenna, M.; Cerminara, M.; Tubino, R.; Meinardi, F.; Bradamante, S.; Pagani, G. A. *Org. Lett.* **2005**, *19*, 4257-4260.

21. Santos, P. F.; Reis, L. V.; Duarte, I.; Serrano, J. P.; Almeida, P.; Oliveira, A. S.; Ferreira, L. F. V. *Helv. Chim. Act* **2005**, *88*, 1135-1143.

22. Das, S.; Kamat, P. V.; De la Barre, D.; Thomas, K. G.; Ajayaghosh, A.; George, M. V. *J. Phys. Chem.* **1992**, *96*, 10327-10330.

23. Das, S.; Thomas, K. G.; George, M. V.; Kamat, P. V. *J. Chem. Soc. Faraday Trans.* **1992**, *88*, 3419-3422.

24. Law, K. -Y. *J. Phys. Chem*. **1989**, *93*, 5925-5930.

25. Das, S.; Thomas, K. G.; Thomas, K. J.; Bedja, I.; Kamat, P. V. George, M. V. *Anal. Proc*. **1995**, *32*, 213-215.

26. Das, S.; Thomas, K. G.; Thomas, K. J.; Kamat, P. V.; George, M. V. *J. Phys. Chem.* **1994**, *98*, 9291-9296.

27. Akkaya, E. U.; Turkyilmaz, S. *Tetrahedron Lett.* **1997**, *38*, 4513-4516.

28. Dilek, G.; Akkaya, E. U. *Tetrahedron Lett.* **2000**, *41*, 3721-3724.

29. Chenthamarakshan, C. R.; Eldo, J.; Ajayaghosh, A. *Macromolecules* **1999**, *32*, 5846-5851.

30. Arunkumar, E.; Ajayaghosh, A.; Daub, J. *J. Am. Chem. Soc.* **2005**, *127*, 3156-3164.

31. Arun, K. T.; Epe, B.; Ramaiah, D. *J. Phys. Chem. B* **2002**, *106*, 11622-11627.

32. Dimitriev, O. P.; Dimitriyeva, A. P.; Tolmachev, A. I.; Kurdyukov, V. V. *J. Phys. Chem. B* **2005**, *109*, 4561-4567.

33. Chen, H.; Farahat, M. S.; Law, K-Y.; Whitten, D. G. *J. Am. Chem. Soc.* **1996**, *118,* 2584-2594.

34. Yagi, S.; Fujie, Y.; Hyodo, Y.; Nakazumi, H. *Dyes and Pigments* **2002**, *52*, 245-252.

35. Ros-Lis, J. V.; Martínez-Máñez, R.; Rurack, K.; Sancenón, F.; Soto, J.; Spieles, M. *Inorg. Chem.* **2004**, *43*, 5183-5185.

36. Wallace, K. J.; Gray, M.; Zhong, Z.; Lynch, V. M.; Anslyn, E. V. *Dalton Trans.* **2005**, 2436-2441.

37. Kim, S. H.; Han, S. K.; Park, S. H.; Lee, S. M.; Lee, S. M.; Koh, K. N.; Kang, S. W. *Dyes and Pigments* **1999**, *41*, 221-226.

38. Ros-Lis, J. V.; García, B.; Jiménez, D.; Martínez-Máñez, R.; Sancenón, F.; Soto, J.; Gonzalvo, F.; Valldecabres, M. C. *J. Am. Chem. Soc.* **2004**, *126*, 4064-4065.

39. Ros-Lis, J. V.; Martínez-Máñez, R.; Soto, J. *Chem. Commun.* **2002**, 2248-2249.

40. Peters, T. *All about Albumin*: *Biochemistry, Genetics and Medicinal Applications*; Academic Press: San Diego, CA, 1996.

41. Kumar, C. V.; Buranaprapuk, A.; Opiteck, G. J.; Moyer, M. B.; Jockusch, S.; Turro, N. J. *Proc. Natl. Acad. Sci. U. S. A.* **1998**, *95*, 10361-10366.

42. Kumar, C. V.; Buranaprapuk, A. *Angew. Chem., Int. Ed. Engl.* **1997**, *36*, 2085-2087.

43. He, X. M.; Carter, D. C. *Nature* **1992**, *358*, 209-215.

44. Dockal, M.; Carter, D. C.; Ruker, F. *J. Biol. Chem*. **1999**, *274*, 29303-29310.

45. Lhiaubet-Vallet, V.; Sarabia, Z.; Bosca, F.; Miranda, M. A. *J. Am. Chem. Soc*. **2004**, *126*, 9538-9539.

46. Jimenez, M. C.; Miranda, M. A.; Vaya, I. *J. Am. Chem. Soc.* **2005**, *127*, 10134-10135.

47. Terpetsching, E.; Lakowicz, J. R. *Dyes Pigm*. **1993**, *21*, 227-234.

48. Terpetschnig, E.; Szmacinski, H.; Lakowicz, J. R. *Anal. Chim. Acta* **1993**, *282*, 633-641.

49. Terpetschnig, E.; Szmacinski, H.; Ozinskas, A.; Lakowicz, J. R. *Anal. Biochem*. **1994**, *217*, 197-204.

50. Terpetschnig, E.; Szmacinski, H.; Lakowicz, J. R. *Proc. SPIE-Int. Soc. Opt. Eng.* **1994**, *2137*, 608.

51. Terpetschnig, E.; Szmacinski, H.; Lakowicz, J. R. *J. Flouoresc*. **1993**, *3*, 153-155.

52. Oswald, B.; Simon, L.; Lehmann, G.; Terpetschnig, E.; Wolfbeis, O. S. *Anal. Biochem.* **2000**, *280*, 272-277.

53. Nizomov, N.; Ismailov, Z. F.; Nizamov, S. N.; Salakhitdinova, M. K.; Tatarets, A. L.; Patsenker, L. D.; Khodjayev, G. *J. Mol. Struct.* **2006**, *788*, 36-42.

54 Nakazumi, H.; Colyer, C. L.; Kaihara, K.; Yagi, S.; Hyodo, Y. *Chem. Lett.* **2003**, *32*, 804-805.

55. Nakazumi, H.; Ohta, T.; Etoh, H.; Uno, T.; Colyer, C. L.; Hyodo, Y.; Yagi, S. *Synth. Met.* **2005**, *153*, 33-36.

56. Jisha, V. S.; Arun, K. T.; Hariharan, M.; Ramaiah, D. *J. Am. Chem. Soc.* **2006**, *128*, 6024-6025.

57. Suzuki, Y.; Yokoyama, K. *Angew. Chem., Int. Ed.* **2007**, *46*, 4097-4099.

58. Snee, P. T.; Somers, R. C.; Nair, G.; Zimmer, J. P.; Bawendi, M. G.; Nocera, D. G. *J. Am. Chem. Soc.* **2006**, *128*, 13320-13321.

CHAPTER 2

A Squaraine Based Chemosensor for Selective Detection of Hg^{2+} and Pb^{2+}

2.1. Abstract

*A novel unsymmetrical cationic squaraine dye (**USqH**$^+$) absorbing in the near infrared region (600–850 nm), was synthesized by reacting a semisquaric acid derivative 3-[4-(N,N-dioctylamino)phenyl]-4-hydroxycyclobutene-1,2-dione with the squarylium dye, bis(3-methylbenzothiazol-2-ylidene)squaraine. Addition of micromolar amounts of Hg^{2+} and Pb^{2+} to solutions of **USqH**$^+$ in dichloromethane brought about significant changes in its absorption spectra, resulting in a change in colour of the solution from green to pink. The absorption spectrum of the dye was relatively insensitive to other environmentally relevant metal ions, making it possible to visually detect Hg^{2+} and Pb^{2+} in the presence of these metal ions. Molecular modeling of the complexes at the density functional theory (DFT) and semiempirical PM3 levels strongly suggests that the oxygen atoms are the most likely choice for cation binding. The calculations also indicate a high affinity of Hg^{2+} and Pb^{2+} towards the formation of 2:1 complexes, which are in good agreement with the experimental results.*

2.2. Introduction

The design of molecular probes for sensing metal ions using the concept of photo-induced electron transfer (PET),[1-7] host-guest chemistry[8-10] or metal ion induced changes in aggregation behaviour[11,12] has been attracting considerable attention in recent years. Of particular interest are the detection of Hg^{2+} and Pb^{2+}, highly toxic environmental pollutants arising from both natural and industrial sources. Their presence in the environment even in trace concentrations causes adverse long-term health effects.[13]

Currently, sophisticated analytical techniques such as atomic absorption spectroscopy, inductively coupled plasma mass spectroscopy, anodic stripping voltammetry and X-ray fluorescent spectroscopy are used in estimating the presence of these metal ions in the environment. There is hence a significant interest in developing rapid and inexpensive methods for detecting Hg^{2+} and Pb^{2+} and a number of fluorescence based molecular sensors have recently been reported.[14-19]

Martínez *et al.*[20] reported an electro-optical triple channel system, in which two molecular systems containing tricyanovinyl dyes act as signaling subunits and crown ether macrocycles as the binding sites (**1**–**2**, Chart 2.1). Signaling was observed through UV–vis absorption, fluorescence and electrochemical measurements. The advantage of tricyanoethylene group is that it can

simultaneously act as a redox-active group and an acceptor moiety in the amino-phenyl-tricyanoethylene chromo/fluorophores.

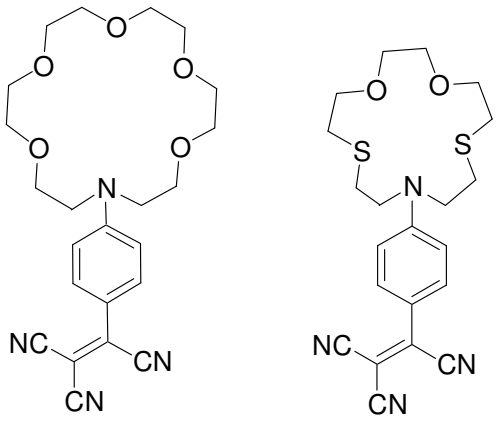

1 **2**

Chart 2.1

In acetonitrile, **1** and **2** showed absorption maxima at around 520 nm and 518 nm respectively. Addition of equimolar quantities of Li^+, Na^+, K^+, Ca^{2+}, Ba^{2+}, Mg^{2+}, Cu^{2+}, Cd^{2+} and Hg^{2+} cations to acetonitrile solutions of **1** produced negligible changes in the UV–vis absorption spectrum of these molecules. However, on adding Pb^{2+}, the absorption band shifted from 520 to 470 nm and this was marked by a colour change from red pink to yellow. The aza–thia–oxa crown containing molecule **2**, exhibited selectivity towards Hg^{2+}. The absorption spectrum blue shifted from 518 to 400 nm on addition of Hg^{2+}, which resulted in a colour change of the acetonitrile solution from reddish pink to yellow. The fluorescence of **2** was highly sensitive to Hg^{2+}. Addition of Hg^{2+} also led to an enhancement in its fluorescence intensity. In contrast, the sensitivity of the

fluorescence property of **1** towards Pb^{2+} was less specific. The electro-chemical response of both receptors **1** and **2** was also less selective. However, remarkably large anodic shifts of near 370 mV were obtained on addition of Hg^{2+}, Pb^{2+} and Fe^{3+} for **1** and Hg^{2+} and Pb^{2+} for **2**.

Qian *et al.*[21] investigated a water soluble chemosensor **3** (Chart 2.2), which is made up of two aminonaphthalimide fluorophores and a non macrocycle receptor of 2,6-bis(aminomethyl)pyridine.

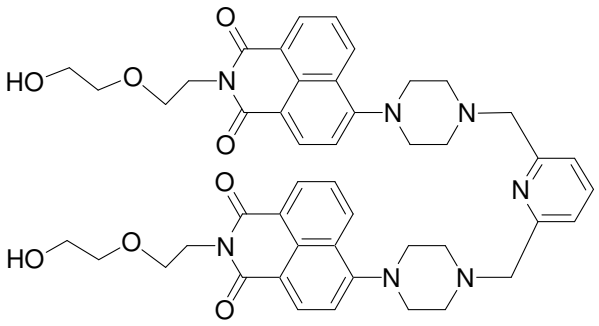

3

Chart 2.2

The fluorescence emission (FE) of **3** exhibited highly selective and sensitive response toward Hg^{2+} in neutral buffered aqueous solutions. The weak emission band of **3** (Φ = 0.007, λ_{max} 548 nm) was hardly affected on addition of biologically relevant metals such as Fe^{3+}, Co^{2+}, Ni^{2+}, Cu^{2+}, Cr^{3+}, Ca^{2+}, K^{+} and Mg^{2+}, whereas a small enhancement in fluorescence was observed upon the addition of Cd^{2+}, Pb^{2+}, Ag^{+} and Zn^{2+}. However, a significant enhancement in fluorescence intensity and a red shift of the emission maximum by about 8 nm was

observed on addition of Hg^{2+}. The red shift in emission may be due to the intramolecular excimer formation caused by the decrease in the distance between two fluorophores on binding with mercury ions. It was noticed that only d^{10} ions such as Hg^{2+}, Cd^{2+}, Pb^{2+}, Ag^{+} and Zn^{2+} led to FE changes of this type, since only such ions do not introduce low-energy metal centered or charge-separated excited states into the molecule, which can prevent energy transfer or electron transfer processes. Hg^{2+} could be detected at least down to 1.0×10^{-8} M when **3** was employed at 1.0×10^{-6} M in 0.001 M tris-HCl buffer aqueous solution, and its fluorescence intensity also increased linearly with the concentration of Hg^{2+} up to a mole ratio (**3**/Hg^{2+}) of 1:1. Competition experiments conducted in the presence of Hg^{2+} at 1.0×10^{-5} M mixed with Ca^{2+}, Fe^{3+}, Co^{2+}, Mg^{2+}, Ni^{2+}, Cu^{2+}, Cr^{3+}, Zn^{2+}, Ca^{2+}, Pb^{2+}, Cd^{2+}, K^{+} and Ag^{+} at 5.0×10^{-5} M, as well as the mixture of the metal ions indicated that the presence of the other metal ions had no effect on the ability of the molecule to sense Hg^{2+}.

The use of Rhodamine 6G based fluorescent probes **4** for selective detection of Hg^{2+} in mixed DMF/water media have recently been reported by Duan and coworkers[22]. The normal form of **4** in solution is the spirolactam form, which is colourless and nonfluorescent. The absorption spectra of **4** in 50% (v/v) water/DMF showed only a very weak band above 500 nm, which was ascribed to its spirolactam form. On addition of 2.5 equiv of Hg^{2+}, formation of a new peak at 538 nm with significant enhancement in intensity of absorption indicated the

formation of the ring-opened amide form of **4** (Chart 2.3)**.** This resulted in the solution turning from colourless to pink.

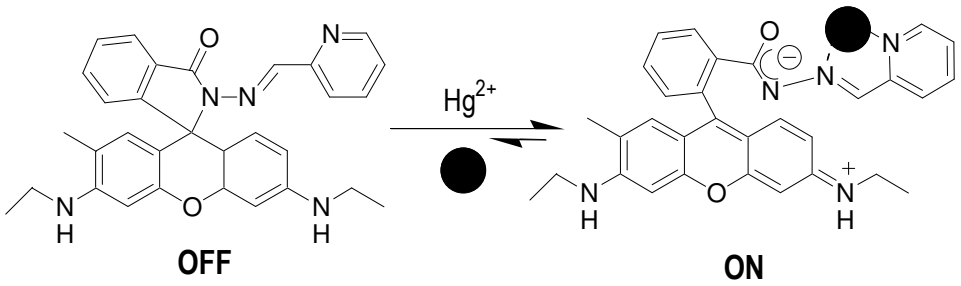

4

Chart 2.3

The fluorescence also increased with the formation of a new peak at 560 nm (Φ = 0.42). The fluorescence titration profile of **4** with Hg^{2+} demonstrated that the detection limit of Hg^{2+} was at the parts per billion level in solutions containing 5 μM of **4**. Addition of alkali or alkaline earth metals such as Na^{+}, K^{+}, Mg^{2+} and Ca^{2+}, and the first row transition metals Mn^{2+}, Fe^{2+}, Co^{2+}, Ni^{2+} and Cu^{2+} did not bring about any significant spectral changes.

Chang and coworkers[23] have reported ratiometric determination of Hg^{2+} ions using a dioxaoctanediamide-based chemosensor possessing two pyrene moieties **5** (Chart 2.4), which makes use of the changes in the ratio of monomer and excimer emissions of the pyrene fluorophores. The fluorescence of compound **5** was switched OFF by addition of Hg^{2+} ions. The molecule exhibited an intense excimer emission of the pyrene at around 489 nm and a very weak monomer emission at around 380–410 nm.

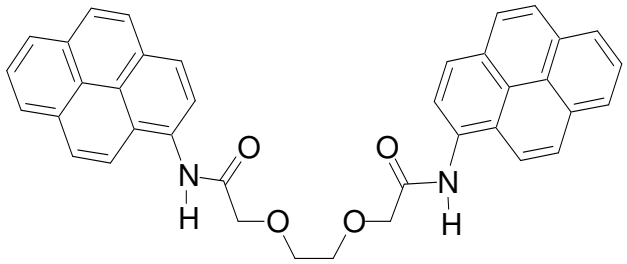

5

Chart 2.4

The ratio of fluorescence intensity of the excimer and monomer observed at 489 and 383 nm respectively, was very large, being 24.9 in a 50% aqueous methanol solution. This indicated that the compound exists in mainly the stacked or folded conformation with the two pyrene moieties situated closely enough to yield the excimer. The fluorescence intensity at 489 nm was remarkably quenched only on the addition of Hg^{2+} (100 equivalents) compared to the various other metal ions tested.

Another Hg^{2+} selective fluoroionophore based on 8-hydroxyquinoline possessing an appended boron-dipyromethene functionality (**6**, Chart 2.5) has been reported by the same group.[24] Solutions of the compound in aqueous dioxane showed a pronounced Hg^{2+} selective ON-OFF switching of fluorescence as compared to some other transition and heavy metal ions. The fluorescence was efficiently quenched (>98%) on addition of 5 equiv of Hg^{2+} ions, and the detection limit was found to be 5×10^{-6} M in a dioxane/water (1:3, v/v) solvent system. The ionophore also showed a selective chromogenic behaviour toward Hg^{2+} ions by

changing the colour of the solution from light amber to red, which was possible to detect with the naked eye.

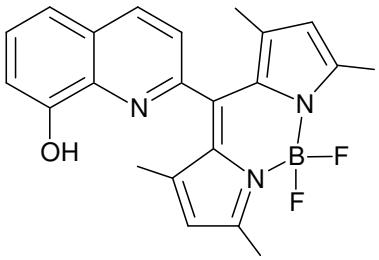

6

Chart 2.5

Most of the systems discussed in this section have absorption and emission properties in the UV and visible region and suffer from the need for short wavelength excitation. A near infrared absorbing cationic squaraine dye **7** (Chart 2.6) capable of detecting trace amounts of transition and lanthanide metal ions in aqueous media, in the presence of excess alkali and alkaline earth metal ions was reported earlier by Das and coworkers.[25] In this chapter we describe the design of a novel cationic squaraine based PET probe which made possible the visual detection of trace amounts Hg^{2+} and Pb^{2+}.[25-27]

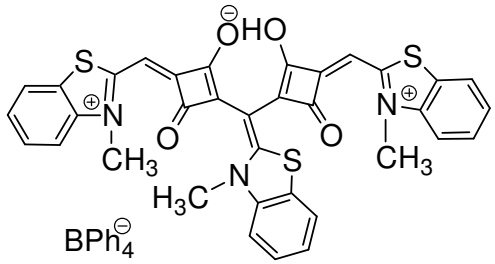

7

Chart 2.6

2.3. Results and Discussion

2.3.1. Synthesis

Nakazumi *et al*.[28] had earlier reported a symmetric cationic squaraine dye **7** (Chart 2.6) which was formed along with the conventional 1,3-disubstituted squaric acid derivatives, during the reaction of *N*-alkylbenzothiazolium iodide with squaric acid. The proposed mechanism for the formation of the cationic dye is as shown in Scheme 2.1.

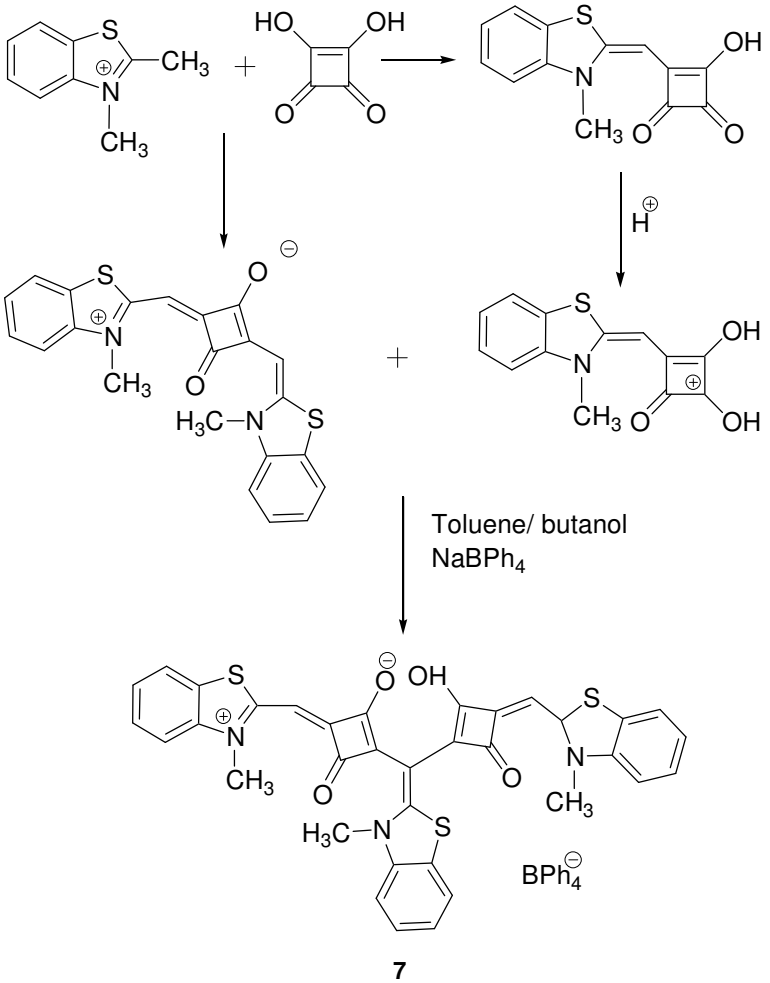

Scheme 2.1. Mechanism for the formation of cationic dye **7**.

Using this strategy, we were able to synthesize a new cationic dye by reacting the semisquaric acid 3-[4-(*N,N*-dioctylamino)phenyl]-4-hydroxycyclobut-ene-1,2-dione with a methylene group containing squarylium dye, namely bis(3-methylbenzothiazol-2-ylidene)squaraine to yield novel unsymmetrically substituted cationic squaraine dye with a 9 % yield (Scheme 2.2).

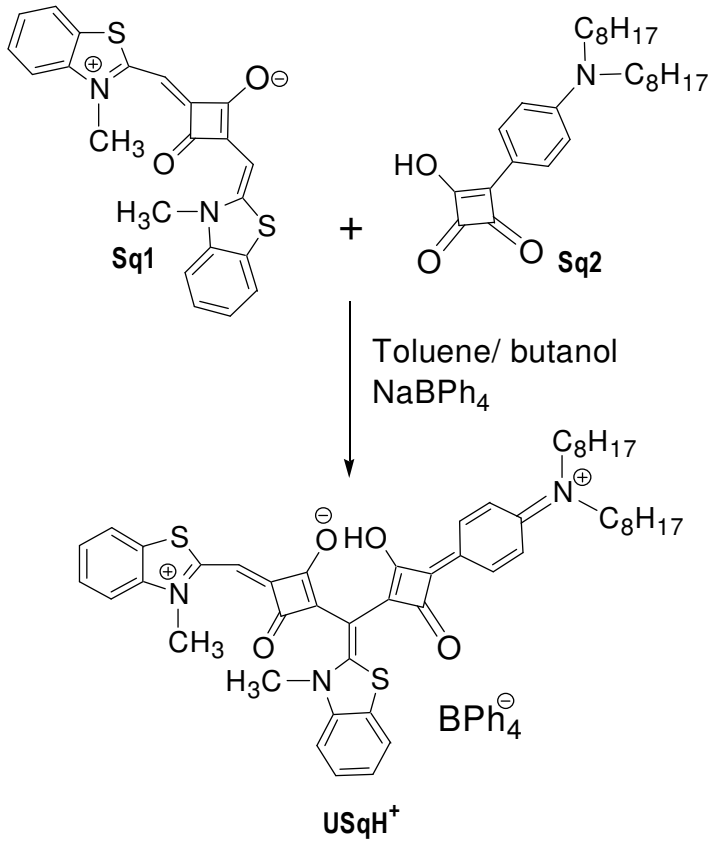

Scheme 2.2. Scheme for synthesis of **USqH⁺**.

2.3.2. Absorption and Emission Properties

Figure 2.1 shows absorption spectra of **USqH⁺** in aprotic solvents, namely dichloromethane, chloroform and acetonitrile. In dichloromethane and chloroform,

the dye showed an absorption maximum at around 782 nm. The absorption spectrum was however blue shifted in acetonitrile. The absorption spectrum in alcoholic solvents such as methanol, butanol and isopropanol was also blue shifted (Figure 2.2).

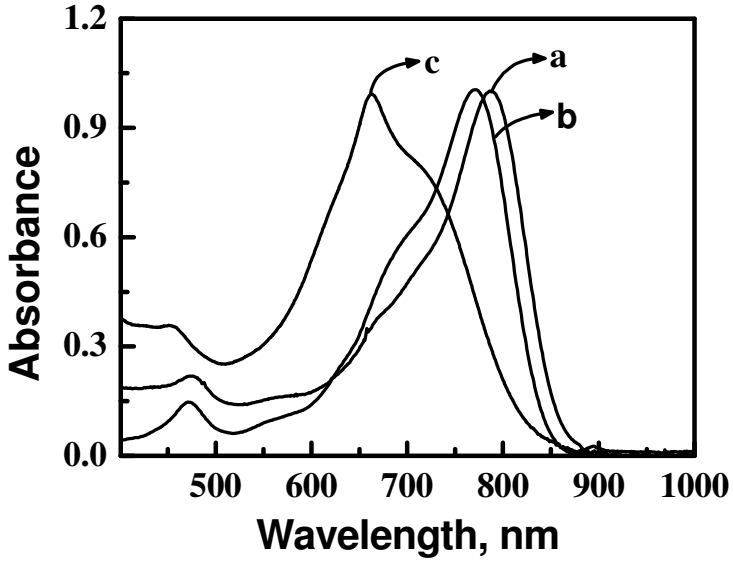

Figure 2.1. Absorption spectra of **USqH⁺** in a) Chloroform, b) Dichloromethane and c) Acetonitrile.

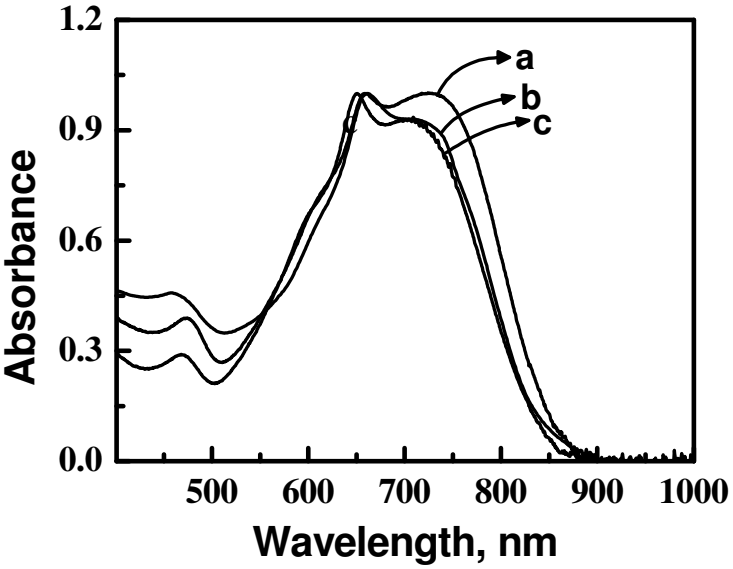

Figure 2.2. Absorption spectra of **USqH⁺** in a) Isopropanol, b) Butanol and c) Methanol.

In solvents such as chloroform, dichloromethane and acetonitrile, the dye showed two emission bands centered at around 840 nm and 660 nm (Figure 2.3).

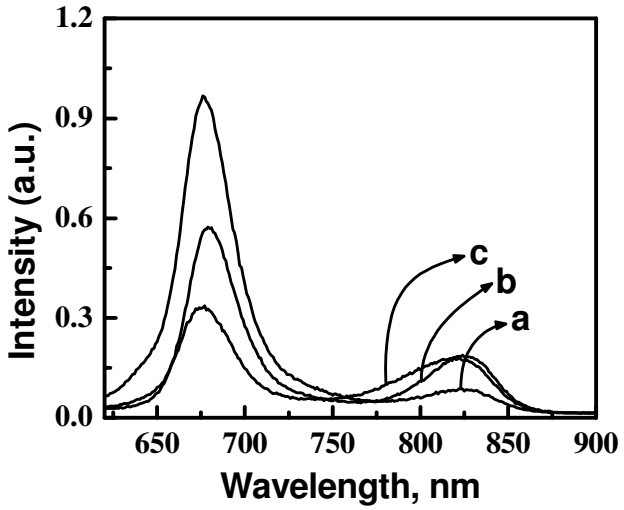

Figures 2.3. Emission spectra of **USqH⁺** in a) Chloroform, b) Dichloromethane and c) Acetonitrile.

In the alcoholic solvents where the emission bands are blue shifted compared to chloroform and dichloromethane, only a blue shifted emission band was observed (Figure 2.4).

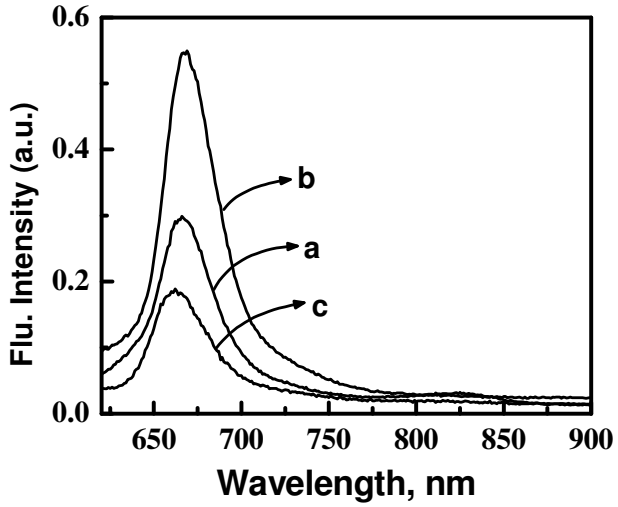

Figures 2.4. Emission spectra of **USqH⁺** in a) Isopropanol, b) butanol and c) Methanol.

It is interesting to note that in acetonitrile, where the absorption band is blue shifted similar to what is observed in the alcoholic solvents, two emission bands were observed. Since the observation of an emission band blue shifted to the long wavelength absorption band is usually an indication of luminescent impurities, rigorous efforts were undertaken to purify the dye by column chromatography. However, even after repeated purification, the absorption and emission properties of the dye remained unchanged, indicating that the observed results could not be attributed to the presence of impurities. A possible explanation could be that the dye can exist in two conformationally different forms, which could possess different absorption and emission properties. In order to test this, the absorption and emission properties of the dye were investigated in solvent mixtures containing different ratios of chloroform and methanol ($CHCl_3$/MeOH). A clear blue shift in the absorption band with increase in percentage of MeOH in the solvent mixture could be observed (Figure 2.5).

This change was observed in decrease in intensity of the long wavelength fluorescence band and an increase in intensity of the short wavelength fluorescence band until in solvent mixtures with high methanol content the long wavelength fluorescence band disappeared completely (Figure 2.6).

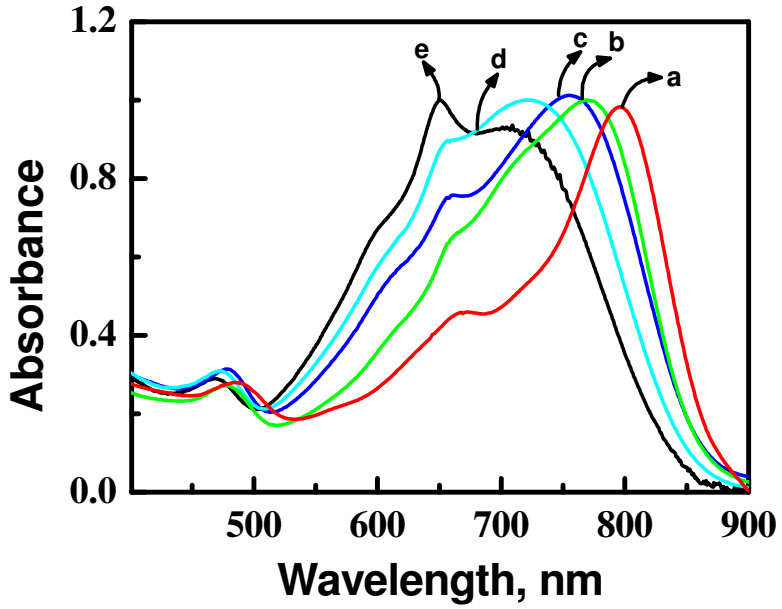

Figure 2.5. Change in the absorption spectra of **USqH⁺** with change in composition of the $CHCl_3$/MeOH solvent mixture: a) $CHCl_3$, b) 3:1 $CHCl_3$/MeOH, c) 2:2 $CHCl_3$/MeOH, d) 1:3 $CHCl_3$/MeOH and e) MeOH.

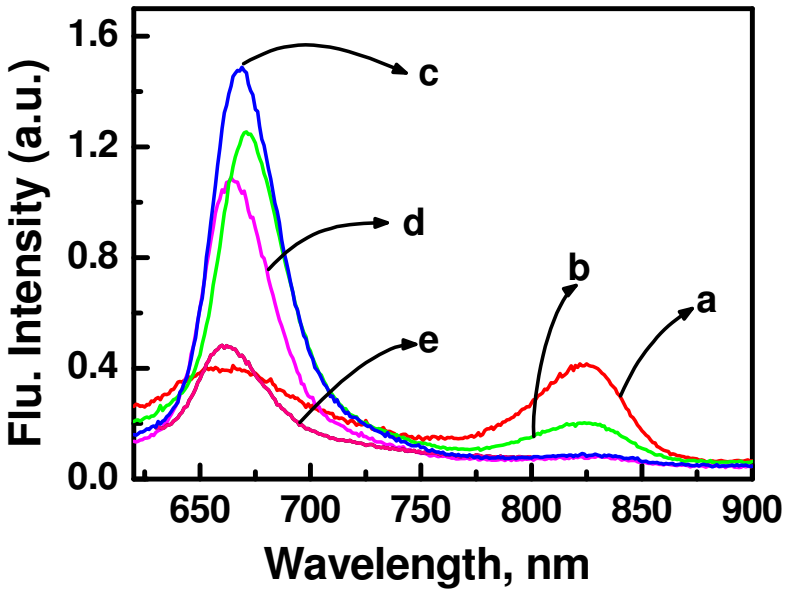

Figure 2.6. Change in the emission spectra of **USqH⁺** with change in composition of the $CHCl_3$/MeOH solvent mixture: a) $CHCl_3$, b) 3:1 $CHCl_3$/MeOH, c) 2:2 $CHCl_3$/MeOH, d) 1:3 $CHCl_3$/MeOH and e) MeOH.

We propose that the observed results can be explained by assuming that the dye can exist in two forms. In aprotic solvents, all parts of the molecule can exist in the same plane due to hydrogen bonding between the two cyclobutane moieties, which would result in conjugation extending to all the three arms of the molecule. In protic solvents, the intramolecular H-bond can break, resulting in the semisquaraine part of the dye twisting out of plane (Scheme 2.3). The absorption and emission spectra under these conditions were very similar to that of the symmetrical dyes reported earlier.[29]

Molecular modeling calculation at the density functional theory level using the Becke's exchange functional in conjunction with the Lee-Yang-Parr correlation functional (BLYP method)[30,31] as implemented in the Gaussian 03 suite of programs[32] are in conformation of the proposed mechanism. In the optimized geometry of **USqH$^+$**, both the squaraine arms were found to lie in the same plane due to a strong O–H••O hydrogen bond (Figure 2.7(a)) while in **USq**, the squaraine arms were twisted due to the electrostatic repulsion between the negatively charged carbonyl oxygens (Fig. 2.7(b)).[33] For instance, a twist angle of 62 ^{o} was found between the two C=O groups facing each other in **USq**.

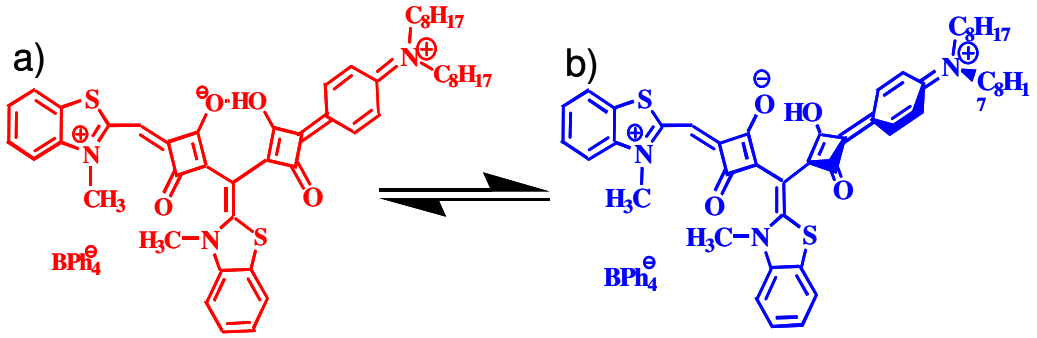

Scheme 2.3. Proposed conformational forms of **USqH⁺** .

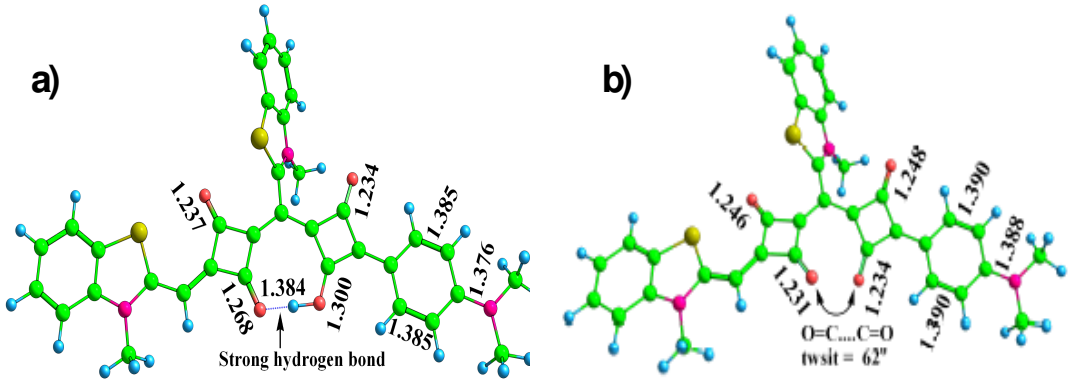

Figure 2.7. Geometries of a) **USqH⁺** and b) **USq** optimized at BLYP/6-31G(d) level.

2.3.3. Selective Sensing of Hg^{2+} and Pb^{2+}

The unsymmetrical cationic squaraine dye **USqH⁺** possesses a sharp absorption peak centered on 782 nm in dichloromethane. Addition of mercury ions ≥20 μM to a dichloromethane solution of **USqH⁺** led to a hypsochromic shift of the main absorption band to 770 nm, along with the formation of a new band with a maximum centered on 551 nm. Further addition of Hg^{2+} led to a decrease in the intensity of the 770 nm peak and an increase in intensity of the 551 nm band

(Figure 2.8), resulting in a change in colour of the solution from green to pink. These changes were marked by the presence of an isosbestic point at 599 nm.

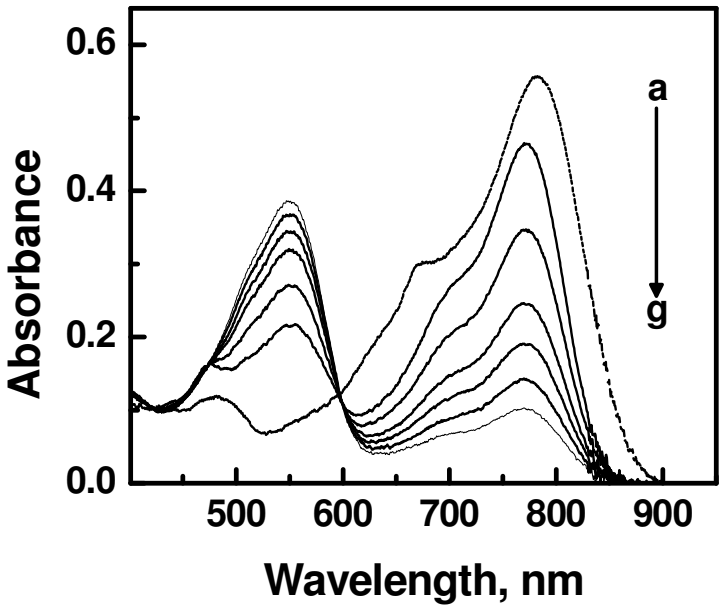

Figure 2.8. Effect of Hg^{2+} on the absorption spectrum of **USqH⁺** (12.9×10^{-6} M) in dichloromethane a) 0, b) 25, c) 28, d) 31, e) 34, f) 38 and g) 49 μM Hg^{2+}.

The Job's plot which is extensively used to find the complexation mode in the host-guest interactions,[34-36] showed a maximum value for absorbance at 551 nm when the mole fraction of **$USqH^+$** was 0.668, which was clearly indicative of a 2:1 **USq-Hg^{2+}** stoichiometry (Figure 2.9).

Similar observations were made on the addition of Pb^{2+}. Upon addition of small amounts of ≥ 15 μM of Pb^{2+}, the absorption at 782 nm was blue shifted to 772 nm and subsequent addition of Pb^{2+} made a decrease in intensity of absorption maximum and was hypsochromically shifted to 549 nm through an isosbestic point 607 nm as shown in Figure 2.10.

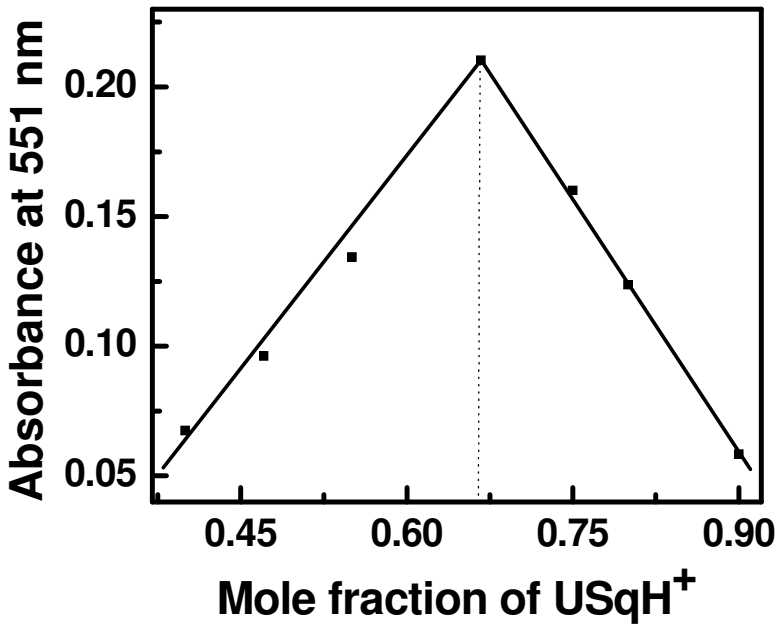

Figure 2.9. Job's plot for the binding of **USqH$^+$** with Hg^{2+}.

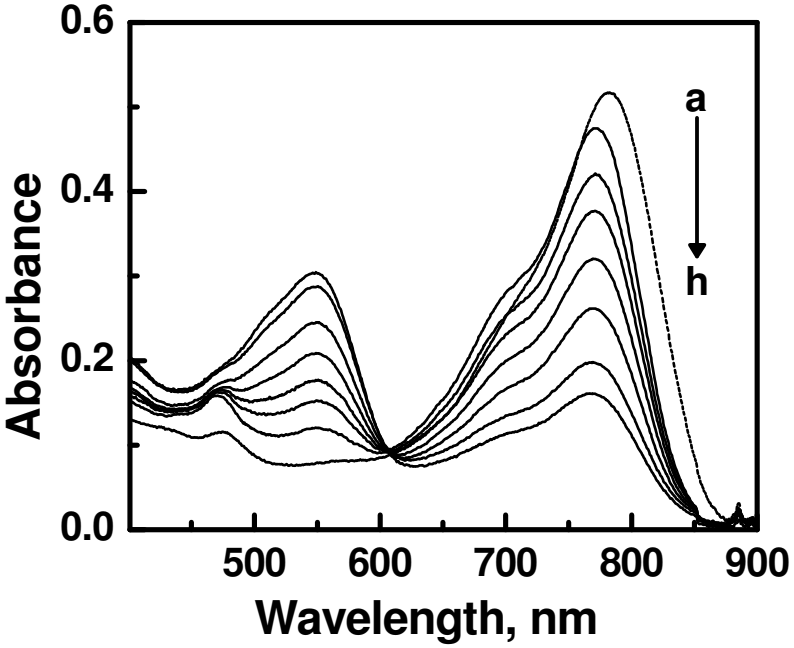

Figure 2.10. Effect of Pb^{2+} on the absorption spectrum of **USqH$^+$** (12×10^{-6} M) in dichloromethane a) 0, b) 36, c) 47, d) 53, e) 59, f) 68, g) 82 and h) 93 μM Pb^{2+}.

2.3.4. Selective Complexation of $USqH^+$ with Hg^{2+} and Pb^{2+} in the Presence of Alkali, Alkaline Earth and Transition Metal Ions

Effect of addition of various alkali, alkaline earth and some transition metal ions such as Li^+, Na^+, Mg^{2+}, Ca^{2+}, Ba^{2+} and Zn^{2+} on the absorbance of **$USqH^+$** in dichloromethane solution was investigated. Figure 2.11 shows the effect of addition of Li^+, Na^+, Mg^{2+}, Ca^{2+}, Ba^{2+} and Zn^{2+} on the absorption spectrum of **$USqH^+$** in dichloromethane. There was no noticeable change either in absorption spectra of **$USqH^+$** even on addition of excess amounts of these metal ions. Instead, a small increase in intensity of the absorption and a small blue shift was observed upon addition of micromolar amounts of these metal ions.

Figure 2.12 shows the effect of addition of various metal ions on the absorbance of **$USqH^+$** in dichloromethane at 770 nm. Addition of Li^+, Na^+, Mg^{2+}, Ca^{2+}, Ba^{2+} and Zn^{2+} led to negligible changes in the absorbance of **$USqH^+$**. Addition of Pb^{2+} to a solution of **$USqH^+$** resulted in a significant decrease in the absorbance at 770 nm. Similar results were also obtained on the addition of Hg^{2+}. The effect of addition of Hg^{2+} to a solution containing Na^+, Ca^{2+} and Zn^{2+} metal ions is also shown. The high specificity for detection of Hg^{2+} by **$USqH^+$** compared to the other metal ions is clearly evident from the figure.

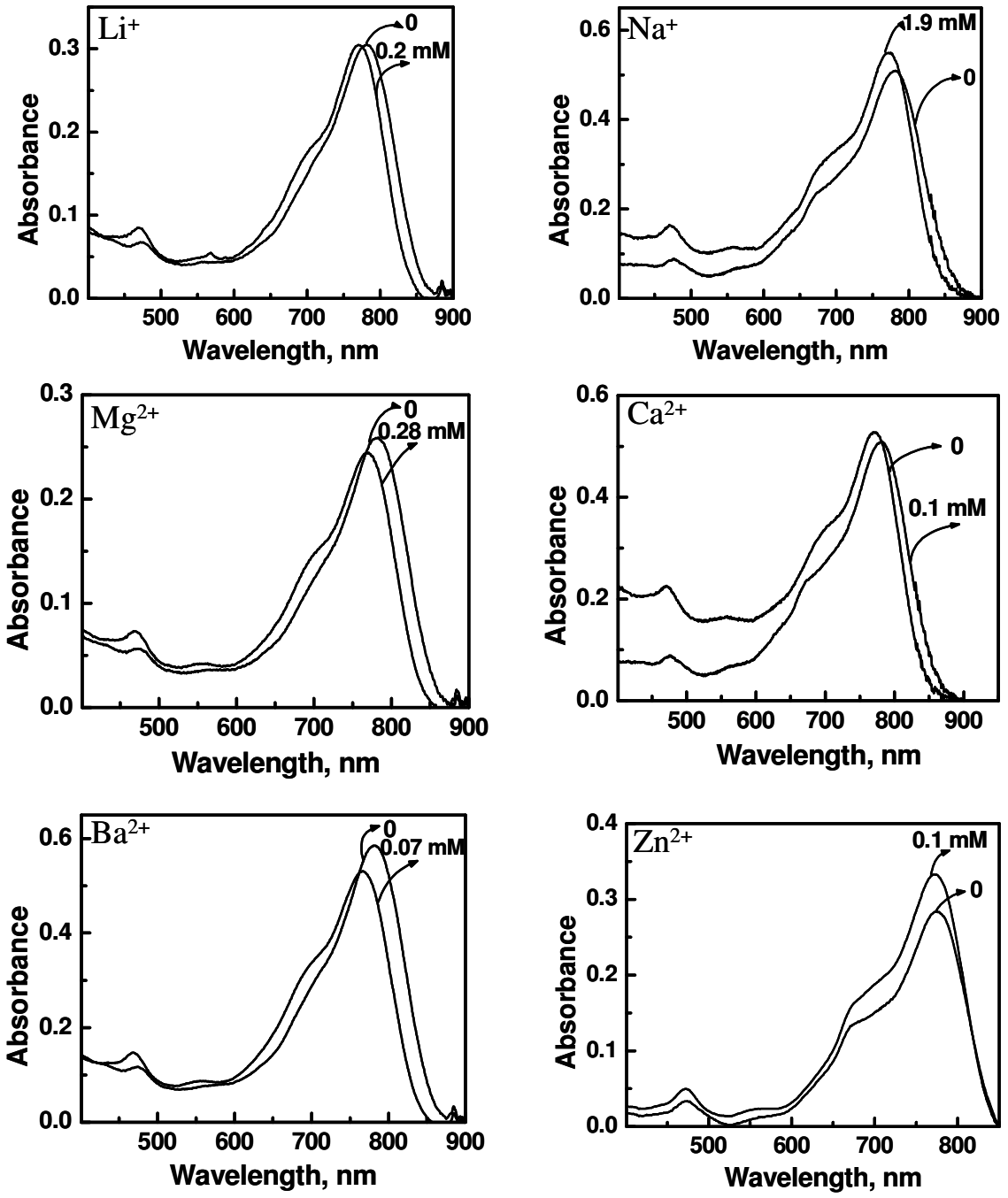

Figure 2.11. Effect of addition of Li^+, Na^+, Mg^{2+}, Ca^{2+}, Ba^{2+} and Zn^{2+} on the absorption spectrum of **USqH$^+$** in DCM.

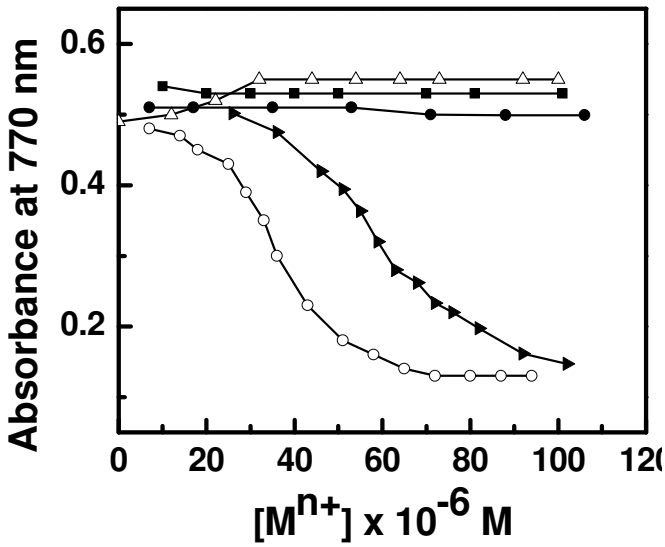

Figure 2.12. Effect of metal ions on the absorbance at 770 nm for solutions of **USqH⁺** (11.6×10^{-6} M) in dichloromethane. Δ) Na^+, ■) Ca^{2+} ●) Zn^{2+} ▶) Pb^{2+} and ○) Hg^{2+} containing Na^+ (0.1 mM), Ca^{2+} (0.1 mM) and Zn^{2+} 0.1 mM).

Addition of micromolar amounts of Cu^{2+} to an 8.7 μM solution of **USqH⁺** in dichloromethane also resulted in a gradual decrease in the intensity of absorption at 782 nm and a concomitant growth of absorption at 750 nm with an isosbestic point at 765 nm. The hypsochromic shift in the absorption band induced by Cu^{2+} was however much less than that caused by Hg^{2+} and Pb^{2+}, and there was no perceivable change in the colour of the solution. At higher concentrations of Cu^{2+} (>120 μM), an irreversible loss of colour indicating oxidation of the dye was observed.

Addition of micromolar amounts of Hg^{2+} into solutions of **USqH⁺** (7.9×10^{-6} M) containing Cu^{2+} in the micromolar range (Figure 2.13) resulted in a change in colour of the solution from green to pink, making it possible to visually

detect Hg^{2+} in the presence of Cu^{2+}. Figure 2.14 shows the effect of addition of different metal ions on the colour of **USqH$^+$** in dichloromethane.

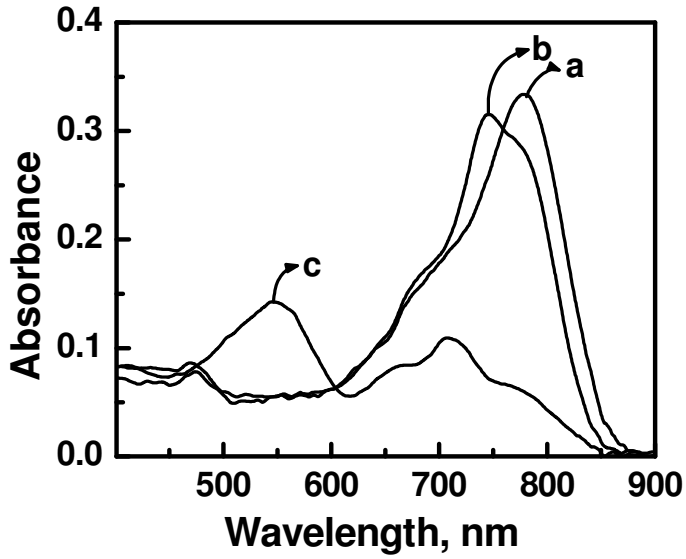

Figure 2.13. Absorption spectra of **USqH$^+$** (7.9×10^{-6} M) in dichloromethane containing a) no metal ions b) 90 μM Cu^{2+} and c) 29 μM Hg^{2+} + 90 μM Cu^{2+}.

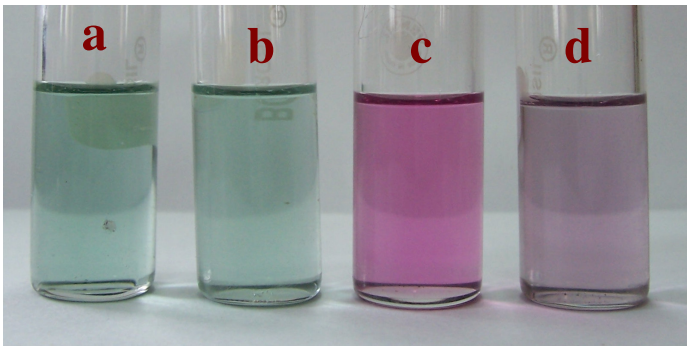

Figure 2.14. Colour of dichloromethane solutions of **USqH$^+$** (15 μM) a) in the absence of metal ions, b) in the presence of 0.3 mM of Li^+, Na^+, Mg^{2+}, Ca^{2+}, Ba^{2+}, Zn^{2+} and 100 μM Cu^{2+}, c) in the presence of 40 μM Hg^{2+} and d) in the presence of 87 μM Pb^{2+}.

Complexation of the metal ions is most likely to involve oxygen atoms of the central cyclobutane ring of **USqH$^+$**. Participation of the oxygen atoms in the

complexation process could be expected to decrease their electron donating ability, thus resulting in destabilization of intra molecular charge transfer (ICT) and formation of the blue shifted band. It is interesting to note that the new absorption band of **USqH$^+$** formed on complexation with Hg^{2+} or Pb^{2+} was blue shifted by about 230 nm compared to the main band, whereas the shift for the symmetric dye **7** on complexation with Hg^{2+} was only 141 nm. As a result, the effect of addition of Hg^{2+} to solutions of **7** was not visually perceptible.

2.3.5. Molecular Modeling of the Complexes at the DFT and Semiempirical PM3 Levels

The geometry of **USqH$^+$** and its deprotonated form **USq** were optimized at DFT level by using BLYP method[30,31] as implemented in the Gaussian 03 suite of programs.[32] For H, C, N, O and S, 6-31G(d) basis functions were selected.[37] For geometry optimization of a **USq**-**Hg** complex, LanL2DZ basis set was selected for Hg.[38,39] For other systems studied here, PM3 level geometry optimization was carried out. Molecular electrostatic potential (MESP)[40-43] was also calculated for **USq** at the BLYP level.

In the optimized geometry of **USqH$^+$**, a strong O–H••O hydrogen bond between squaraine arms was found which results in all the nucleophiles being in the same plane, while in **USq**, the squaraine arms were twisted at an angle of 62 ^{o} due to the electrostatic repulsion between the negatively charged carbonyl oxygen. Although **USq** is neutral, the planarization of the terminal amino group and a short

C–N(Me)$_2$ bond of length 1.388 Å are in favour of its expected zwitterionic structure.[44] This electronic feature was further revealed in the MESP analysis, which showed a very high and localized negative MESP around the oxygen atoms of four membered rings (Figure 2.15). This strongly suggests that the oxygen atoms are the most likely choice for cation binding.

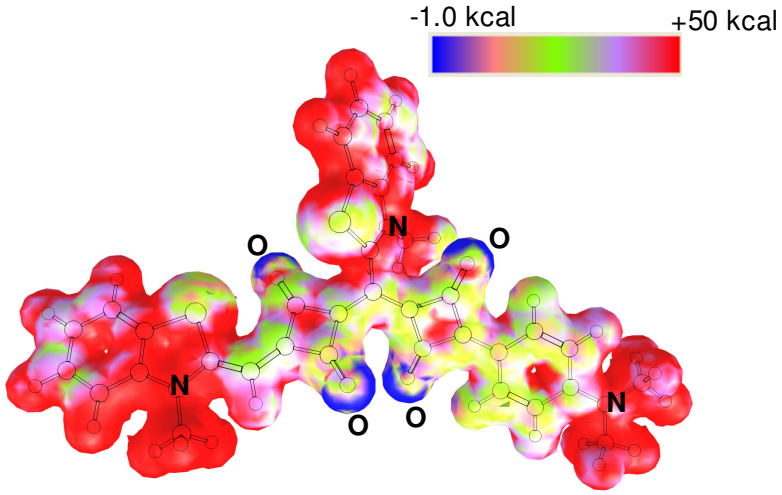

Figure 2.15. The MESP mapped on to the van der Waals' surface of **USqH**$^+$ at BLYP/6-31G* level showing the high negative potential around oxygen atoms and high positive potential around nitrogen atoms revealing the zwitterionic character of the system.

We have modeled several possible structures for the 1:1 and 2:1 complexes of **USq** with Zn^{2+}, Hg^{2+} and Pb^{2+}, and their binding energies have been calculated at the semiempirical PM3 level. For this, the oxygen and sulfur atoms were considered as possible metal binding site. Starting geometries containing the cation interacting with (O1, O2), (O3, S1), (O3, S2), (O1, O2, S3) and the methyl group of the amine ligand were included in the calculations.

In the case of 1:1 **(USq)Zn^{2+}** complex, although the oxygen atoms of **USq** is electron rich, a structure containing the expected **O1••Zn^{2+}••O2** interaction could not be located. The nearest inter atomic distance of around 7.065 Å obtained suggests a negligible interaction between the **USq** and Zn^{2+}. The most stable geometry **(USq)Zn^{2+}**(1) obtained is shown in Figure 2.16. The difference in the heat of formation (HF) value of the complex (HF = 485.3 kcal mol^{-1} **(USq)Zn^{2+}**(1)) and unbound system (HF = 492.6 kcal mol^{-1} **(USq)Zn^{2+}**(2)) turns out to be 7.3 kcal mol^{-1} for the 1:1 **(USq)Zn^{2+}** complex (Figure 2.16). This value is considered as the binding energy.

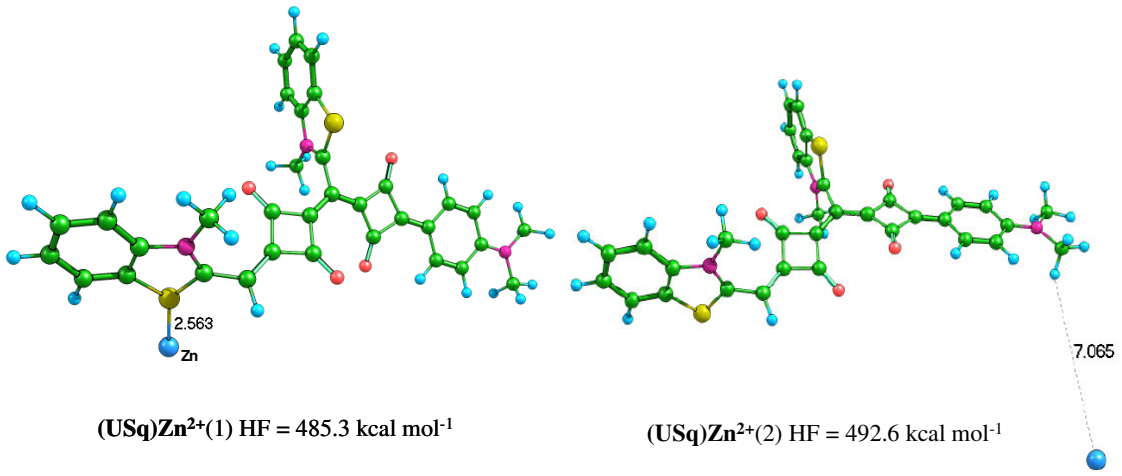

Figure 2.16. Optimized geometries at PM3 level for 1:1 complexes of Zn^{2+}.

In the case of 1:1 **(USq)Hg^{2+}** complex, the most stable geometry **(USq)Hg^{2+}**(1) does not show significant interaction between cation and Hg^{2+}. Although a structure containing **O1••Hg^{2+}••O2** interaction was located

(USq)Hg^{2+}(2), it was unstable by 12.0 kcal mol^{-1} compared to the unbound system **(USq)Hg^{2+}**(1) (Figure 2.17).

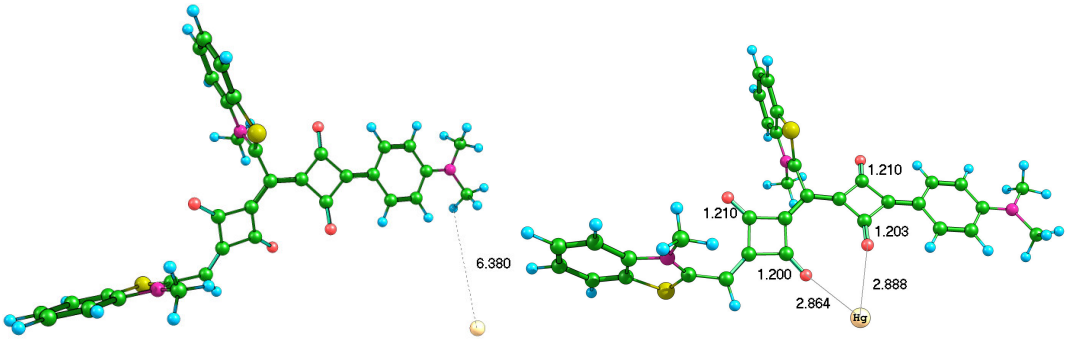

(USq)Hg^{2+}(1) HF = 476.2 kcal mol^{-1} **(USq)Hg^{2+}**(2) HF = 488.2 kcal mol^{-1}

Figure 2.17. Optimized geometries at PM3 level for 1:1 complexes of Hg^{2+}.

Unlike the 1:1 complexes of Zn^{2+} and Hg^{2+}, the structure of 1:1 complex of Pb^{2+} (**(USq)Pb^{2+}**) showed a strong **O1••Pb^{2+}••O2** interaction. Based on the HF value of the unbound system **(USq)Pb^{2+}**(2), a binding energy of 49.5 kcal mol^{-1} was assigned for **(USq)Pb^{2+}**(1) (Figure 2.18).

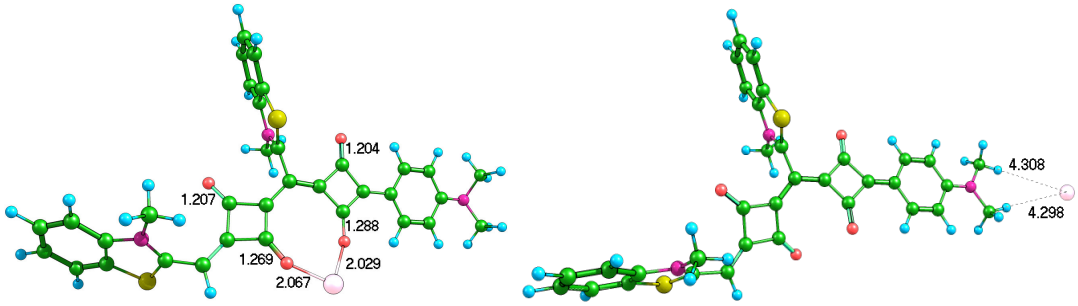

(USq)Pb^{2+}(1) HF = 461.4 kcal mol^{-1} **(USq)Pb^{2+}**(2) HF = 510.9 kcal mol^{-1}

Figure 2.18. Optimized geometries at PM3 level for 1:1 complexes of Pb^{2+}.

In the case of 2:1 complexes, several possible structures were optimized that contain the metal••oxygen and metal••sulfur interactions. In case of **(USq)$_2$-**

Zn^{2+} complex, the most stable one has a tetrahedral structure (**$(USq)_2Zn^{2+}$**(1), Figure 2.19).

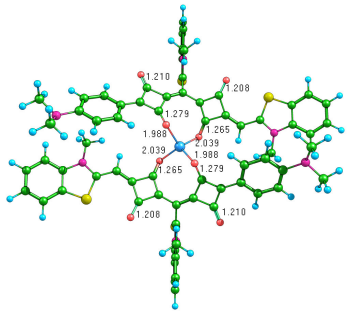

$(USq)_2Zn^{2+}$(1) HF = 621.9 kcal mol^{-1}

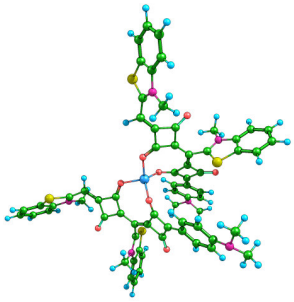

$(USq)_2Zn^{2+}$(2) HF = 628.5 kcal mol^{-1}

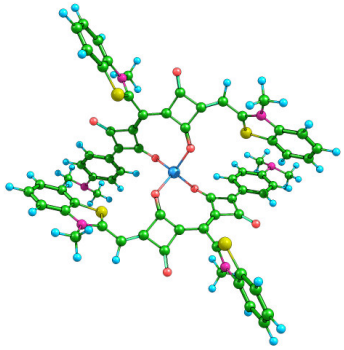

$(USq)_2Zn^{2+}$(3) HF = 630.8 kcal mol^{-1}

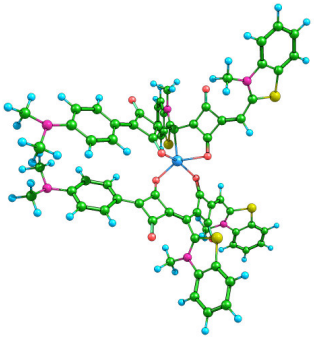

$(USq)_2Zn^{2+}$(4) HF = 658.4 kcal mol^{-1}

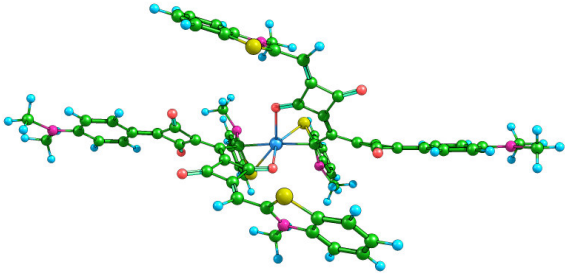

$(USq)_2Zn^{2+}$(5) HF = 658.5 kcal mol^{-1}

Figure 2.19. Optimized geometries at PM3 level for 2:1 complexes with Zn^{2+}.

The binding energy was calculated from the difference in value of heat of formation of the complex (2:1) with the sum of value of HF of 1:1 complex and unbound system (**USq,** HF = 154.4). **$(USq)Zn^{2+}$**(2) complex reported earlier was

taken as a 1:1 complex since it is an unbound system. This energy turned out to be 25.1 kcal mol^{-1}.

$$\mathbf{(USq)Zn^{2+}}(2) + \mathbf{USq} \rightarrow \mathbf{(USq)_2Zn^{2+}}(1) \qquad 2.1$$

USq also forms a tetrahedral 2:1 complex with Hg^{2+} (Figure 2.20). The most stable complex ($\mathbf{(USq)_2Hg^{2+}}(1)$) was found to be very similar to the most stable 2:1 Zn^{2+} complex. In contrast to the earlier case, a very high binding energy of 81.2 kcal mol^{-1} was calculated for the 2:1 complex from the following equation and from the known value of $\mathbf{(USq)Hg^{2+}}(1)$ for the 1:1 complex and **USq**.

$$\mathbf{(USq)Hg^{2+}}(1) + \mathbf{USq} \rightarrow \mathbf{(USq)_2Hg^{2+}}(1) \qquad 2.2$$

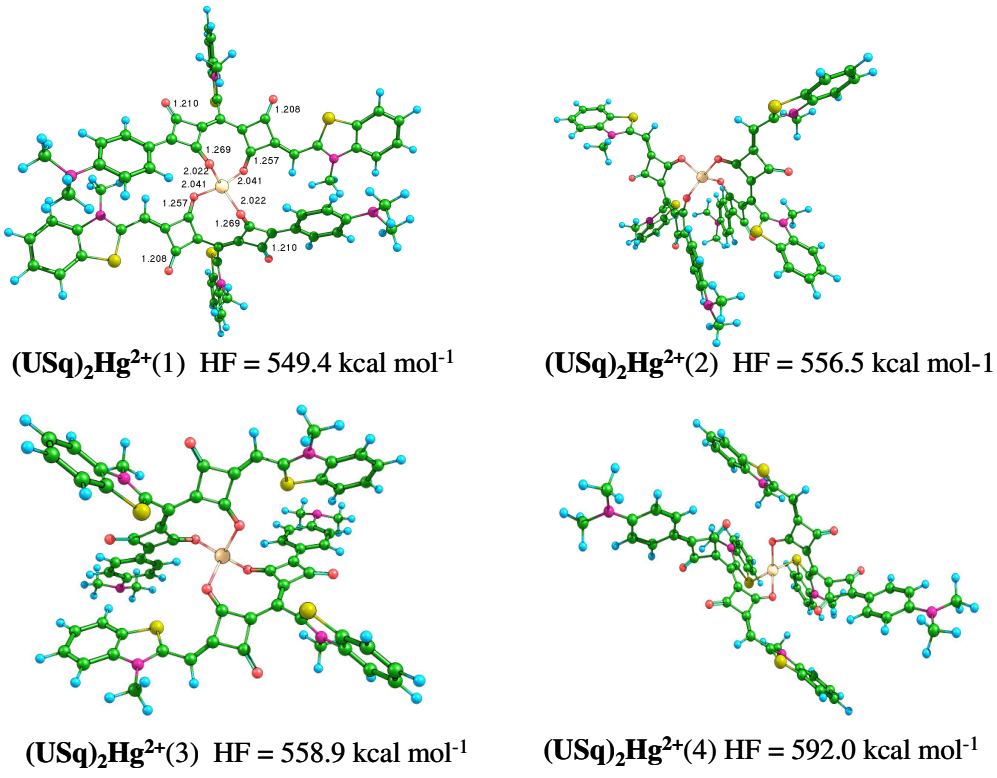

$\mathbf{(USq)_2Hg^{2+}}(1)$ HF = 549.4 kcal mol^{-1} $\mathbf{(USq)_2Hg^{2+}}(2)$ HF = 556.5 kcal mol-1

$\mathbf{(USq)_2Hg^{2+}}(3)$ HF = 558.9 kcal mol^{-1} $\mathbf{(USq)_2Hg^{2+}}(4)$ HF = 592.0 kcal mol^{-1}

Figure 2.20. Optimized geometries at PM3 level for 2:1 complexes with Hg^{2+}.

In case of the 2:1 complex of Pb^{2+}, square pyramidal structure **$(USq)_2Pb^{2+}$**(1) was the most stable one (Figure 2.21). For this complex, a binding energy of 108.3 kcal mol^{-1} was obtained from the following equation.

$(USq)Pb^{2+}$ (2) + **USq** → **$(USq)_2Pb^{2+}$** (1) 2.3

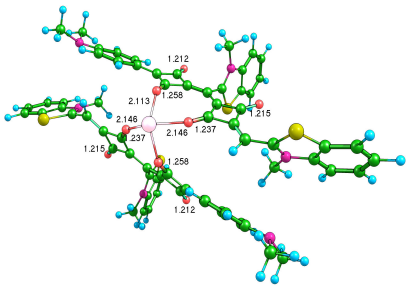

$(USq)_2Pb^{2+}$(1) HF = 557.0 kcal mol^{-1}

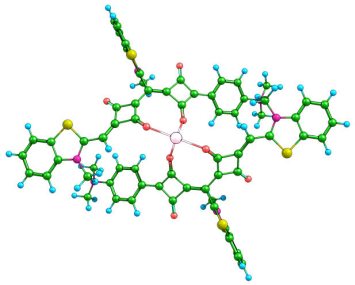

$(USq)_2Pb^{2+}$(2) HF = 563.1 kcal mol^{-1}

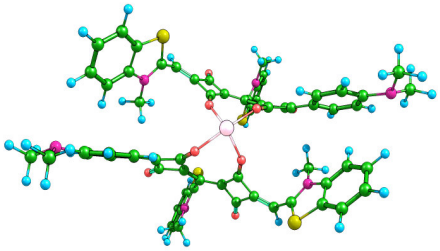

$(USq)_2Pb^{2+}$(3) HF = 565.2 kcal mol^{-1}

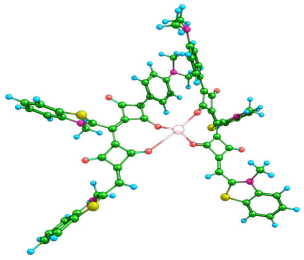

$(USq)_2Pb^{2+}$(4) HF = 566.3 kcal mol^{-1}

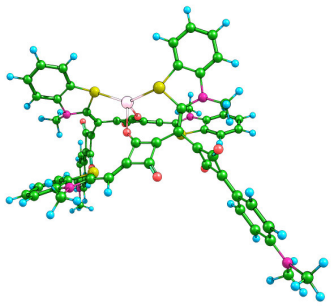

$(USq)_2Pb^{2+}$(5) HF = 607.8 kcal mol^{-1}

Figure 2.21. Optimized geometries at PM3 level for 2:1 complexes of Hg^{2+}.

In the case of Zn^{2+} and Hg^{2+}, the most stable 2:1 complexes **$(USq)_2Hg^{2+}$** and **$(USq)_2Zn^{2+}$** were tetrahedral in nature. On the other hand, in the case of Pb^{2+},

a square pyramidal structure in which Pb occupies the apical position was obtained as the most stable 2:1 complex. Binding energies with values of 25.1, 81.2 and 108.3 kcal mol^{-1} were obtained for the 2:1 complexes of **USq** with Zn^{2+}, Hg^{2+} and Pb^{2+} respectively. The high binding energy values obtained for Hg^{2+} and Pb^{2+} supports the high affinity of these cations towards the formation of 2:1 complexes, as compared to Zn^{2+}, which is in good agreement with the experimental results.

The tetrahedral structure of **$(USq)_2Hg^{2+}$** obtained at the PM3 level was further optimized at the BLYP/6-31G* level method (Figure 2.22). In this complex, both squaraine arms of each **USq** unit were coplanar. Further, the O••Hg bonding leads to the elongation of the corresponding CO bond lengths from 1.23 Å in free **USq** to 1.28 Å in the complex.

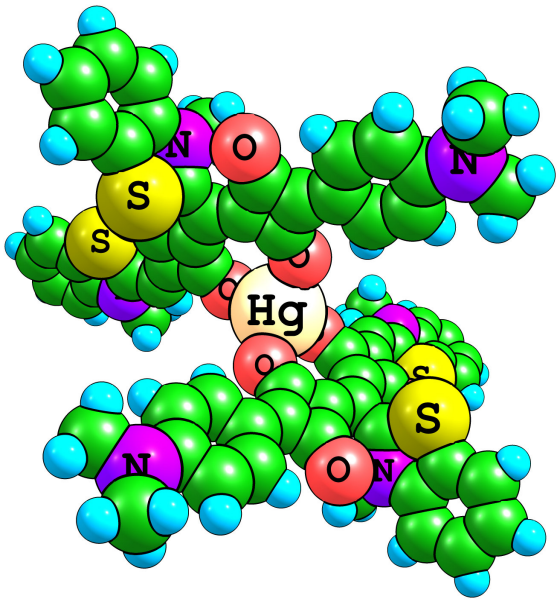

Figure 2.22. Molecular structures of **$(USq)_2Hg^{2+}$** complex obtained from BLYP/6-31G* level calculation.

2.4. Conclusions

In summary, we have designed a new squaraine-based chromoionophore **USqH$^+$**, capable of selectively detecting Hg^{2+} and Pb^{2+} in solution. Photophysical studies of this dye indicated that it could exist in two different conformational forms in equilibrium with each other. It is proposed that in aprotic solvents the dye exists in its planar form due to intramolecular hydrogen bonding between the oxygen and hydroxyl groups in the neighbouring cyclobutane rings of the molecule. As a result of planar configuration of this molecule in such solvents, the conjugation extends over the entire molecule, resulting in highly red shifted absorption and emission bands. In protic solvents, such hydrogen bonding interactions can be disrupted resulting in an out of plane twisting of one of the arms of the molecule. As a result, the conjugation to this arm could become less favoured and this could result in a blue shift in the absorption and emission bands of the molecule. Solutions of this dye in dichloromethane showed a significant shift in the absorption spectrum on addition of Hg^{2+} and Pb^{2+}, whereas, addition of most other metal ions had negligible effect. This made it possible to visually detect Hg^{2+} and Pb^{2+} in the presence of micromolar amounts of alkali, alkaline and transition metal ions such as Li^+, Na^+, Mg^{2+}, Ca^{2+}, Ba^{2+}, Zn^{2+} and Cu^{2+}. Theoretical calculations are in support of the oxygen atom in the central cyclobutane ring being the main binding site and high affinity for the formation of 2:1 complexes of the dye with Hg^{2+} and Pb^{2+}. In view of the wide range of 1,3-

disubstituted symmetric squaraine dyes and semisquaraine esters reported in the literature,[45,46] it should be possible to tune the cation sensing ability of the unsymmetrical cationic squaraine dyes by systematically varying the reaction components in the synthetic strategy shown in Scheme 2.2.

2.5. Experimental Section

2.5.1. Materials

Sq1 and **Sq2** were prepared according to the reported procedures.[45] Squaric acid and 2-methylbenzothiazole and all perchlorate salt of metal ions used for the metal binding studies were purchased from Sigma-Aldrich. Solvents used were of highest available purity obtained from local companies.

2.5.2. General Techniques

Melting points were determined on a Mel-Temp II melting point apparatus. ^{1}H NMR spectra were recorded on Bruker 300 MHz NMR spectrometer. IR spectra were recorded on a Shimadzu IRPrestige 21 FT-IR Spectrophotometer. Mass spectra were measured on a JEOL JMS 600H mass spectrophotometer. Elemental analyses were carried out on a Perkin-Elmer series II 2400 CHN Analyzer. Absorption spectra were recorded on a Shimadzu UV-3101 PC UV-vis-NIR Scanning Spectrophotometer. Emission spectra were recorded on a SPEX-Fluorolog, F112X spectrofluorimeter. Modeling of the complexes at the DFT and semiempirical PM3 levels were optimized by using Gaussian software.

2.5.3. General Procedure for the Metal Ion Binding Studies

Stock dye solutions were made by dissolving the dye (**$USqH^+$**) in spectroscopic grade dichloromethane. Metal perchlorate solutions were prepared in spectroscopic grade acetonitrile. Absorption measurements were carried out in a 4 mL quartz cuvette. Metal ion titrations were carried out by adding micro litre quantities of the metal solution by using micro litre syringe. The measurements were carried out immediately after the addition of metal ions.

2.5.4. General Procedure for Obtaining the Job's Plot

Aliquots of equimolar solutions of the dye (P) and metal perchlorate (X) were mixed in such a way that the total concentration of P+X remained constant. The absorbance of each of the solution was measured at a suitable wavelength, and a graph of the corrected absorbance was plotted against the mole fraction of X or P. Maximum absorbance is obtained at the composition corresponding to the stoichiometry of the predominant complex.

2.5.5. Synthesis of Bis(3-methylbenzothiazol-2-ylidene)squaraine, Sq1

The squaraine dye **Sq1** was prepared by refluxing a mixture of 3-methyl-2-methylbenzothiazolium iodide (1.6 g, 5.7 mmol) and squaric acid (0.32 g, 2.8 mmol) in a mixture (2:1) of benzene and n-butanol (30 mL) in presence of quinoline (2.5 mL, 5.7 mmol) under azeotropic distillation of water. After cooling,

the reaction mixture was concentrated to approximately 2 mL under reduced pressure. The precipitate formed on adding hexane was filtered. The crude product was purified by column chromatography using silica gel (100-200 mesh) and a mixture (1:9) of methanol and chloroform as eluent to yield 1.75 g (80%) of the pure product, mp 241-242 °C (decomp.).

^{1}H NMR (300 MHz, $CDCl_3$) δ 3.7-4.2 (m, 6H, NCH_3), 6.2 (s, 2H, vinylic) 7.2-8.3 (m, 8H, aromatic).

2.5.6. Synthesis of 1-(p-N,N-Dioctylaniline)-2-hydroxycyclobutene-3,4-dione, Sq2

1,2-Dichlorocyclobutene-3,4-dione (1.4 g, 9.7 mmol), and *N,N*-dioctylaniline (3.0 g, 9.7 mmol) were dissolved in dry benzene (30 mL) and refluxed for 6 h. After cooling, the reaction mixture was poured into ice water (200 mL) and the two layers formed were separated. The organic layer was washed with water, and the crude product obtained by evaporation of the solvent under reduced pressure was dissolved in a mixture of acetic acid (25 mL), water (25 mL) and 2N HCl (10 mL) and the resulting mixture was refluxed for 2 h. After cooling this solution to room temperature, the crystallized product was isolated by filtration, washed with ether, and dried to yield 2 g (50%) of the pure product.

^{1}H NMR (300 MHz, $CDCl_3$) δ 0.80-0.93 (m, 6H, CH_3), 0.90-1.16 (m, 24H, CH_2), 3.30-3.50 (m, 4H, NCH_2), 7.60-8.40 (m, 4H, aromatic).

2.5.7. Synthesis of Cationic Squaraine Dye ($USqH^+$)

3-[4-(*N,N*-Dioctylamino)phenyl]-4-hydroxycyclobutene-1,2-dione, (0.22 g, 0.52 mmol) and bis(3-methylbenzothiazol-2-ylidene)squaraine (0.20 g, 0.4 mmol) were added to a mixture (2:1) of toluene and n-butanol (30 mL) and this was refluxed for 3 h, followed by azeotropic removal of water. To the cooled reaction mixture, sodium tetraphenyl borate (0.14 g, 0.40 mmol) was added and the solution was stirred at 60 ºC for 3 h. The mixture was concentrated to 1 mL by removing the solvent under reduced pressure. To this concentrated solution, excess hexane (20 mL) was added to precipitate out the product. The crude product was filtered and purified by column chromatography using neutral alumina as the stationary phase and a mixture (1:9) of methanol and chloroform as eluent to give 50 mg (8.5%) of the pure product, mp 175 ºC (decomp.).

IR ν_{max} (neat): 3415, 1590, 1263, 781 cm^{-1}; ^1H NMR (300 MHz, $CDCl_3$) δ 0.88-1.1 (m, 6H, CH_3), 0.9-1.3 (m, 24H, CH_2), 3.1-3.9 (m, 10H, NCH_2, NCH_3), 6.1-8.1 (m, 33H, aromatic); HRMS (EI) calcd for $C_{48}H_{54}N_3O_4S_2$, 800.3556. Found: 800.3582; CHN Anal. calcd for $C_{48}H_{54}N_3O_4S_2$: C, 71.97; H, 6.79; N, 5.25; Found: C, 71.59; H, 6.49; N, 5.42.

2.6. References

1. Callan, J. F.; de Silva A. P.; Magri, D. C. *Tetrahedron* **2005**, *61*, 8551-8588.

2. de Silva, A. P.; de Silva, S. A. *J. Chem. Soc., Chem. Commun*. **1986**, 1709-1710.

3. Bryan, A. J.; de Silva, A. P.; de Silva, S. A.; Rupasinghe, R. A. D. D.; Sandanayake, K. R. A. S. *Biosensors* **1989**, *4*, 169-179.

4. Bissel, R. A.; de Silva, A. P.; Gunaratne, H. Q. N.; Lynch, P. L. M.; Maguire, G. E. M.; Sandanayake, K. R. A. S. *Chem. Soc. Rev.* **1992**, *21*, 187-195.

5. de Silva, A. P.; Fox, D. B.; Huxley, A. J. M.; Moody, T. S. *Coord. Chem. Rev.* **2000**, *205*, 41-57.

6. Czarnik, A. W. *Fluorescence Chemosensors for Ions and Molecular Recognition*; ACS Books: Washington, DC, 1993.

7. Kijima, H.; Takeuchi, M.; Robertson, A.; Shinkai, S.; Cooper, C.; James, T. D. *Chem. Commun.* **1999**, 2011-2012.

8. Lehn, J. M. *Supramolecular Chemistry Concepts and Perspectives*; Wiley-VCH: Weinheim, 1995.

9. Gokel, G. W. *Molecular Recognition for Cationic Guests, In Comprehensive Supramolecular Chemistry*; Gokel, G. W. Ed. Elsevier Science: Oxford, 1996, 2.

10. J. W. Steed and J. L. Atwood, *Supramolecular Chemistry*; John Wiley & Sons Ltd.: England, 2000.

11. Arunkumar, E.; Ajayaghosh, A.; Daub, J. *J. Am. Chem. Soc.* **2005**, *127*, 3156-3164.

12. Ros-Lis, J. V.; Martínez Máñez, R.; Rurack, K.; Sancenón, F.; Soto, J.; Spieles, M. *Inorg. Chem.* **2004**, *43*, 5183-5185.

13. For informative websites dealing with the problem of and other heavy metals in the environment see: (a) http;//www.epa.gov/opptintr/lead/; (b) http://www.orcbs.msu.edu/AWARE/pamphlets/hazwaste/mercuryfacts.html

14. Kim, I. B.; Erdogan, B.; Wilson, J. N.; Bunz, U. H. F. *Chem. Eur. J.* **2004**, *10*, 6247-6254.

15. Metivier, R.; Leray. I.; Valeur, B. *Chem. Eur. J.* **2004**, *10*, 4480-4490.

16. Chen, Q.-Y.; Chen, C.-F. *Tetrahedron Lett.* **2005**, *46*, 165-168.

17. Descalzo, A. B.; Martínez Máñez, R.; Radegli, R.; Rurack, K. *J. Am. Chem. Soc.* **2003**, *125*, 3418-3419.

18. Nolan, E.M.; Lippard, S. J. *J. Am. Chem. Soc.* **2003**, *125*, 14270-14271.

19. Al Shihadeh, Y.; Benito, A.; Lloris, J. M.; Martínez Máñez, R.; Pardo, T.; Soto, J.; Marcos, M. D. *J. Chem. Soc., Dalton Trans.* **2000**, 1199-1205.

20. Jiménez, D.; Martínez Máñez, R.; Sancenón, F.; Soto, J. *Tetrahedron Lett.* **2004**, *45*, 1257-1259.

21. Guo, X.; Qian, X.; Jia, L. *J. Am. Chem. Soc.* **2004**, *126*, 2272-2273.

22. Wu, D.; Huang, W.; Duan, C.; Lin, Z.; Meng, Q. *Inorg. Chem.* **2007**, *46*, 1538-1540.

23. Kim, J. S.; Choi, M. G.; Song, K. C.; No, K. T.; Ahn, S.; Chang, S. K. *Org. Lett.* **2007**, *9*, 1129-1132.

24. Moon, S. Y.; Cha, N. R.; Kim, Y. H.; Chang, S. K. *J. Org. Chem.* **2004**, *69*, 181-183.

25. Thomas, K. G.; Thomas, K. J.; Das, S.; George, M. V. *Chem. Commun.* **1997**, 597-598.

26. Das, S.; Thomas, K. G.; Kamat, P. V.; George, M. V. *J. Phys. Chem.* **1994**, *98*, 9291-9296.

27. Das, S.; Thomas, K. G.; Bedja, I.; Kamat, P. V.; George, M. V. *Anal. Proc.* **1995**, *32*, 213-215.

28. Nakazumi, H.; Natsukawa, K.; Nakai, K.; Isagawa, K. *Angew. Chem., Int. Ed. Engl.* **1994**, *33*, 1001-1003.

29. Das, S.; Thomas, K. G.; Ramanathan, R.; George, M. V.; Kamat, P. V. *J. Phys. Chem.* **1993**, *97*, 13625-13628.

30. Becke, A. D. *J. Chem. Phys.* **1993**, *98*, 5648-5652.

31. Lee, C.; Yang, W.; Parr, R. G. *Phys. Rev. B: Condens. Matter Mater. Phys.* **1988**, *37*, 785-789.

32. Gaussian 03, Revision C.02, Frisch, M. J.; Trucks, G. W.; Schlegel, H. B.; Scuseria, G. E.; Robb, M. A.; Cheeseman, J. R.; Montgomery, Jr., J. A.; Vreven, T.; Kudin, K. N.; Burant, J. C.; Millam, J. M.; Iyengar, S. S.; Tomasi, J.; Barone, V.; Mennucci, B.; Cossi, M.; Scalmani, G.; Rega, N.;

Petersson, G. A.; Nakatsuji, H.; Hada, M.; Ehara, M.; Toyota, K.; Fukuda, R.; Hasegawa, J.; Ishida, M.; Nakajima, T.; Honda, Y.; Kitao, O.; Nakai, H.; Klene, M.; Li, X.; Knox, J. E.; Hratchian, H. P.; Cross, J. B.; Adamo, C.; Jaramillo, J.; Gomperts, R.; Stratmann, R. E.; Yazyev, O.; Austin, A. J.; Cammi, R.; Pomelli, C.; Ochterski, J. W.; Ayala, P. Y.; Morokuma, K.; Voth, G. A.; Salvador, P.; Dannenberg, J. J.; Zakrzewski, V. G.; Dapprich, S.; Daniels, A. D.; Strain, M. C.; Farkas, O.; Malick, D. K.; Rabuck, A. D.; Raghavachari, K.; Foresman, J. B.; Ortiz, J. V.; Cui, Q.; Baboul, A. G.; Clifford, S.; Cioslowski, J.; Stefanov, B. B.; Liu, G.; Liashenko, A.; Piskorz, P.; Komaromi, I.; Martin, R. L.; Fox, D. J.; Keith, T.; Al-Laham, M. A.; Peng, C. Y.; Nanayakkara, A.; Challacombe, M.; Gill, P. M. W.; Johnson, B.; Chen, W.; Wong, M. W.; Gonzalez, C.; Pople, J. A. Gaussian, Inc.,Wallingford CT, 2004.

33. For graphics, ChemCraft, Ver. 1.4 (build 234) by Zhurko, G. A.; Zhurko, D. A. is used (www.chemcraftprog.com).

34. Specht, A.; Bernard, P.; Goeldner, M.; Peng, L. *Angew. Chem., Int. Ed. Engl.* **2002**, *41*, 4706-4708.

35. Huang, F.; Gibson, H. W.; Bryant, W. S.; Nagvekar, D. S.; Fronczek, F. R. *J. Am. Chem. Soc.* **2003**, *125*, 9367-9371.

36. Huang, F.; Fronczek, F. R.; Gibson, H. W. *Chem. Commun.* **2003**, 1480-1481.

37. Hariharan, P. C.; Pople, J. A. *Mol. Phys.* **1974**, *27*, 209.

38. Wadt, W. R.; Hay, P. J. *J. Chem. Phys.* **1985**, *82*, 284-298.

39. Hay, P. J.; Wadt, W. R. *J. Chem. Phys.* **1985**, *82*, 299-310.

40. Politzer, P. *In Chemical Applications of Atomic and Molecular Electrostatic Potentials*; Politzer, P., Truhlar, D. G., Eds. Plenum: New York, 1981.

41. Gadre, S. R.; Shirsat, R. N. *Electrostatics of Atoms and Molecules*; Universities Press (India): Hyderabad, 2000.

42. Suresh, C. H.; Gadre, S. R. *J. Am. Chem. Soc.* **1998**, *120*, 7049-7055.

43. Suresh, C. H.; Koga, N.; Gadre, S. R. *Organometallics* **2000**, *19*, 3008-3015.

44. A typical single bond length for C-N bond is around 1.45 Å. For X-ray geometries related to **USq** system, see (b) Ashwell, G. J.; Bahra, G. S.; Brown, C. R.; Hamilton, D. G.; Kennard, C. H. L.; Lynch, D. E. *J. Mater. Chem.* **1996**, *6*, 23-26.

45. Sprenger, H.-E.; Ziegebien, W. *Angew Chem., Int. Ed. Engl.* **1967**, *6*, 553-554.

46. Keil, D.; Hartmann, H. *Dyes and Pigments*, **2001**, *49*, 161-179.

CHAPTER 3

Design and Synthesis of Near Infrared Squaraine Based Fluorescent Probes

3.1. Abstract

A novel class of dialkylanthracene containing squaraine dyes possessing intense absorption and emission in the near infrared (NIR) region has been synthesized. Structural and electronic features investigated using Density Functional Theory (DFT) methods suggest that the significant bathochromic shifts observed on replacing dialkylaniline by dialkylanthracene in this class of molecules can be attributed to a reduction in the HOMO–LUMO gap mainly due to enhanced hydrogen bonding between the carbonyl group of the cyclobutane ring and the neighbouring aromatic hydrogen in the dyes containing the anthracene moiety. The absence of fluorescence in aqueous media and high fluorescence when encapsulated into hydrophobic domains such as cetyltrimethylammonium bromide (CTAB), sodium dodecylsulfate (SDS) and polyethylene-t-octylphenol (Triton X-100) make this class of dyes particularly useful as probes for mapping such domains in biological systems. Since water compatibility is an important criterion for use of dyes in biological systems, one of the dyes was designed such that it would have improved water solubility.

3.2. Introduction

The development of new dyes with strong emission in the NIR region (700-900 nm) plays a crucial role in advancing techniques for noninvasive monitoring of diseased tissues.[1-3] Cells excited at wavelength below 500 nm produce considerable autofluorescence mainly from flavins, flavoproteins and NADH, which can very often swamp the probe fluorescence. Hemoglobin and melanin, the primary endogenous chromophores of the skin absorb over a broad range, from 300-500 nm, but their absorption decreases steadily on progressing from the visible to the NIR region as shown in Figure 3.1.

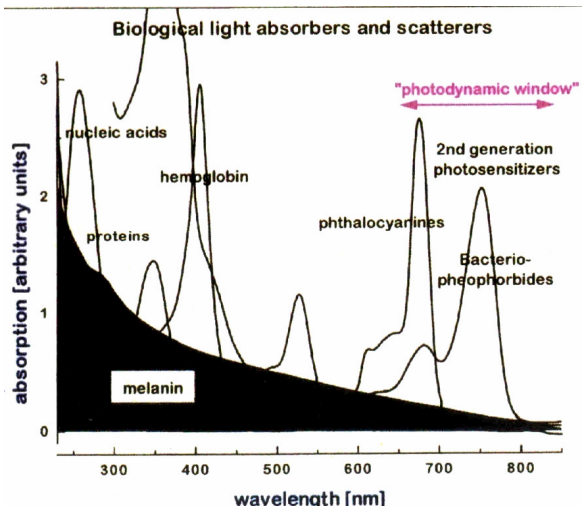

Figure 3.1. Absorbance of major biological molecules.

Since NIR light can penetrate several centimeters into the tissues, use of probes sensitive to this region of light can be useful for imaging deeper parts of the tissues. Figure 3.2 demonstrates the penetration power of NIR light to the

tissues. The combined aspects of greater tissue penetration and reduced photochemical damage of cells make fluorescence microscopy in the NIR region especially attractive for biomedical applications.[4,5] The limited number of photostable fluorochromes with strong emission in the NIR region however forms a major bottleneck in the use of fluorescence microscopy for such applications.

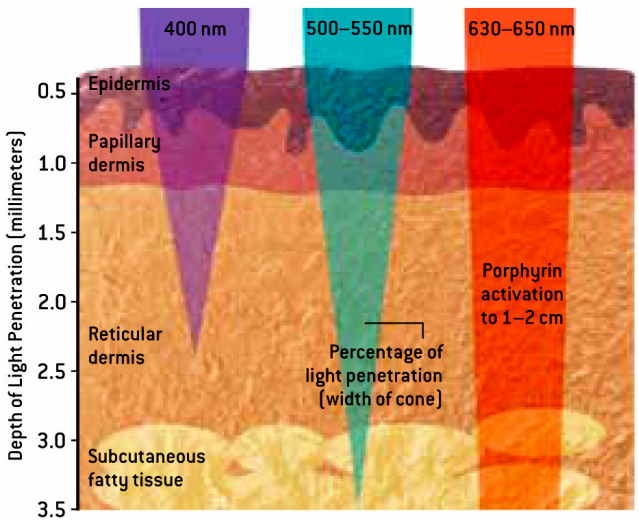

Figure 3.2. Penetration power of light into tissues.

Cyanine fluorochromes have attracted considerable attention in cellular imaging, due to the fact that the NIR absorption of these dyes could be tuned by varying the length of the polymethine chain connecting the terminal heterocyclic rings. Other dyes such as oxazines, rhodamines and pthalocyanines have also found application in cellular imaging. Anna Moore and coworkers[6] reported the synthesis and application of novel water soluble cyanine dyes (**1**–**3**, Chart 3.1) for the optical imaging of cancerous cells. The presence of a single carboxylic group in **2** also helped in the selective conjugation of this molecule to biomolecules.

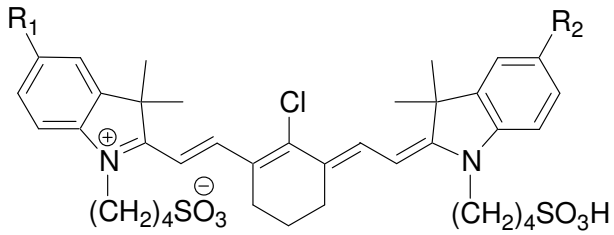

1, $R_1 = R_2 = COOH$, **2**, $R_1 = SO_3H$, $R_2 = COOH$
3, $R_1 = SO_3H$, $R_2 = CONH(CH_2)_6$AREPPTRTFAYWG

Chart 3.1

The molar extinction coefficient and quantum yield of **2** in water were 200000 $M^{-1}cm^{-1}$ and 0.18, respectively, compared to 180000 $M^{-1}cm^{-1}$ and 0.08 for **1**. The broad absorption spectrum of **2** enabled excitation of the molecule several nanometers below the absorption maximum (λ_{max} = 790 nm) using a commercially available 720 nm excitation filter and collection of emission 50 nm away from the excitation wavelength using a narrow-band emission filter at 790 nm. This strategy could help diminish the high background that normally results from the cross-talk when the excitation and emission filter wavelengths are too close. Conjugation of **2** to an EPPT peptide, which showed specific accumulation in tumors expressing the uMUC-1 antigen, gave **3**, which could be used for *in vivo* optical imaging studies. The authors anticipate potential and broad applications of this dye in developing molecular based beacons for cancer detection.

Oxazine and rhodamine based fluorophores with absorption and emission in the visible region are also used for intracellular imaging applications. These are structurally similar classes of compounds containing two nitrogen atoms forming

the push-pull conjugated system, with oxazine having an additional oxygen atom to bridge the conjugation. The main advantage of these dyes is that they are structurally more compact than cyanine dyes. Burgess *et al.* reported the synthesis of a water soluble rhodamine based dye **4** (Chart 3.2) for intracellular imaging applications.[7] The presence of four carboxylic acid functionalities in **4** facilitated water solubility and conjugation to proteins. In addition, the aryl bromide group in the molecule could be used to functionalize the molecule for special applications.

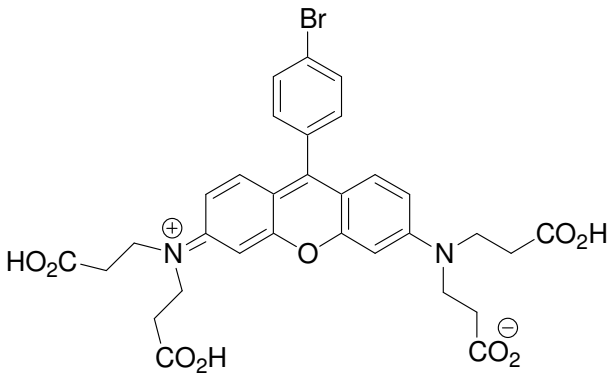

4

Chart 3.2

Following activation of **4** with *N*-hydroxysuccinimide, it was coupled to acyl-CoA Binding Protein (ACBP). ACBP-labeled **4** could be successfully delivered into COS–7 cells. Various amounts of the ACBP-labeled dye varying from 0.5 to 2 μg, were preincubated with Chariot (from Active Motif, Carlsbad, CA) in protein-to-peptide ratio of 1:20 (w/w) for 30 min at room temperature and then was added to COS-7 cells in the presence of serum-free DMEM. After 30 min incubation, the protein-Chariot mixes were washed off and the cells with PBS

were incubated with 10% FBS/DMEM at 37 °C and 5% CO_2 for 2 h before conducting confocal microscopy. The cell nuclei were counterstained by adding 1 μg/mL of Hoechst 33342 nuclear marker solution (from Molecular Probes, Eugene, OR) about 30 min before the confocal microscopy observation.

Figure 3.3A shows the fluorescence images of **4**–ACBP in cells (detected in the red channel, with an emission filter at 598 nm and excitation at 568 nm). The fluorescence signals from **4**–ACBP (in red) and Hoechst stained nuclei (in green) clearly indicated better distribution of ACBP molecules inside the cells relative to the nuclei (Figure 3.3B). Most of the fluorescently labeled ACBP molecules appeared in the cytoplasm, around the nuclei, but a fraction of the **4**–ACBP molecules were also observed inside the nuclei. The yellow pixels in Figure 3.3C indicates the colocalization of **4**–ACBP with the nuclear marker.

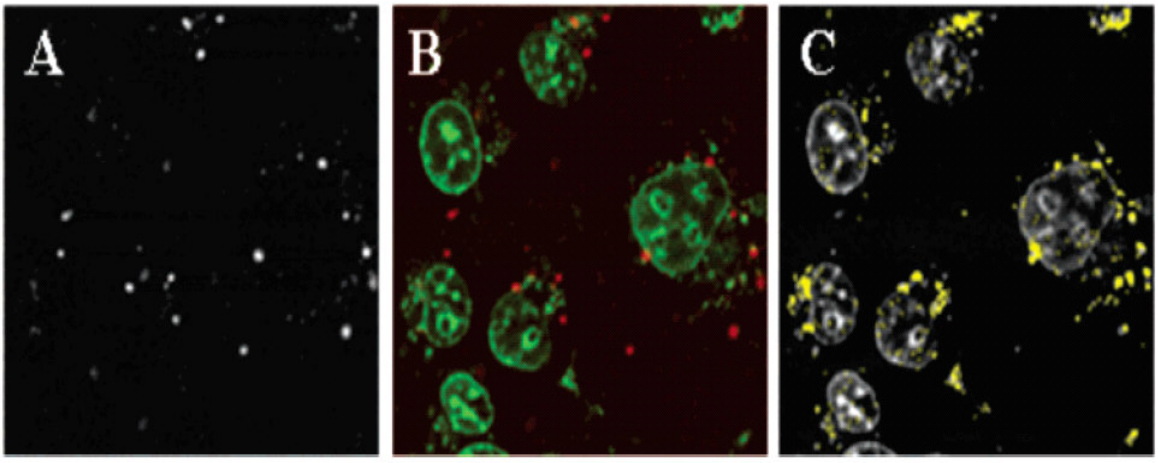

Figure 3.3. Intracellular imaging of **4**–ACBP labeled COS-7 cells by confocal microscopy. A) **4**–ACBP with excitation at 568 nm, and emission filter HQ 598/40; B) overlay of **4**–ACBP image (red) with nuclei image (green, given by the nuclear marker Hoechst 33342 that emits at 530 nm with excitation at 408 nm); C) colocalized pixels (yellow) from **4**–ACBP and the nuclear marker (From Ref 7).

A major limitation of using cyanine and related linear dye systems for the design of NIR dyes with absorption far into the NIR region is that the system undergoes symmetry collapse and bond localization at long chain lengths. As a result, the absorption of the dyes cannot be shifted into the NIR region beyond a certain point. In addition, the increased conjugation between terminal groups is also known to result in the reduction in the photo and thermal stability of the dyes, which is a major limitation in the use of cyanine dyes. In the case of the rhodamine based systems discussed above, the dyes suffer the problem of short wavelength excitation. For intracellular applications, NIR absorbing water soluble dyes would be highly desirable.

It is evident from the literature scenario presented above that there is a requirement for finding alternate strategies for developing NIR dyes. Squaraine is a suitable candidate for this kind of studies due to its intense absorption and emission properties.[8-9] Their unique photochemical and photophysical properties[10-13] make these dyes useful in a variety of applications such as in copiers,[14,15] solar cells,[16,17] optical discs[18,19] and sensors.[20-24] Among the various classes of squaraine dyes, the one possessing tertiary arylamine end groups are known to be more stable and possess good solubility compared to those containing heterocyclic end groups.[9,25,26] However, the maximum red shifted absorbance for this class of dyes is around 700 nm.[9,27] Recently, Ramaiah and coworkers[28] reported the synthesis of amphiphilic squaraine dyes where absorption is in the range of 630–650 nm (**5**–

8, Chart 3.3). The fluorescence spectra of these dyes showed emission maxima ranging from 660 to 675 nm, depending on the nature of substituents. The fluorescence quantum yields were in the 0.15–0.21 range in ethanol, and 0.01–0.02 in aqueous media.

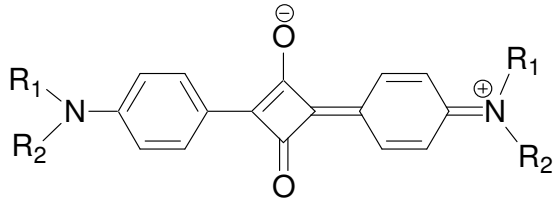

5, $R_1 = R_2 = -CH_2-CH_2-OH$, **6**, $R_1 = -CH_3$, $R_2 = -(CH_2)_3CO_2H$
7, $R_1 = -CH_3$, $R_2 = -(CH_2-CH_2-O)_4 - CH_3$, **8**, $R_1 = R_2 = -(CH_2-CH_2-O)_4 - CH_3$

Chart 3.3

Das and coworkers had earlier reported the synthesis of a NIR dye (**Sq1**, Chart 3.4) absorbing around 800 nm region.[29] In the work described in this Chapter, we have shown that the absorption spectra of this class of dyes can be fine tuned by synthesizing unsymmetrical squaraine dyes (**Sq2** and **Sq3**, Chart 3.4). A major drawback of the earlier dyes was that they were not water compatible. Since water compatibility is an important criterion for use of dyes in biological systems, one of the dyes was designed such that it would have improved water solubility.

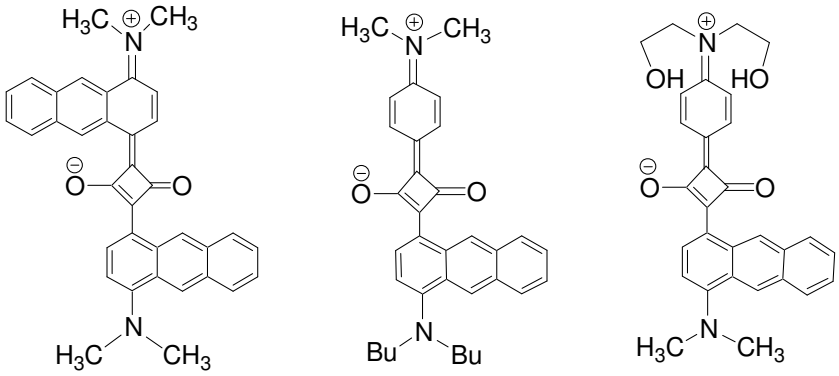

Sq1 **Sq2** **Sq3**

Chart 3.4

3.3. Results and Discussion

3.3.1. Absorption and Emission Properties of Sq1–3

Figure 3.4 shows the absorption and emission spectra of **Sq1** and **Sq2** along with that of bis[4-(*N*,*N*-dibutylamino)phenyl]squaraine (**DBAS**).[30]

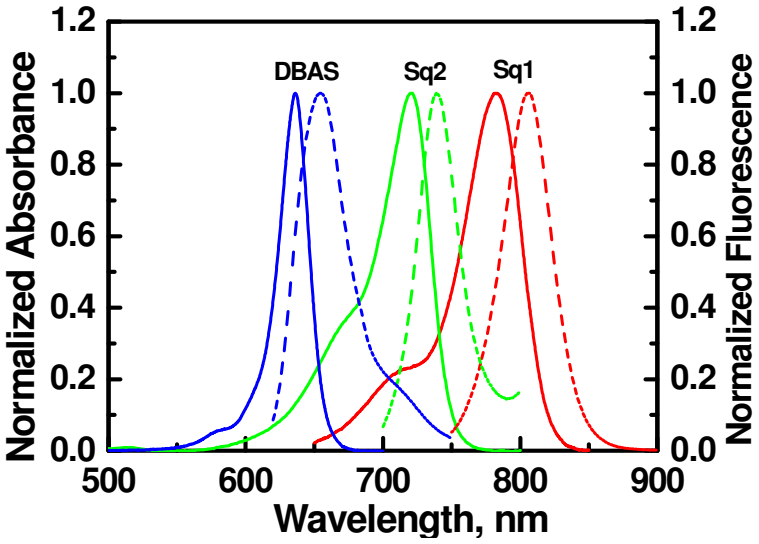

Figure 3.4. Normalized absorption (solid line) and emission spectra (dashed line) of **DBAS**, **Sq1** and **Sq2** in toluene.

The photophysical properties of these dyes in toluene and ethanol are summarized in Table 3.1. Replacement of each dialkylaminophenyl group with a dialkylaminoanthracene moiety resulted in a significant red shift in the absorption and emission bands of the dyes. Thus a 140 nm shift was observed between the absorption spectra of **DBAS** and **Sq1**, while it was nearly 60 nm between **Sq2** and **Sq1**. These dyes are characterized by fairly high quantum yields of fluorescence, better than or comparable to some of the best dyes reported with absorption and emission in the 700–800 nm region.[31-34]

Thus, the use of dialkylaminoanthracene instead of dialkylaniline provides a facile strategy for obtaining squaraine dyes with increasingly red shifted absorption and emission, and this strategy has been used to develop a series of new NIR dyes which are described in Chapter 4.

Table 3.1. Photophysical properties of **Sq1–3** in Toluene and Ethanol.

	Toluene			Ethanol		
	λ_{max} (nm)		Φ_f[b]	λ_{max} (nm)		Φ_f[b]
	Abs	Em		Abs	Em	
Sq1	782	805	0.24	789	811	0.03
Sq2	720	739	0.30	726	749	0.05
Sq3	a	a	a	720	743	0.06

a) **Sq3** is insoluble in Toluene, b) Quantum yield was determined by using **DDI** (1,1'-Diethyl-2,2'-dicarbocyanine iodide) Φ_{EtOH} = 0.0028[35] (for **Sq2** and **Sq3**) and **IR-125** Φ_{dmso} = 0.13[34] (for **Sq1**) as standard. error ca. ± 5 %.

3.3.2. Photophysical Properties of Sq3 in Aqueous Media

Water compatibility is an important criterion for biological applications of sensing dyes. The presence of hydroxyethyl substituents in **Sq3** made it much more soluble in aqueous media compared to **Sq1** and **Sq2**. In fact, the latter two dyes were practically insoluble in aqueous media. The absorption and emission properties of **Sq3** were studied in various ethanol/water solvent mixtures. Increase in water content of the solvent mixture resulted in a blue shift, broadening and reduction in intensity of its absorption band. This was accompanied by a significant decrease in its fluorescence intensity (Figure 3.5).

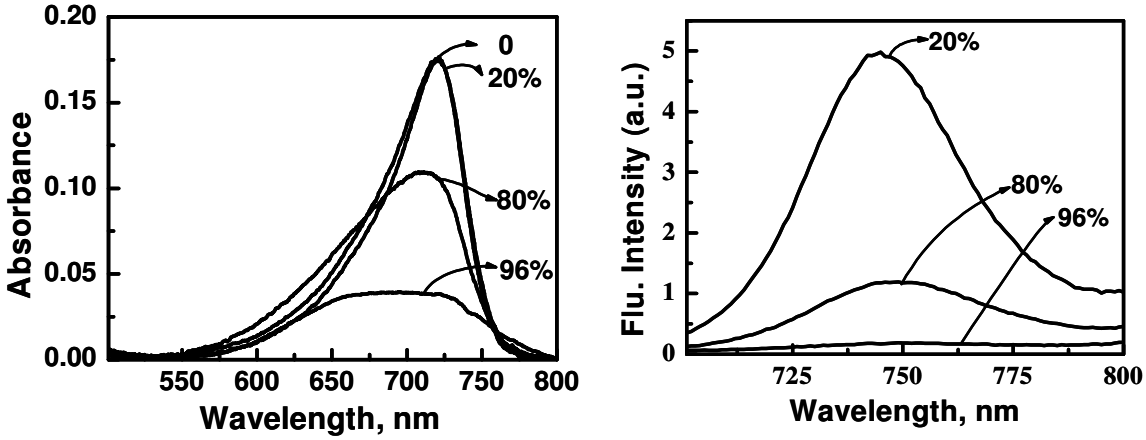

Figure 3.5. Absorption and emission spectrum of **Sq3** in water/ethanol binary mixtures. The % of water in the solvent mixture is shown in the figure.

These effects could be attributed to the formation of H-aggregates[36-38] as well as hydrogen bonding interactions of the dye with water.[39] Table 3.2 summarizes photophysical properties of **Sq3** in various water/ethanol binary mixtures. The photostability of the dyes under these conditions was ascertained by

the lack of change in their absorption and emission spectra in ethanol/water on extended irradiation (>4h) with 690 nm light from the 450 W excitation lamp of the SPEX Fluorolog.

Table 3.2. Absorption, emission maximum, fluorescence life time and extinction coefficients of **Sq3** in various water/ethanol binary mixtures.

% Water/Ethanol	λ_{max}, Abs	λ_{max}, Em	Φ_f	$\varepsilon \times 10^4$ $mol^{-1}cm^{-1}$
20	720	754	0.06	1.5
40	721	747	0.05	1.5
60	720	749	0.03	1.4
80	711	749	0.013	1.2
96	704	735	0.004	0.3

3.3.3. Effect of Surfactants on Absorption and Fluorescence Properties of Sq3

In biological systems, the dyes can encounter hydrophobic environments marked by relatively high microviscosity, low dielectric constant, low polarity and poor hydrogen bond donor capabilities, compared with that of free solutions. Thus, investigation of the photophysical properties of dyes in micellar media, which can mimic some of these conditions, can provide useful information on the behaviour of the dyes in such environments. In view of this, the absorption and fluorescence properties of **Sq3** were examined in the presence of CTAB, SDS and Triton X-100. Figure 3.6 shows the effect of SDS on the absorption spectrum of **Sq3** in 96% (v/v) water/ethanol mixtures.

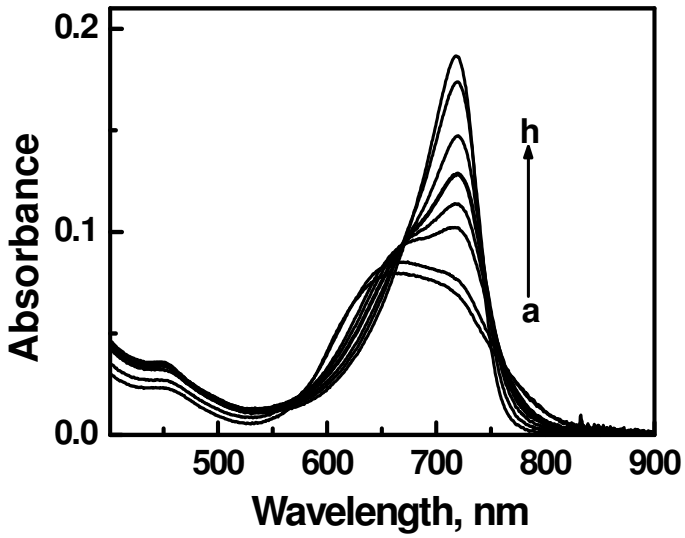

Figure 3.6. Effect of SDS on absorption properties of **Sq3** [2.43 × 10^{-5} M] in 96% (v/v) water/ethanol mixture [SDS] a) 0, b) 0.28, c) 0.83, d) 1.39, e) 1.95, f) 2.5, g) 3.1 and h) 9.2 mM.

On addition of SDS, a bathochromic shift and increase in intensity of the absorption band was observed. These absorption changes were accompanied by a significant enhancement of fluorescence (Fig. 3.7, Table 3.3).

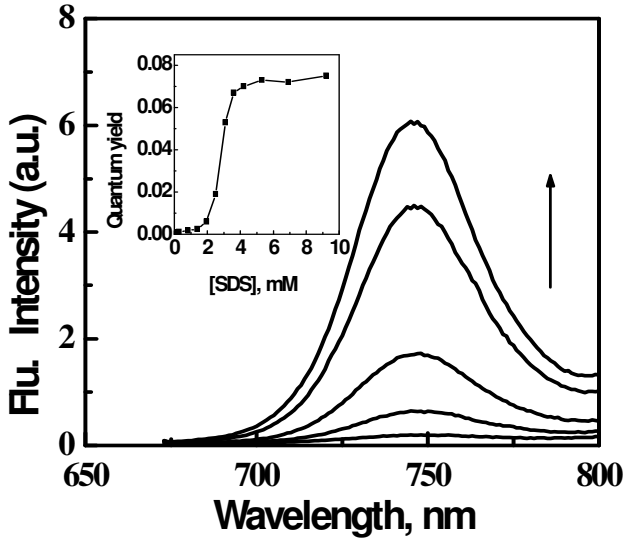

Figure 3.7. Effect of addition of SDS on the fluorescence spectrum of **Sq3** [2.43 × 10^{-5} M], [SDS] a) 0, b) 1.95, c) 2.5, d) 3.1 and e) 9.2 mM, λ_{ex} = 662 nm. Inset shows plot of quantum yield of fluorescence of **Sq3** *vs* concentration of SDS in 96% (v/v) water/ethanol mixture.

Table 3.3. Absorption, emission maximum and quantum yield of fluorescence of **Sq3** in 96% water/ethanol binary mixtures and surfactant solutions.

Solvent %H_2O[a]	CMC	λ_{max} (nm)		Φ_f
		Abs	Em	
96		704	735	0.004
96 + 1.5 mM CTAB	9.2×10^{-4}	727	753	0.09
96 + 9.2 mM SDS	8.0×10^{-3}	719	747	0.08
96 + 2.1 mM TX-100	2.6×10^{-4}	731	755	0.13

Maximum enhancement of fluorescence was observed above the critical micellar concentration (CMC), which is 8.0 mM for SDS. Similar observations were made for the cationic micelle CTAB and the nonionic micelle Triton X-100. The absorption maximum of **Sq3** is at 704 nm in a 96% water/ethanol mixture. Addition of CTAB to this solution resulted in a maximum bathochromic shift of 20 nm, while the emission maximum shifted from 735 nm to 753 nm. This change was accompanied by a significant enhancement in fluorescence efficiency. Addition of Triton X-100 also resulted in maximum of 27 nm shift in absorption and a shift in emission maximum from 735 nm to 755 nm.

These effects could be attributed to break up of the dye aggregates on addition of surfactants such as CTAB, SDS and Triton X-100 at concentrations above their CMC. The break up of the dye aggregates, which would occur as a consequence of microencapsulation of the dye within the hydrophobic micellar cavity, was indicated by the recovery of the monomer absorption and increased

emission intensity. The absence of fluorescence in aqueous media and high fluorescence when encapsulated into hydrophobic domains makes this dye specially useful as a probe for mapping hydrophobic domains of high microviscosity in biological systems.[28,40-42]

3.3.4. Effect of β-CD on Absorption and Emission Properties of Sq3

Cyclodextrins (CD) are cyclic oligosaccharides which have a central cavity capable of accommodating guest molecules in aqueous solutions. These oligosaccharide molecules contain six α-CD, seven β-CD or eight γ-CD glucose units, each having a different cavity diameter of approximately 4.5, 6.5 and 8.5 Å, respectively. The primary hydroxyl groups are on the narrower side and the secondary hydroxyl groups reside in the broader side. β-CD has an internal diameter of 6.5 Å and a height of 7.9 Å. The interiors of the cavities encircled by ether oxygen provide a hydrophobic microenvironment in an aqueous solution. The guest molecules that are accommodated in these cavities are relatively isolated from the bulk water environment and often have enforced and constrained conformation.

Figure 3.8 shows the effect of adding β-CD on the absorption spectra of **Sq3** in 96% (v/v) water/ethanol mixture. On addition of β-CD, a bathochromic shift from 650 nm to 690 nm accompanied by an increase in intensity of the absorption band was observed. As discussed earlier for the micellar solutions, this effect can be attributed to break up of the aggregate and recovery of the monomer

due to formation of inclusion complexes between β-CD and the dye molecules. The absorption changes were accompanied by a significant enhancement of fluorescence quantum yield (Figure 3.9).

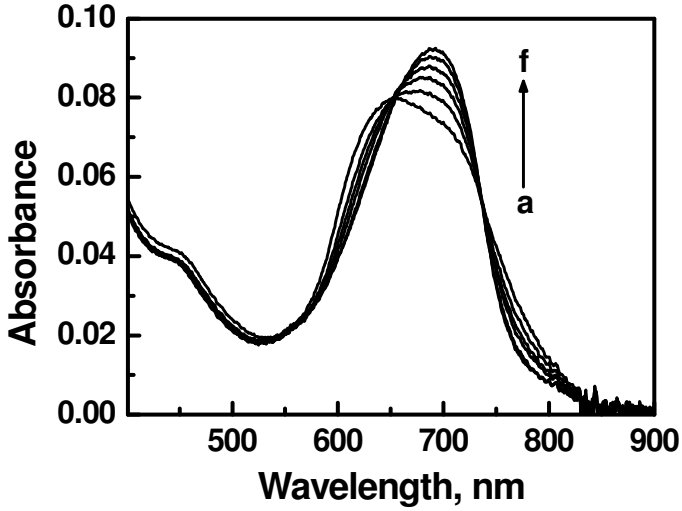

Figure 3.8. Effect of β-CD on absorption spectra of **Sq3** [21.9×10^{-6} M] in 96% (v/v) water/ethanol mixture. [β-CD] a) 0, b) 0.19, c) 0.38, d) 0.57, e) 0.95 and f) 1.33 mM.

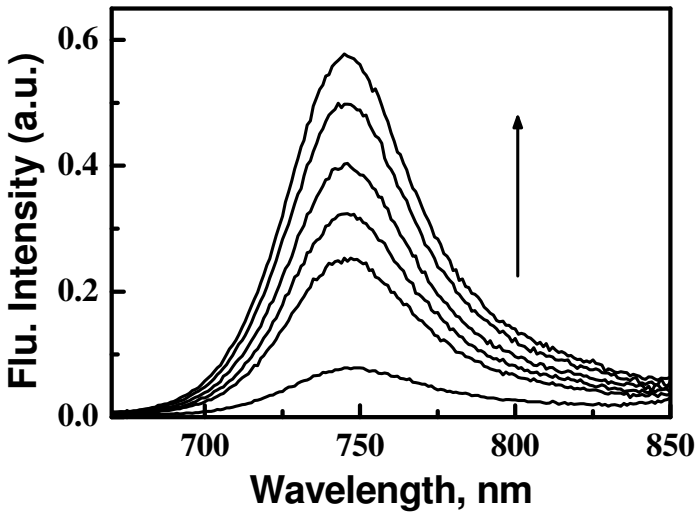

Figure 3.9. Effect of β-CD on emission spectra of **Sq3** [21.9×10^{-6} M] in 96% (v/v) water/ethanol mixture. [β-CD] a) 0, b) 0.19, c) 0.38, d) 0.57, e) 0.95 and f) 1.52 mM.

The mode of complexation was obtained from the Benesi-Hildebrand equation,

$$1/(\Phi_f-\Phi_{ob}) = 1/(\Phi_f-\Phi_c) + 1/K(\Phi_f-\Phi_c)\,[\beta\text{-CD}] \qquad 3.1$$

where, K is the association constant, Φ_f is the quantum yield of emission of the free dye, Φ_{ob} is the observed quantum yield and Φ_{fc} is the quantum yield of emission of the dye-β-CD complex. A plot of $1/(\Phi_f-\Phi_{ob})$ *vs* 1/ [β-CD] was found to be linear which indicated that the dye forms 1:1 complex with β-CD (Figure 3.10).

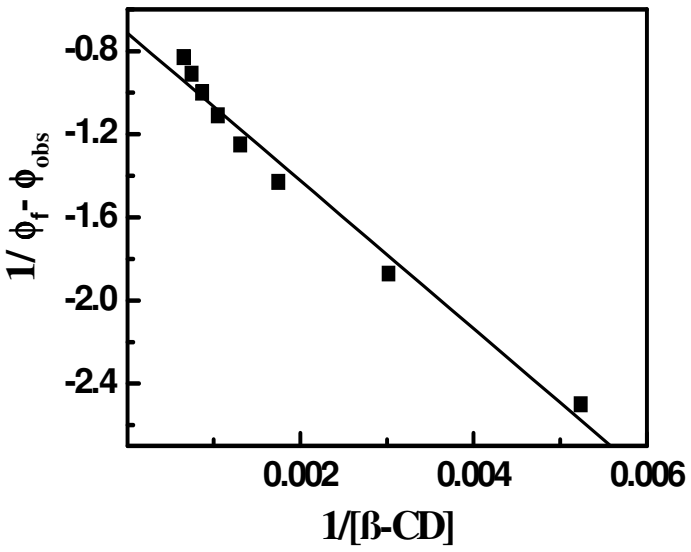

Figure 3.10. Plot of $1/(\Phi_f-\Phi_{ob})$ *vs* 1/ [β-CD] for qauntum yield of **Sq3** [21.9×10^{-6} M] in 96% (v/v) water/ethanol mixture.

3.3.5. Fluorescence Lifetimes of Sq1–3

Figure 3.11 shows fluorescence decay profiles for **Sq1–3** in toluene and ethanol along with the instrument response function. In each case a single

exponential decay was observed. Table 3.4 summarizes the fluorescence lifetime values of these dyes in toluene and ethanol. In toluene, **Sq1** and **Sq2** exhibited longer lifetime of 1.52 ns and 2.22 ns respectively when compared to that in ethanol which was in the range 0.2–0.4 ns.

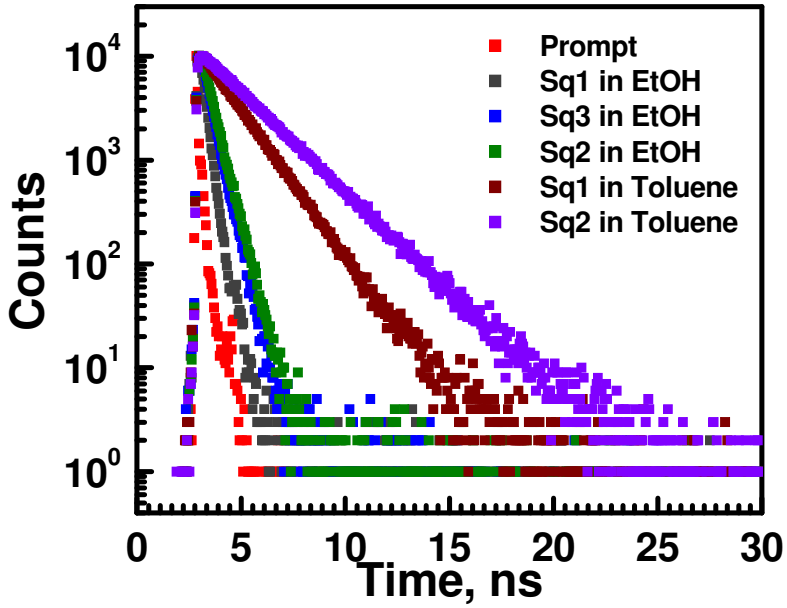

Figure 3.11. Singlet excited state decay of **Sq1–3** in Ethanol and Toluene. Lamp profile also is shown. Emission is monitored at 750 nm for **Sq2**, **Sq3** and 825 nm for **Sq1**, λ_{ex} = 635 nm.

Table 3.4. Fluorescence lifetime properties of **Sq1–3** in toluene and ethanol.

	Toluene		Ethanol	
	$\tau_{f,}$ (ns)	χ^2	$\tau_{f,}$ (ns)	χ^2
Sq1	1.52	1.09	0.22	1
Sq2	2.22	1.05	0.47	1.04
Sq3	-	-	0.44	1

Figure 3.12 shows the singlet excited state decay of **Sq3** in 96% (v/v) water/ethanol mixture before and after the addition of micelles such as CTAB (1.5 mM), SDS (9.2 mM) and Triton X-100 (2.1 mM). The enhancement in fluorescence lifetime in the presence of micelles is clearly observable from this figure.

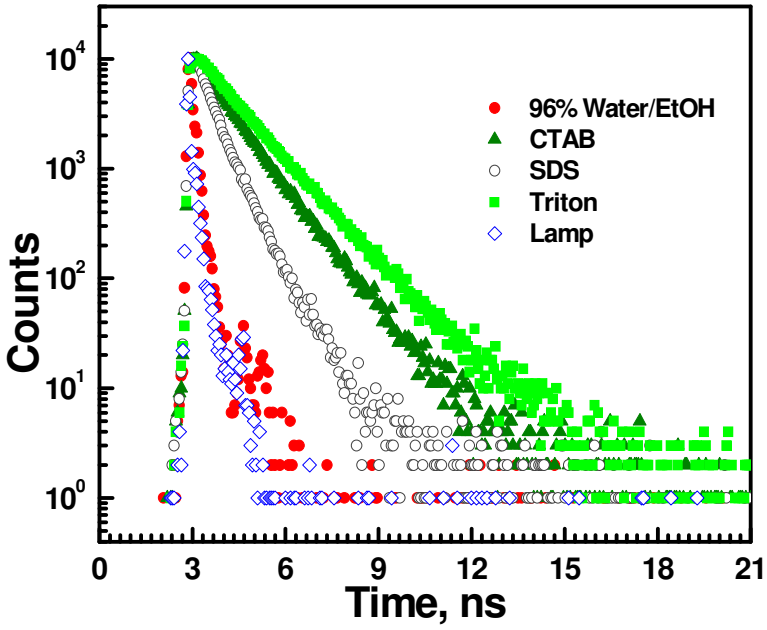

Figure 3.12. Singlet excited state decay of **Sq3** in 96% (v/v) water/ethanol mixture, 1.5 mM CTAB, 9.2 mM SDS, 2.1 mM Triton X-100. Lamp profile also is shown. Emission is monitored at 750 nm, λ_{ex} = 635 nm.

Table 3.5 summarizes time-resolved fluorescence lifetimes of **Sq3** in water/ethanol mixtures and in the presence of micelles. For **Sq3**, the fluorescence lifetime decreased from 0.44 ns (EtOH) to 0.05 ns as the percentage of water increased in the ethanol/water binary mixture. However, addition of micelles

resulted in an enhancement in fluorescence lifetime to 1.06 ns (CTAB), 0.61 ns (SDS) and 1.03 ns (Triton X-100). These effects can be attributed to the microencapsulation of the dye within the hydrophobic micellar cavity as discussed earlier.

Table 3.5. Fluorescence lifetime properties of **Sq3** in water/ethanol binary mixtures and surfactant solutions.

Solvent Composition $\%H_2O$[a]	CMC	λ_{max} (nm)		Φ_f
		Abs	Em	
96		704	735	0.004
96 + 1.5 mM CTAB	9.2×10^{-4}	727	753	0.09
96 + 9.2 mM SDS	8.0×10^{-3}	719	747	0.08
96 + 2.1 mM TX-100	2.6×10^{-4}	731	755	0.13

3.3.6. Molecular Modeling of the Complexes at the DFT and Semiempirical PM3 Levels of Sq1 and Sq2

In order to understand the structural and electronic features of this class of molecules, the solution phase geometries in ethanol were optimized for **DBAS**, **Sq1** and **Sq2** at the BLYP/6-31G* level of density functional theory in conjunction with the polarizable continuum (PCM) model of Tomasi and co-workers (Figure 3.13).[43-45] The Gaussian 03 suite of programs were used for the calculations.[46]

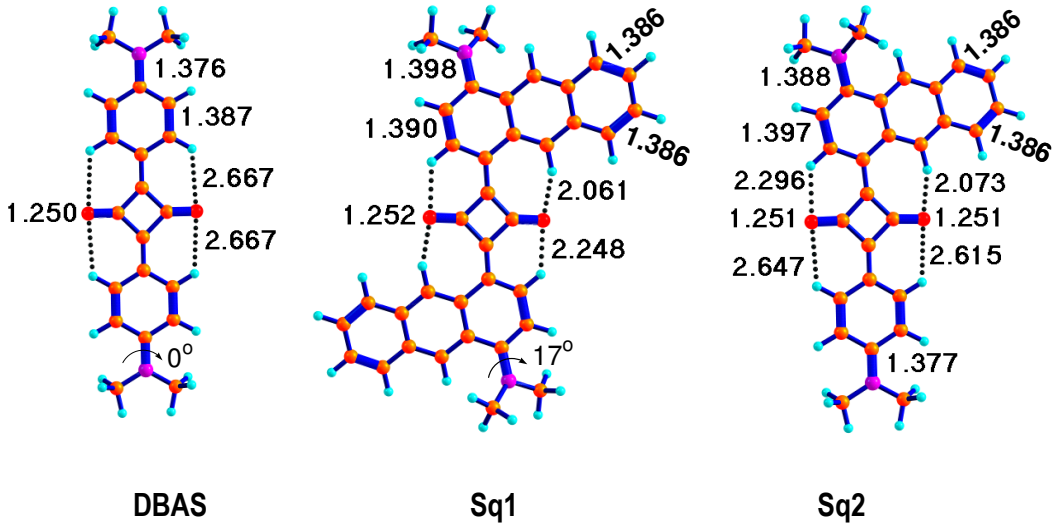

Figure 3.13. Optimized geometries of **DBAS**, **Sq1** and **Sq2** at BLYP/6-31G*-PCM level. Important bond lengths in Å are also given. Bond lengths below 1.40 Å are shown in thick lines.

In **DBAS** and **Sq2**, the dimethylamino group is coplanar to the phenyl moiety whereas a twist angle of 17° was observed between this group and the anthracene moiety in **Sq1** and **Sq2**. Further, the C–N bond lengths in the range of 1.376 to 1.398 Å observed in these systems are much shorter than a typical C–N single bond length of 1.48 Å, indicating a partial double bond character and partial positive charge on the nitrogen. This can be attributed mainly to the strong electron donating mesomeric effect of the nitrogen lone pair. The C=O bond lengths in the range of 1.250 to 1.252 Å observed in these systems are much longer than the typical value of 1.22 Å, indicative of an anionic C–O^- character. The anionic nature of the C–O facilitates interaction with the nearby C–H bonds on the aromatic moiety (see the CO••HC non-bonded interaction shown in Figure 3.13). In addition, the structural restrictions imposed by the middle ring of the

anthracene moiety in **Sq1** and **Sq2** bring the C–O oxygen and C–H bonds into close proximity making it favourable for the CO••HC interactions. Thus the shortest CO••HC length observed in **Sq1** and **Sq2** are 2.073 Å and 2.061 Å respectively.

In Figure 3.14, the molecular electrostatic potential (MESP) plotted on the van der Waals' surface of **Sq1** illustrates the highly charge separated (zwitterionic) character of the system.[47-50] As expected, the positive MESP is largely localized on the dimethyl amino group (red region) while the negative MESP is mainly on the squaraine oxygens (blue region). This feature of MESP was observed in **DBAS** and **Sq2** also.

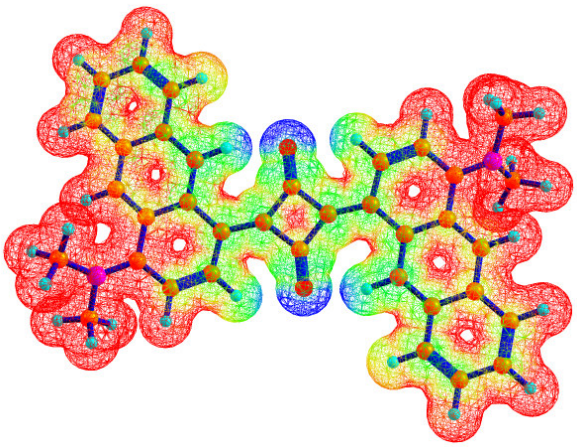

Figure 3.14. Molecular electrostatic potential mapped on to the van der Waals' surface of **Sq1**. Colour coding (▬) red to blue is +44 to -31 kcal mol^{-1}.

The absorption properties of the systems optimized at BLYP/6-31G*-PCM level were further analyzed using the time-dependent DFT (TDDFT) calculations.[51] The calculated values for λ_{max}, oscillator strength and the main MO transitions are

provided in Table 3.6. The calculated values for λ_{max} were in good agreement with the experimental values.

Table 3.6. Theoretical absorption TDDFT at BLYP/6-31G*-PCM level with wavelengths in nm and oscillator strengths (f).

System	λ_{max} (nm)	f	MO transition
DBAS	591	1.6401	HOMO to LUMO (56 %)
Sq1	786	1.0884	HOMO to LUMO (54 %)
Sq2	704	1.0355	HOMO to LUMO (53 %)

In all cases, the main MO transition corresponding to the NIR absorption is from HOMO to LUMO. The HOMO is delocalized over the entire molecule while the LUMO shows more localization on the arene ring directly connected to the squaraine moiety and two of the squaraine carbon atoms (Figure 3.15a). The HOMO–LUMO gap (Figure 3.15b) shows a gradual decrease when going from **DBAS** to **Sq2** to **Sq1** which correlates well with the observed bathochromic shift.

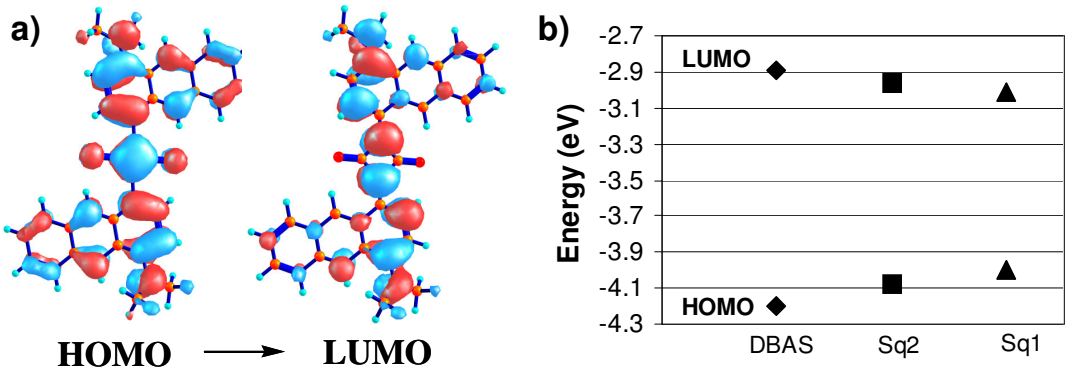

Figure 3.15. a) HOMO and LUMO of **Sq2** and b) HOMO–LUMO gap in **DBAS**, **Sq1** and **Sq2**.

The structural and electronic features, suggest extended π-conjugation in **Sq1** and **Sq2** via the anthracene moiety and strong mesomeric effect of the dimethyl amino group. The CO••HC hydrogen bond interaction further enhances the electron delocalization in these systems.

3.4. Conclusions

In conclusion, a new class of NIR emitting squarylium dyes has been synthesized. The structural and electronic features of **Sq1**–**3** were investigated using DFT methods. The absorption and emission bands of these dyes are substantially red shifted compared to most of the reported squaraine dyes. The high extinction coefficients, good quantum yields of fluorescence, long fluorescence lifetimes and good photostability make these dyes suitable for application as fluorescent probes. The water compatibility and substantial enhancement of fluorescence of **Sq3** in micellar media suggest that these dyes can be potentially useful as fluorescent probes in biological applications.

3.5. Experimental Section

3.5.1. Materials

Squaric acid, 1-aminoanthracene, cetyltrimethylammonium bromide (CTAB), sodium dodecyl sulfate (SDS) and polyethylene-*t*-octylphenol (Triton X-100) were purchased from Aldrich. 3-[4-(*N,N*-dialkylamino)phenyl]-4-hydroxycyclobutene-

1,2-dione, 3-[4-(*N,N*-dialkylamino)anthracene]-4-hydroxycyclobutene-1,2-dione was prepared according to the reported procedure.[52] All other starting materials and reagents were purchased from commercial suppliers and used without further purification. The solvents used were purified and dried by standard methods prior to use. All the dye solutions were made in spectroscopic grade solvents. The aqueous solutions of the dyes were prepared by dissolving the dye in ethanol and then diluting the same with appropriate volume of doubly distilled water.

3.5.2. General Techniques

Melting points were determined with a Mel-Temp-II melting point apparatus and were uncorrected. ^{1}H NMR spectra were measured on a 300 MHz Bruker Avance DPX NMR Spectrometer. FT-IR spectra were recorded on a Shimadzu IRPrestige-21 Fourier Transform Infrared Spectrophotometer. High Resolution Mass Spectral (HRMS) analysis was obtained from JEOL JMS600 instrument.

Electronic absorption spectra were recorded on a Shimadzu UV-3101 PC NIR scanning spectrophotometer and the emission spectra were recorded on a SPEX-Fluorolog, F112X spectrofluorimeter. Fluorescence quantum yields were measured by the relative method using optically matched dilute solutions. 1,1'-Diethyl-2,2'-dicarbocyanine iodide (**DDI**) having a quantum yield of 0.0028 in ethanol[35] and **IR–125** having a quantum yield of 0.13 in DMSO[34] were used as

standards. The quantum yield of fluorescence was calculated by using the equation 3.2, where, A_s and A_u are the absorbance of the standard and unknown, respectively. F_s and F_u are the fluorescence peak areas of the standard and unknown and n_s and n_u are the refractive indices of the standard and unknown solvents.

$$\phi_f = \frac{A_s F_u n_u^2}{A_u F_s n_s^2} \qquad 3.2$$

Fluorescence lifetimes were measured using IBH (FluoroCube) time-correlated picosecond single photon counting (TCSPC) system using a 635 nm IBH NanoLED source and Hamamatsu C4878-02 MCP detector. The fluorescence decay profiles were deconvoluted using IBH data station software V2.1, fitted with monoexponential decay and minimizing the χ^2 values of the fit to 1 ± 0.3.

The solution phase geometries in ethanol were optimized for **DBAS**, **Sq1** and **Sq2** at BLYP/6-31G* level of density functional theory in conjunction with the polarizable continuum (PCM) model. The Gaussian 03 suite of programs was used for the calculations. The absorption properties of the systems optimized at BLYP/6-31G*-PCM level were further analyzed using the time-dependent DFT (TDDFT) calculations.

3.5.3. Synthesis of the Squaraine Dye, Sq2

A mixture of *N,N*-dimethyl-1-aniline (10 mg, 0.08 mmol) and 3-[4-(*N,N*-dibutylamino)anthracene]-4-hydroxycyclobutene-1,2-dione (33 mg, 0.08 mmol)

were heated at 60 °C in a mixture of 1 mL tributylorthoformate (TBOF) and n-BuOH (10 mL) for 3 h (Scheme 3.1).

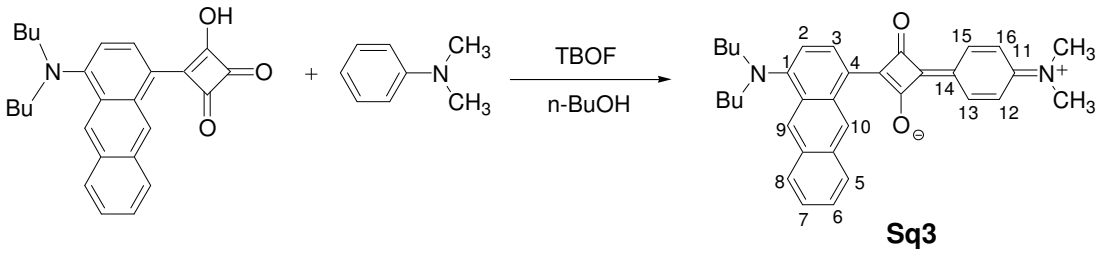

Sq3

Scheme 3.1

After cooling, the reaction mixture was filtered and the residue was purified by column chromatography over silica gel (100-200 mesh) using methanol/chloroform mixture (1:99) as eluent to give the dye **Sq2** (15 mg, 36%). Mp 165-167 °C (decomp.); FT-IR(KBr): ν_{max} 1596 cm^{-1} (CO); UV λ_{max} (toluene) 720 nm, ε 70000 $M^{-1}cm^{-1}$; ^1H NMR (300 MHz, $CDCl_3$, TMS) δ 0.95 (6H, t, aliphatic CH_3), 1.25-1.4 (4H, m, aliphatic CH_2), 1.68-2 (4H, m, aliphatic CH_2), 3.19 (6H, s, NCH_3), 3.64-3.68 (4H, NCH_2), 6.79 (2H, d, J = 8.88 Hz, aromatic C_{13} & C_{15} proton), 6.99 (1H, d, J = 8.67 Hz, aromatic C_2 proton), 7.48-7.58 (2H, t, J = 8.28 Hz, aromatic C_6 & C_7 proton), 7.95 (1H, d, J = 7.86 Hz, aromatic C_8 proton), 8.26 (1H, d, J = 8.1 Hz, aromatic C_5 proton), 8.5 (2H, d, J = 8.388 Hz, aromatic C_{12} & C_{16} proton), 8.51 (1H, s, aromatic C_9 proton), 9.42 (1H, d, J = 8.61 Hz, aromatic C_3 proton), 10.48 (1H, s, aromatic C_{10} proton); (HRMS-EI) Mol. wt. calcd. for $C_{34}H_{36}N_2O_2$ (MH^+) 504.277. Found 504.2801.

3.5.4. Synthesis of the Squaraine Dye, Sq3

A mixture of *N*-phenyldiethanolamine (20 mg, 0.11 mmol) and 3-[4-(*N,N*-dimethylamino)anthracene]-4-hydroxycyclobutene-1,2-dione (35 mg, 0.11mmol) was heated at 60 °C in a mixture of TBOF (1 mL) and n-BuOH (10 mL) for 3 h. After cooling, the reaction mixture was filtered and the residue was purified by column chromatography over silica gel (100-200 mesh) using methanol/chloroform mixture (5:95) as eluent to give the dye **Sq3** as a green solid (15 mg, 29%). Mp 125-130 °C (decomp.); FT-IR(KBr): ν_{max} 1590 (CO) cm^{-1}; UV λ_{max} (EtOH) 720 nm; ε (EtOH) 34000 $M^{-1}cm^{-1}$; ^1H NMR (300 MHz, CD_3OD, TMS) δ 3.47 (6H, s, NCH_3), 3.76 (4H, t, $-CH_2OH$), 3.84 (4H, t, NCH_2), 6.92 (2H, d, J = 8.85 Hz, aromatic C_{13} & C_{15} proton), 7.47-7.52 (2H, t, J = 7.17 Hz, aromatic C_6 & C_7 proton), 7.54 (1H, d, J = 9.1 Hz, aromatic C_2 proton), 7.95 (1H, d, J = 8.19 Hz, aromatic C_8 proton), 8.12 (1H, d, J = 8.25 Hz, aromatic C_5 proton), 8.28 (2H, d, J = 8.91 Hz, aromatic C_{12} & C_{16} proton), 8.53 (1H, s, aromatic C_9 proton), 9.18 (1H, d, J = 8.94 Hz, aromatic C_3 proton), 10.12 (1H, s, aromatic C_{10} proton); (HRMS-EI) Mol. wt. calcd. for $C_{30}H_{28}N_2O_4$ (MH^+) 480.2049. Found 480.2120.

3.6. References

1. Ye, Y.; Bloch, S.; Kao, J.; Achilefu, S. *Bioconjugate Chem.* **2005**, *16*, 51-61.

2. Ntziachristos, V.; Bremer C.; Weissleder, R. *Eur. Radiol.* **2003**, *13*, 195-208.

3. Sevick-Muraca, E. M.; Houston, J. P.; Gurfinkel, M. *Curr. Opin. Chem. Biol.* **2002**, *6*, 642-650.

4. Frangioni, J. V. *Curr. Opin. Chem. Biol.* **2003**, *7*, 626-634.

5. Pham, W.; Lai, W. F.; Weissleder R.; Tung, C. H. *Bioconjugate Chem.* **2003**, *14*, 1048-1051.

6. Pham, W.; Medarova, Z.; Moore, A. *Bioconjugate Chem.* **2005**, *16*, 735-740.

7. Bandichhor, R.; Petrescu, A. D.; Vespa, A.; Kier, A. B.; Schroeder, F.; Burgess, K. *Bioconjugate Chem*. **2006**, *17*, 1219-1225.

8. Das, S.; Thomas, K. G.; George, M. V. *Mol. Supramol. Photochem.* **1997**, *1*, 467-517.

9. Law, K.-Y. *Chem. Rev.* **1993**, *93*, 449-486.

10. Stoll, R. S.; Severin, N.; Rabe, J. P.; Hecht, S. *Adv. Mater.* **2006**, *18*, 1271-1275.

11. Liang, K.; Farahat, M. S.; Perlstein, J.; Law, K.-Y.; Whitten, D. G. *J. Am. Chem. Soc.* **1997**, *119*, 830-831.

12. Das, S.; Thomas, K. G.; Kamat, P. V.; George, M. V. *J. Phys. Chem.* **1994**, *98*, 9291-9296.

13. Kamat, P. V.; Das, S.; Thomas, K. G.; George, M. V. *J. Phys. Chem.* **1992**, *96*, 195-199.

14. Law, K.-Y.; Bailey, F. C. *J. Imaging Sci.* **1987**, *31*, 172.

15. Tam, A. C.; Balanson, R. D. *IBM J. Res. Develop.* **1982**, *26*, 186-197.

16. Alex, S.; Santhosh, U.; Das, S. *J. Photochem. Photobiol., A* **2005**, *172*, 63-71.

17. Liang, K. N.; Law, K.-Y.; Whitten, D. G. *J. Phys. Chem.* **1995**, *99*, 16704-16708.

18. Fabian, J.; Nakazumi, H.; Matsuoka, M. *Chem. Rev.* **1992**, *92*, 1197-1226.

19. Emmelius, M.; Pawlowski; G.; Volmann, H. W. *Angew. Chem., Int. Ed. Engl.* **1989**, *28*, 1445-1471.

20. Basheer, M. C.; Alex, S.; Thomas, K. G.; Suresh, C. H.; Das, S. *Tetrahedron* **2006**, *62*, 605-610.

21. Ajayaghosh, A. *Acc. Chem. Res.* **2005**, *38*, 449-459.

22. Ros-Lis, J. V.; García, B.; Jiménez, D.; Martínez Máñez, R.; Sancenón, F.; Soto, J.; Gonzalvo, F.; Valldecabres, M. C. *J. Am. Chem. Soc.* **2004**, *126*, 4064-4065.

23. Yagi, S.; Fujie, Y.; Hyodo, Y.; Nakazumi, H. *Dyes Pigm.* **2002**, *52*, 245-252.

24. Thomas, K. G.; Thomas, K. J.; Das, S.; George, M. V. *Chem. Commun.* **1997**, 597-598.

25. Bello, K. A.; Corns, S. N.; Griffiths, J. *J. Chem. Soc. Chem. Commun.* **1993**, 452-453.

26. Sprenger, H. E.; Ziegenbein, W. *Angew. Chem., Int. Ed. Engl*. **1966**, *5*, 893-894.

27. Keil, D.; Hartmann, H.; Moschny, T. *Dyes Pigm.* **1991**, *17*, 19-27.

28. Arun, K. T.; Ramaiah, D. *J. Phys. Chem. A*. **2005**, *109*, 5571-5578.

29. Das, S.; Thomas, K. G.; Biju, P. V.; Santosh, U.; Suresh, V. *U. S. Patent* 6,417,402, 2002.

30. Law, K.-Y. *J. Phys. Chem.* **1989**, *93*, 5925-5930.

31. Haugland, R. P. *Handbook of Fluorescent Probes and Research Chemicals*; Sixth Ed., Molecular Probes: Eugene, OR, 1996.

32. Pham, W.; Lai, W. F.; Weissleder, R.; Tung, C. H. *Bioconjugate Chem.* **2003**, *14*, 1048-1051.

33. Pham, W.; Medarova, Z.; Moore, A. *Bioconjugate Chem*. **2005**, *16*, 735-740.

34. Soper, S. A.; Mattingly, Q. L. *J. Am. Chem. Soc.* **1994**, *116*, 3744-3752.

35. Dempster, D. N.; Morrow, T.; Rankin, R.; Thompson, G. F. *J. Chem. Soc., Faraday Trans. 2* **1972**, *68*, 1479-1496.

36. Das, S.; Thomas, K. G.; Thomas, K. J.; Madhavan, V.; Liu, D.; Kamat, P. V.; George, M. V. *J. Phys. Chem.* **1996**, *100*, 17310-17315.

37. Liang, K.; Law, K.-Y.; Whitten, D. G. *J. Phys. Chem.* **1994**, *98*, 13379-13384.

38. Chen, H.; Farahat, M. S.; Law, K.-Y.; Whitten, D. G. *J. Am. Chem. Soc.* **1996**, *118*, 2584-2594.

39. Das, S.; Thomas, K. G.; Ramanathan, R.; George, M. V.; Kamat, P. V. *J. Phys. Chem.* **1993**, *97*, 13625-13628.

40. Jisha, V. S.; Arun, K. T.; Hariharan, M.; Ramaiah, D. *J. Am. Chem. Soc.* **2006**, *128*, 6024-6025.

41. Nizomov, N.; Ismailov, Z. F.; Nizamov, S. N.; Salakhitdinova, M. K.; Tatarets, A. L.; Patsenker, L. D.; Khodjayev, G. *J. Mol. Struct.* **2006**, *788*, 36-42.

42. Nakazumi, H.; Colyer, C. L.; Kaihara, K.; Yagi, S.; Hyodo, Y. *Chem. Lett.* **2003**, *32*, 804-805.

43. Becke, A. D. *Phys. Rev. A* **1988**, *38*, 3098-3100.

44. Lee, C.; Yang, W.; Parr, R. G. *Phys. Rev. B* **1988**, *37*, 785-789.

45. Miertus, S.; Scrocco, E.; Tomasi, J. *J. Chem. Phys.* **1981**, *55*, 117.

46. Gaussian 03, Revision C.02, Frisch, M. J. *et al.*

47. MESP is directly related with the electron density distribution and the the most negative valued MESP is often observed at the electron rich regions such as lone pair and π-bonded regions of a molecule or more on MESP, see (a) Politzer, P.; Truhlar, D. G. *Chemical Applications of Atomic and*

Molecular Electrostatic Potentials; Plenum: New York, 1981. (b) Gadre, S. R.; Shirsat, R. N. *Electrostatics of Atoms and Molecules*; Universities Press: Hyderabad, 2000.

48. Suresh, C. H.; Gadre, S. R. *J. Org. Chem.* **1999**, *64*, 2505-2512.

49. Suresh, C. H.; Gadre, S. R. *J. Am. Chem. Soc.* **1998**, *120*, 7049-7055.

50. Suresh, C. H.; Koga, N. *Inorg. Chem*. **2002**, *41*, 1573-1578.

51. Stratmann, R. E.; Scuseria, G. E.; Frisch, M. J. *J. Chem. Phys.* **1998**, *109*, 8218-8224.

52. Keil, D.; Hartmann, H. *Dyes and Pigm.* **2001**, *49*, 161-179.

CHAPTER 4

Novel Squaraine Based Dyes with Strong Luminescence in the Near Infrared Region: Study of their Photophysical, Metal Ion and Protein Sensing Properties

4.1. Abstract

*The photophysical properties of unsymmetrical squaraine dyes (**Sq1** and **Sq2**) possessing intense absorption and emission in the near infrared (NIR) region have been investigated. These dyes showed good quantum yield of fluorescence, high extinction coefficient, good photostability and a large Stokes' shift in emission (~100–140 nm) in the NIR region. These dyes were characterized by a negative solvatochromism, i.e. their absorption underwent a blue shift with increase in solvent polarity, whereas, their emission spectra were hardly affected by the change in polarity of the solvents. Metal ion sensing and noncovalent interaction of the dyes with proteins were also investigated. The benzothiazolium based dye, **Sq1**, was found to be capable of selectively detecting Hg^{2+} in the presence of other environmentally relevant metal ions in aqueous media. The fluorescence of the benzindolenium based dye, **Sq2** increased significantly on complexation with proteins such as human serum albumin (HSA) and bovine*

serum albumin (BSA) suggesting the suitability of this dye for labeling proteins. A novel class of unsymmetrical squaraine dyes containing N-heteroaromatic ring nitrogen atom remaining non-alkylated is also reported. The presence of a free nitrogen group in these dyes makes them useful as pH sensors.

4.2. Introduction

The advantages of using dyes fluorescing in the NIR region for various biomedical imaging applications have been highlighted in the previous Chapter. In the work described in that Chapter, the use of *N,N*-dialkylaminoanthracene as a substituent instead of *N,N*-dialkylaniline was shown to bring about strong red shift in the absorption and emission spectra. Using the same strategy we have synthesized novel unsymmetrical squaraines **Sq1** and **Sq2** (Chart 4.1), with intense absorption and emission in the NIR region. The emission spectra of these molecules were marked by large Stokes' shift particularly in polar solvents. Dyes with large Stokes' shift are especially suitable for imaging applications, since a small Stokes' shift can cause self-quenching and measurement error due to interference by excitation and scattered light,[1,2] both of which can decrease the detection sensitivity to a great extent.

In this Chapter, we describe the synthesis, solvatochromic and metal ion sensing properties of the benzothiazolium based dye, **Sq1** and the use of the benzindolenium based dye, **Sq2** as a fluorescent probe for proteins.

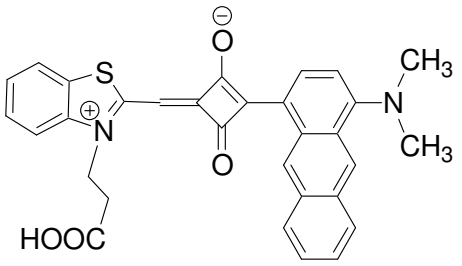

Sq1

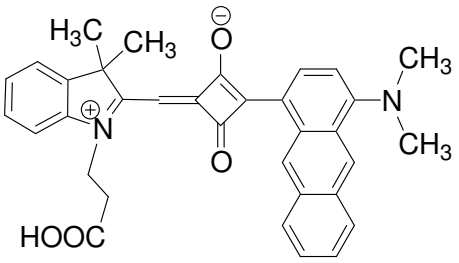

Sq2

Chart 4.1

Conventionally, unsymmetrical dyes possessing nitrogen containing heterocyclic compounds have been prepared by the reaction of semisquaraine with quaternized heterocycles. In this Chapter, we also describe the synthesis and study of a novel class of unsymmetrical squaraine dyes (**Sq3–6**, Chart 4.2), wherein the nitrogen of the *N*-heteroaromatic rings remained non-alkylated.

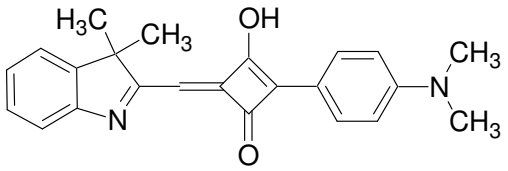

Sq3

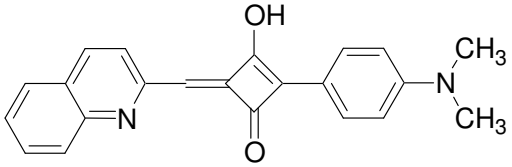

Sq4

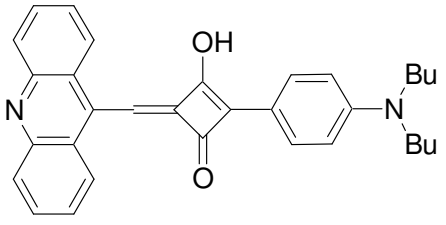

Sq5

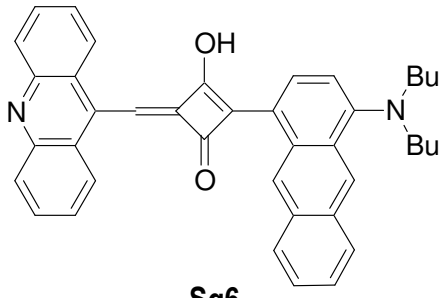

Sq6

Chart 4.2

Due to the presence of free nitrogen at the *N*-heteroaromatic ring, this class of dyes can potentially be used to covalently label biomolecules via quarternization of the nitrogen group.

4.3. Results and Discussion

4.3.1. Absorption and Emission Spectra

Figure 4.1 and 4.2 show the absorption and emission spectra of **Sq1** and **Sq2** in methanol. The absorption spectrum of **Sq1** showed a maximum centered at 596 nm and emission maximum centered at 738 nm, whereas the absorption maximum of **Sq2** was at 631 nm and emission maximum at 731 nm.

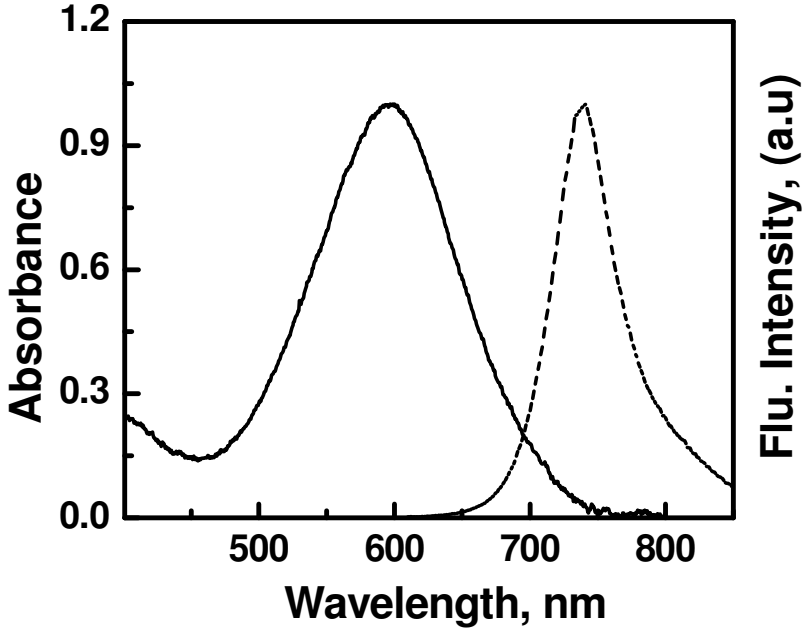

Figure 4.1. Absorption and emission spectra of **Sq1** in methanol.

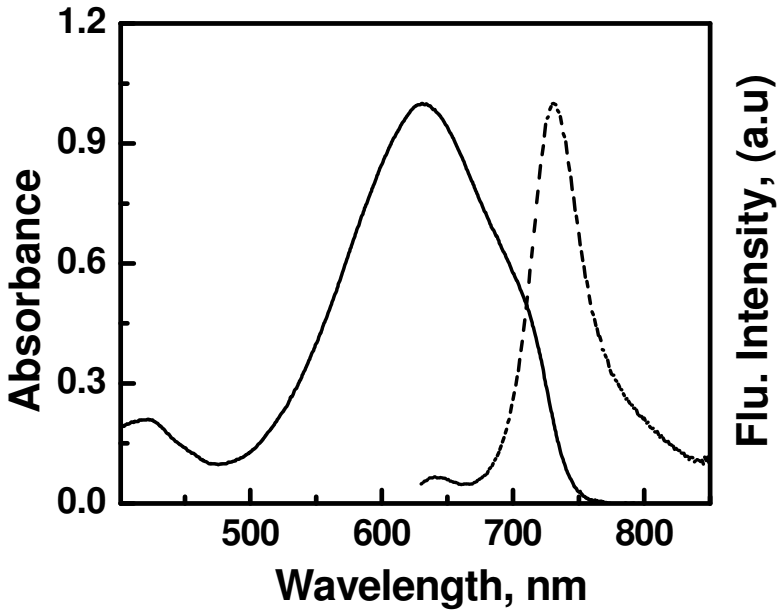

Figure 4.2. Absorption and emission spectra of **Sq2** in methanol

These dyes exhibited good quantum yields of fluorescence, much higher than those of most commercially available dyes emitting in the NIR region, even higher than the dyes reported in the previous Chapter.[3-5] The quantum yield of fluorescence of the benzindolenium based dye was higher compared to that of the benzothiazolium based dye. Time-resolved fluorescence studies indicated mono-exponential decays with lifetimes in the 0.2-2 ns range.

Table 4.1 summarizes the photophysical properties of **Sq1** and **Sq2** and the Stokes' shift in different solvents.

Table 4.1. Photophysical properties of **Sq1** and **Sq2**.

Solvents	**Sq1**					**Sq2**				
	λ_{max} (nm)		Φ_f	ν_{st} cm^{-1}	τ, *ns*	λ_{max} (nm)		Φ_f	ν_{st} cm^{-1}	τ, *ns*
	Abs	Em				Abs	Em			
MeOH	596	738	0.02	3228	0.30	631	731	0.03	2168	0.20
EtOH	603	738	0.04	3033	0.70	638	730	0.08	1975	0.40
2-PrOH	607	734	0.09	2850	1.30	632	727	0.16	2067	0.80
n-BuOH	617	739	0.07	2675	1.34	645	733	0.13	1861	0.65
DMSO	606	757	0.07	3291	1.54	639	746	0.15	2244	0.80
ACN	611	744	0.05	2925	0.72	638	732	0.06	2012	0.32
Acetone	612	743	0.08	2880	1.31	634	729	0.17	2055	0.65
EtOAc	628	737	0.12	2355	2.07	637	726	0.24	1924	1.52
DCM	643	746	0.06	2147	1.66	676	736	0.07	1206	0.69
Toluene	650	736	0.07	1797	1.88	679	731	0.16	1047	1.32

The emission of these dyes showed a very large Stokes' shift. In methanol, **Sq1** and **Sq2** exhibited Stokes' shifts of around 142 nm and 100 nm respectively. The Stokes' shifts were much larger in alcoholic solvents (Methanol, Ethanol) than in aprotic solvents (Toluene, Dichloromethane). Dyes with large Stokes' shift are particularly useful as probes, since a large difference in excitation and emission wavelengths can considerably reduce the background signals due to

significant reduction in the amount of the excitation wavelength reaching the detector.

4.3.2. Solvatochromic Properties

The dyes exhibited interesting solvatochromic properties. Solvatochromism can be defined as positive solvatochromism, when there is a bathochromic shift with increase in solvent polarity or as negative solvatochromism, when a hypsochromic shift is observed with increase in solvent polarity. In the present study negative solvatochromism, *i.e.* a blue shift in absorption with increase in solvent polarity (Figure 4.3) was observed for **Sq1** and **Sq2**. The shift was much more significant for **Sq1**.

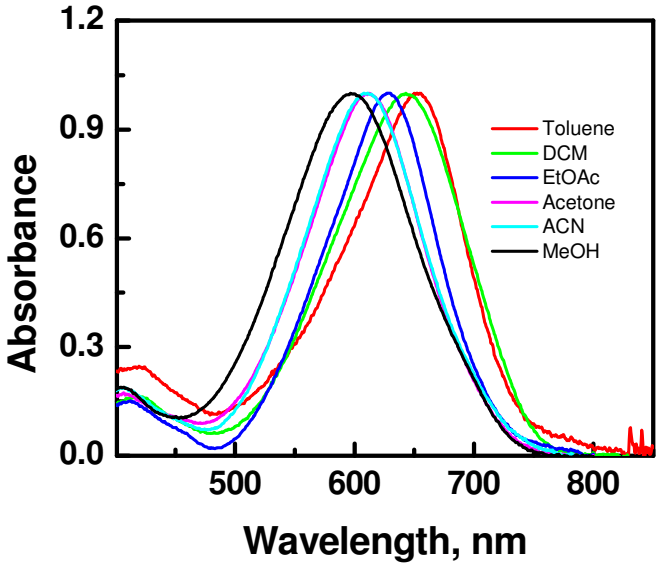

Figure 4.3. Absorption spectra of **Sq1** in solvents of different polarity.

In a nonpolar solvent such as toluene, **Sq1** showed an absorption maximum at 650 nm, whereas the absorption spectrum was significantly blue shifted in

methanol to 596 nm. Interestingly, the emission spectrum was hardly affected by the change in solvent polarity. The emission maximum of **Sq1** was centered at around 736 nm in toluene, whereas in methanol it was centered at 738 nm. It was clear that the emission was not dependent on solvent polarity.

The correlation of the blue shift in the absorption spectra of **Sq1** and **Sq2** as a function of solvent polarity was investigated by plotting the absorption maxima versus $E_T(30)$ (Dimroth solvent polarity scale).[6-10]

$E_T(30)$ values are based on the negatively solvatochromic pyridinium *N*-phenolate betaine dye. This scale is obtained by using equation 4.1, where λ_{max} is the maximum of the longest wavelength *i.e.,* the intramolecular CT π-π^* band of the dye.

$$E_T(30)\ (\text{Kcal mol}^{-1}) = 28951/\lambda_{max}\ (\text{nm}) \qquad 4.1$$

The $E_T(30)$ scale ranges from 63.1 kcal mol^{-1} for water, as the most polar solvent, to 30.7 kcal mol^{-1} for tetramethylsilane (TMS), as the least polar solvent. In order to avoid the non-SI unit kcal mol^{-1}, $E_T(30)$ values are usually convereted into kJ mol^{-1}. In 1983 the normalized $E_T(N)$ scale was introduced as defined by equation 4.2.[11] The dimensionless $E_T(N)$ scale ranges from 1.0 for water to 0.0 for TMS.

$$E_T(N) = \frac{E_T\ \text{Solvent} - E_T\ (\text{TMS})}{E_T\ \text{Water} - E_T\ (\text{TMS})} = \frac{E_T\ (\text{Solvent}) - 30.7}{32.4} \qquad 4.2$$

Figure 4.4 and 4.5 show the plot of observed absorption maxima (in cm^{-1}) of **Sq1** and **Sq2** against molar electronic transition energy of solvents $E_T(30)$ and $E_T(N)$ respectively. A linear relation with correlation coefficient r > 0.9, was obtained for **Sq1**. For **Sq2**, with the exception of ethyl acetate and acetone a good linear fit was observed for all the solvents.

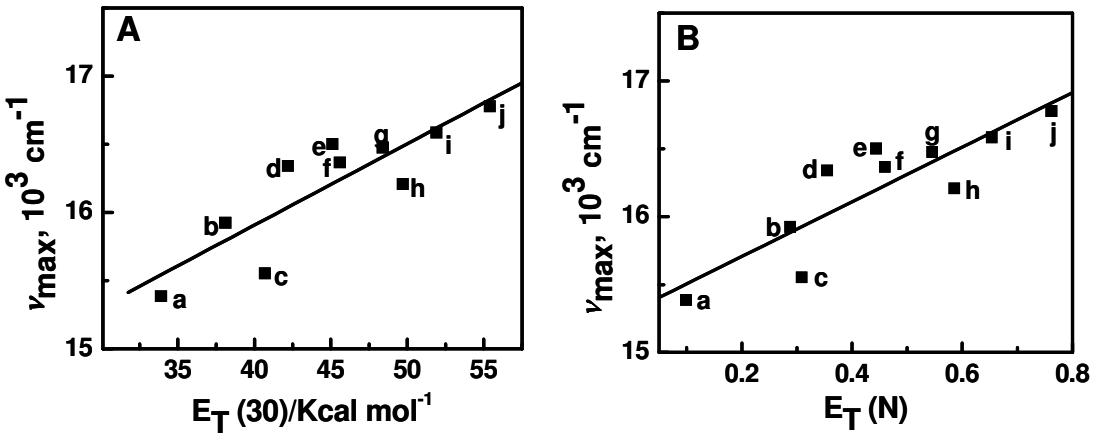

Figure 4.4. Plot of absorption maxima of **Sq1** *vs* A) $E_T(30)$ and B) $E_T(N)$ of corresponding solvents a) Toluene, b) EtOAc, c) DCM, d) Acetone, e) DMSO, f) ACN, g) 2-PrOH, h) n-BuOH, i) EtOH and j) MeOH.

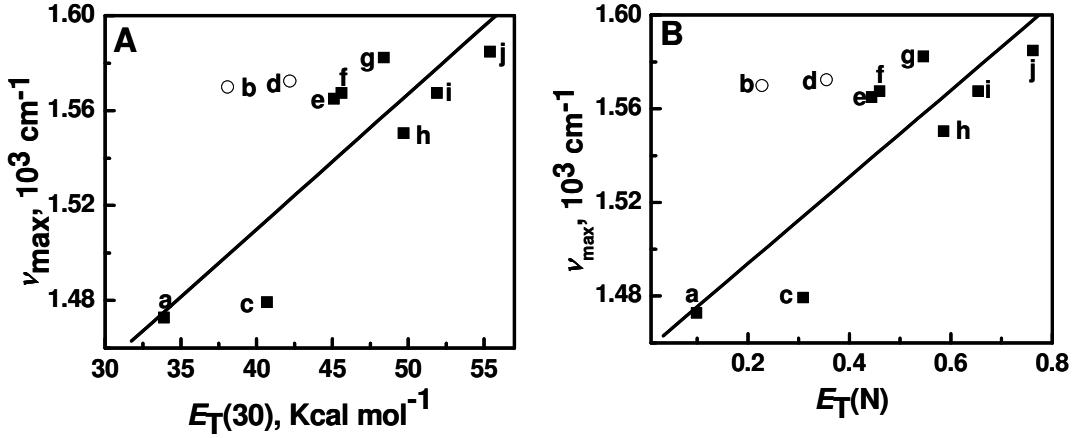

Figure 4.5. Plot of absorption maxima of **Sq2** *vs* A) $E_T(30)$ and B) $E_T(N)$ of corresponding solvents a) Toluene, b) EtOAc, c) DCM, d) Acetone, e) DMSO, f) ACN, g) 2-PrOH, h) n-BuOH, i) EtOH and j) MeOH.

The observation of such large solvent polarity induced hypsochromic shifts associated with hardly any change in the fluorescence spectra is unusual. Recently, Peng and coworkers[12] reported large Stokes' shift for the NIR absorbing heptamethine cyanine dyes (**2a**, **2b** Scheme 4.1).

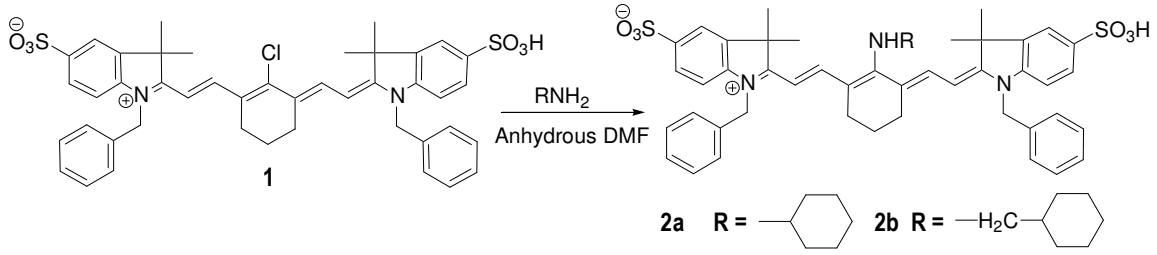

Scheme 4.1. Synthetic scheme for the heptamethine cyanine dyes.

The absorption spectra of **2a** and **2b** exhibited very large blue shifts when compared to **1** (from 783 (**1**) to ~600 nm (**2a**, **b**) in water). The dyes also exhibited large Stokes' shift (>140) nm in water. In addition to a large Stokes' shift, these dyes showed broad and fairly structureless fluorescence spectrum, and no mirror image relationship between the absorption and fluorescence spectra (Figure 4.6), and the authors attributed this effect to an intramolecular charge transfer (ICT) process. Sovatochromism is a widely used criterion to identify charge transfer processes in dyes. In contrast to the dye **1**, marked negative solvatochromism behaviour of the absorption spectrum was observed with increasing polarity of the solvents for the dye **2a**. However no apparent solvatochromism was observed in the emission spectra. The authors suggest that these unusual properties might be

due to the hydrogen bonding interactions between the solvent and dye molecules, however no details have been provided.

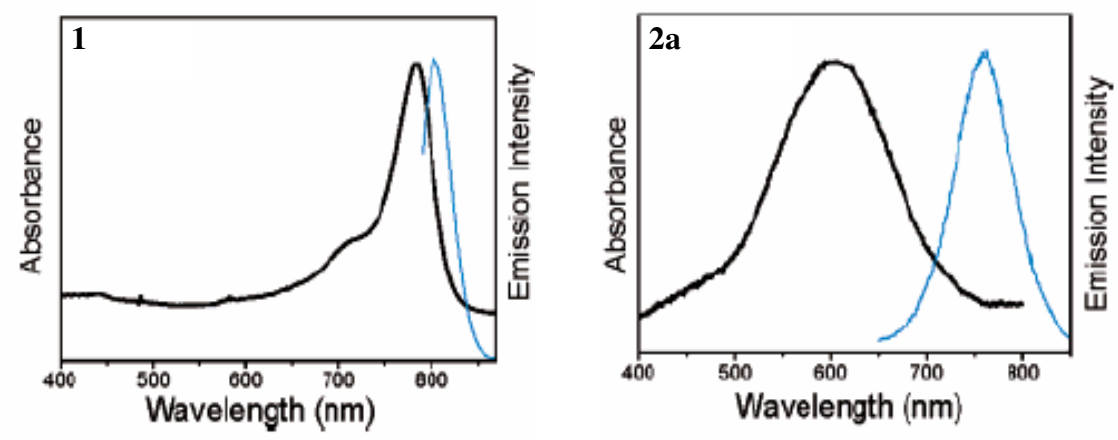

Figure 4.6. Absorption (black) and emission (blue) spectra of dye **1** (left) and **2a** (right) in water. (From Ref. 12).

Similar results were also observed for some styryl pyridinium dyes.[10,13] The absorption maximum of these dyes depends on the polarity and hydrogen bonding ability of the solvents, and a marked hypsochromic shift was observed with increasing polarity or acidity of the solvent. However, no solvatochromism was observed in the emission spectra. A mechanism shown in Scheme 4.2 was proposed to explain this phenomenon.

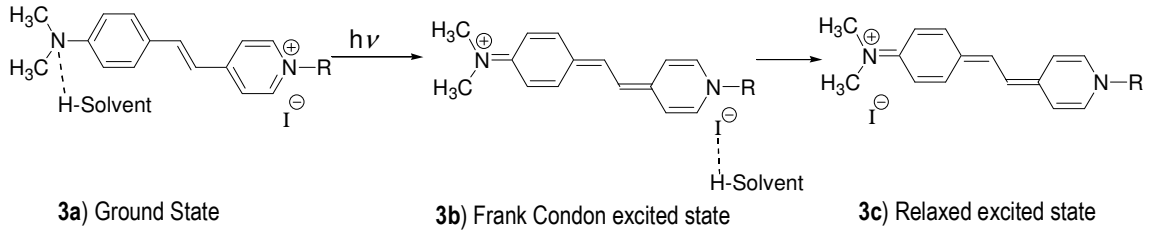

Scheme 4.2. Proposed mechanism for the solvatochromic behaviour of styryl pyridinium dye **3**.

Strong hydrogen bonding solvents were said to stabilize the structure **3a** decreasing the electron donating ability of nitrogen and thereby the ICT interaction with the pyridinium moiety. In the Franck Condon (FC) excited state, hydrogen bonding was proposed to take place between solvent and iodide ions and stabilize **3b.** The energy gap between the FC excited state and relaxed excited state was proposed to be small and increase with a decrease in the acidity of the solvents. Thus it was proposed that **3c** was more stabilized in solvents of low polarity (low acidity), since these solvents would not hydrogen bond with the iodide anions.

In order to explain the unusual behaviour of **Sq1** and **Sq2** observed in the present study, *i.e.* large negative solvatochromism in the absorption spectrum with no apparent effect of solvent polarity on the fluorescence spectra, we propose the scheme shown in Figure 4.7. A possible reason for the observed difference in solvatochromic behaviour of the absorption and emission bands could be that the excited state formed by direct absorption and the excited state responsible for the emission are conformationally different species. Such an explanation has been suggested for a variety of molecules which undergo twist in the excited state due to enhanced charge transfer in the excited state.[14-16] In the present study the blue shifts in absorption with increasing solvent polarity suggests that the ground state of this molecule is highly polar compared to the excited state. Thus in polar solvents, the charge separated state will be highly stabilized compared to nonpolar

solvents and we propose that this can exist in the twisted form similar to the TICT excited state in dimethylaminobenzonitrile.[14]

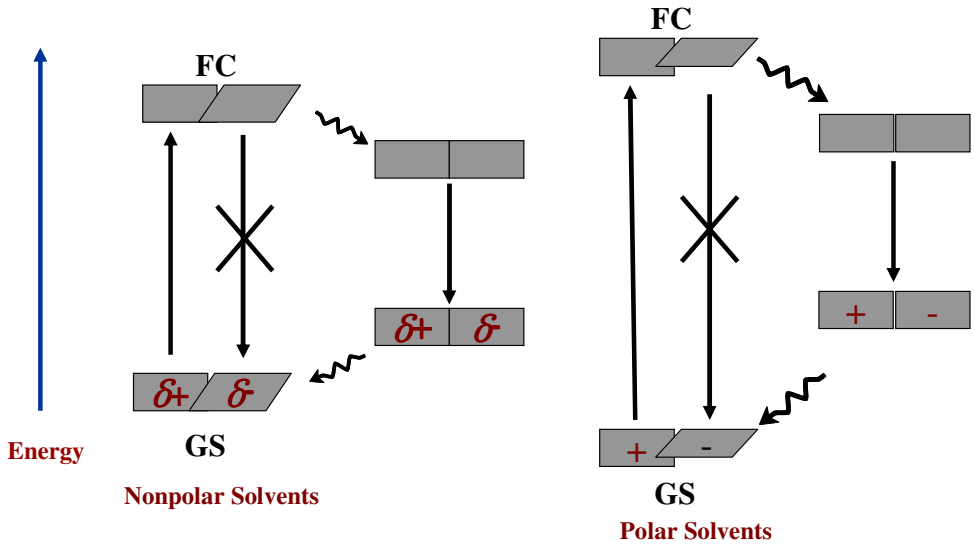

Figure 4.7. Proposed mechanism for explaining the solvatochromic behaviour of **Sq1** and **Sq2**.

This twisting can help in stabilizing the charge separation. Charge transfer excitation will lead to a nonpolar FC excited state with the same conformation. We propose that this FC state is nonfluorescent and that the observed fluorescence could be from a planar relaxed state as shown in the above diagram. In nonpolar solvents, the ground state will have only partial charge transfer and therefore the difference in energy between the FC state and the emitting state will be much lesser.

4.3.3. Metal Ion Sensing Properties

In Chapter 2, we described the use of the cationic squaraine dye as a selective sensor for mercury and lead. However due to limited solubility of the

cationic dye in aqueous media its ability to sense metal ions could be investigated only in organic solvents. Our continued interest in exploring the use of squaraine dyes for selective detection of mercury in water, led us to study the metal ion sensing properties of the water soluble benzothiazolium based dye, **Sq1**. Interestingly, we found that the absorption of the dye was almost insensitive to transition metal ions such as Cu^{2+}, Zn^{2+}, Pb^{2+} and Cd^{2+} (Figure 4.8) and alkali/alkaline earth metals such as Li^{+}, Na^{+}, Ba^{2+}, Mg^{2+} and Ca^{2+} (Figure 4.9) in 2:1 ethanol/water solvent mixture at pH 6.9.

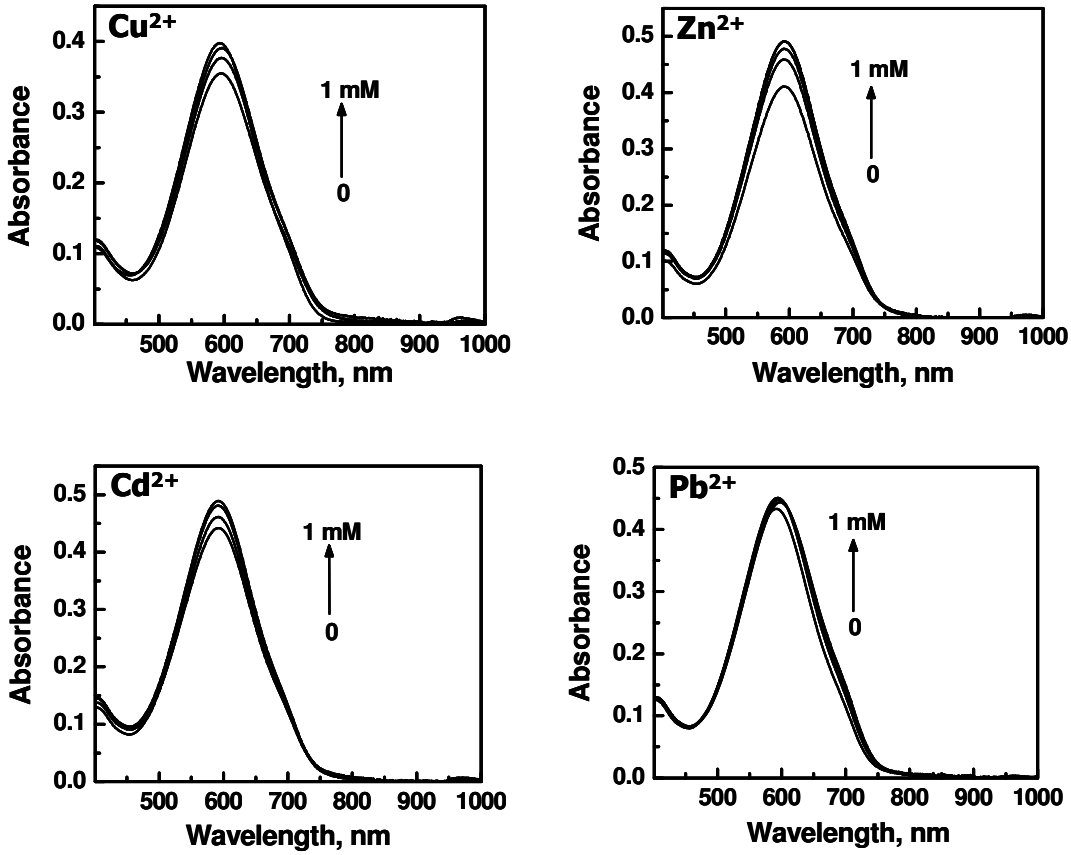

Figure 4.8. Effect of addition of Cu^{2+}, Zn^{2+}, Cd^{2+} and Pb^{2+} on the absorption spectrum of **Sq1** in 2:1 ethanol/water at pH 6.9.

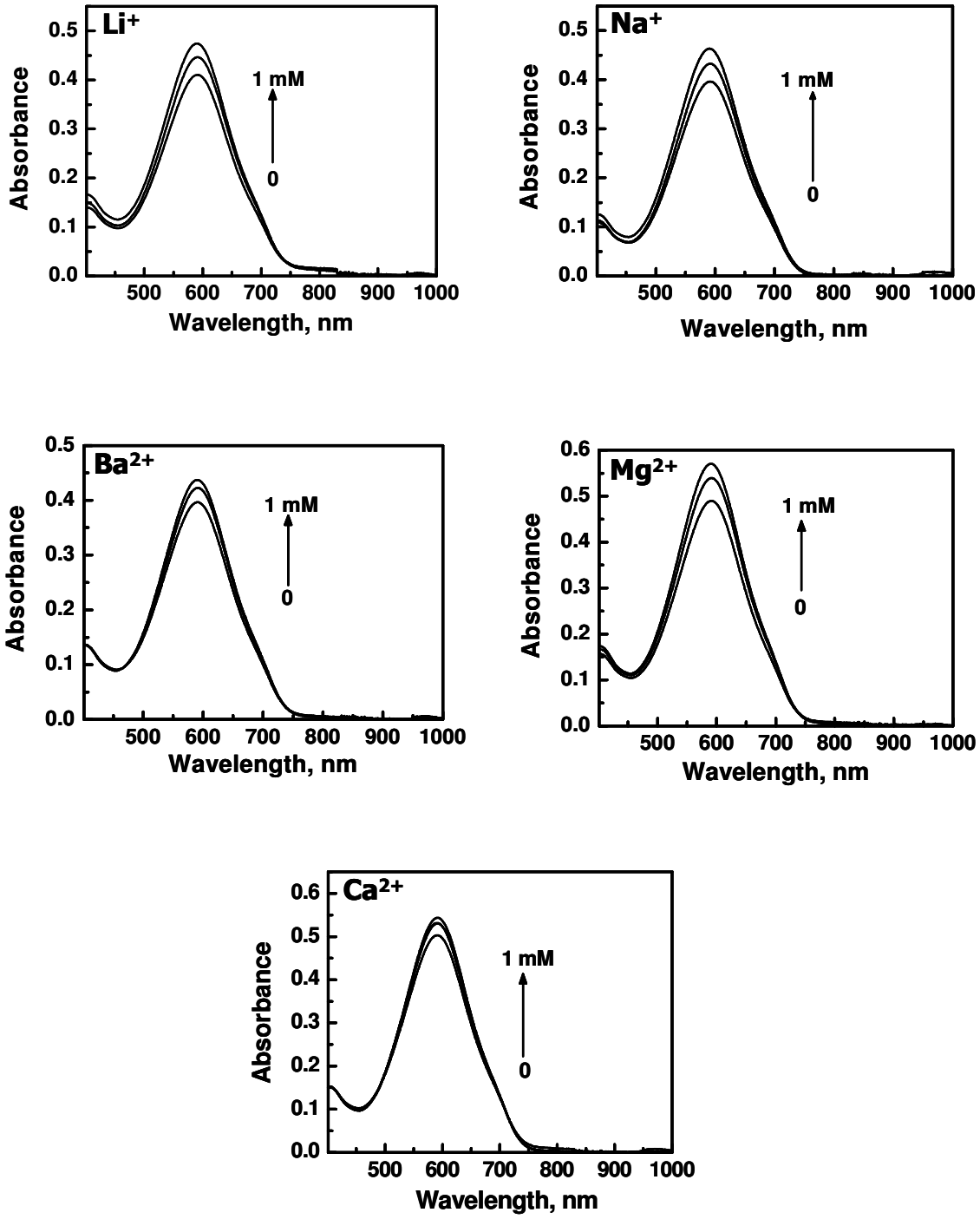

Figure 4.9. Effect of addition of Li^+, Na^+, Ba^{2+}, Mg^{2+} and Ca^{2+} on the absorption spectrum of **Sq1** in 2:1 ethanol/water at pH 6.9.

Addition of micromolar amounts of Hg^{2+} in 2:1 ethanol/water mixture at pH 6.9 however resulted in a significant decrease in the absorption intensity at 592 nm along with the formation of a bathochromically shifted band with a maximum centered on 722 nm (Figure 4.10). These changes were marked by the presence of an isosbestic point and more importantly, the absorption changes were clearly visible to the naked eye. A purple blue solution of **Sq1** became greenish upon titration with Hg^{2+} ions (Inset in Figure 4.10).

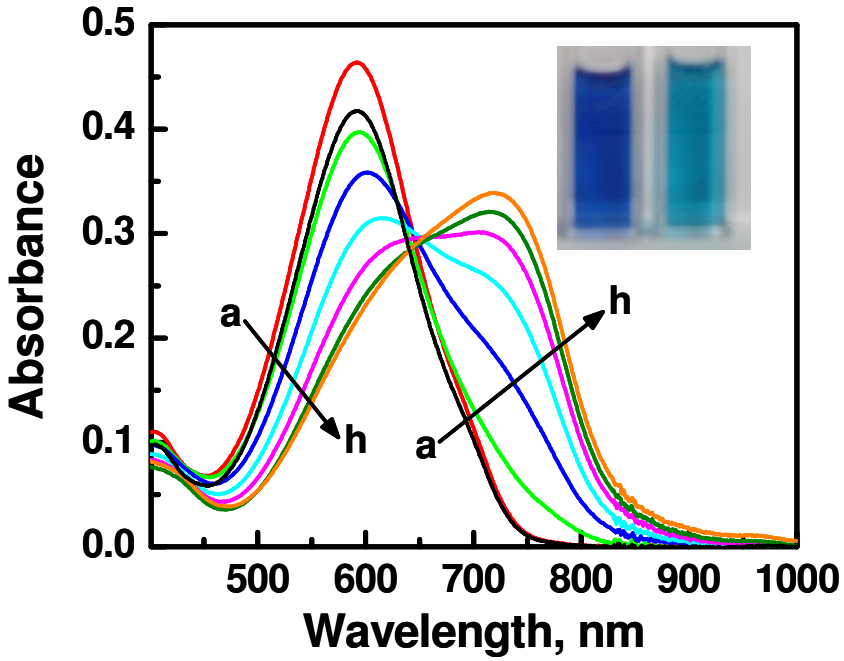

Figure 4.10. Effect of Hg^{2+} on the absorption spectrum of **Sq1** (30.2 μM) in 2:1 ethanol/water at pH 6.9 a) 0 (Dash line), h) 94 μM Hg^{2+}. Inset shows the visible colour change of **Sq1** (78 μM) upon addition of Hg^{2+} (300 μM).

Figure 4.11 shows the dependence of increase in absorbance of **Sq1** at 722 nm and decrease in absorbance at 592 nm and the change in the ratio of

absorbance (A_{722}/A_{592}) against Hg^{2+} concentration. The above studies clearly indicated that the dye can be used for ratiometric colourimetric selective detection of Hg^{2+} in aqueous media.

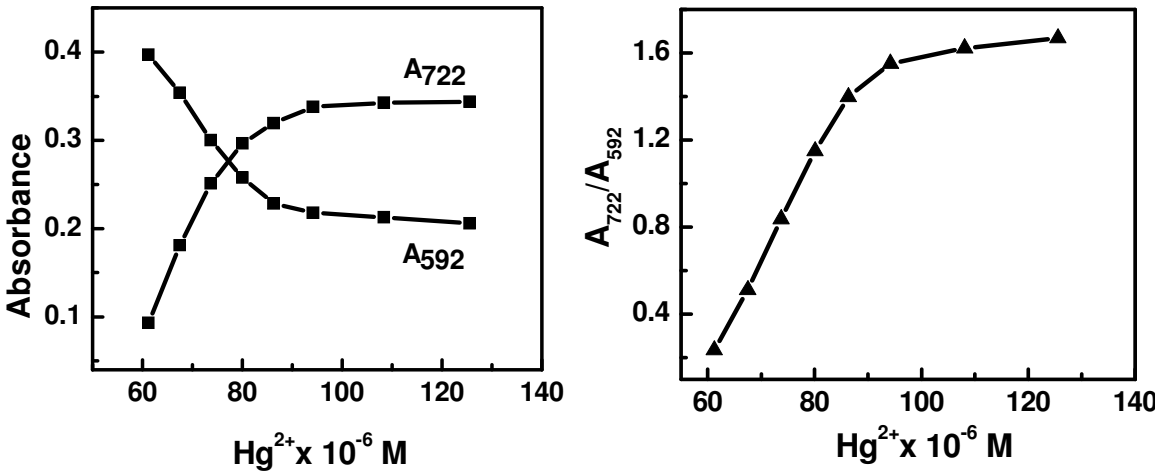

Figure 4.11. Change in absorbance of **Sq1** at 722 and 592 nm and their ratio (A_{722}/A_{592}) with increase in concentration of Hg^{2+} in 2:1 ethanol/water at pH 6.9.

The fluorescence of **Sq1** in presence of Hg^{2+} and other biologically relevant metal ions was also investigated. It was found that fluorescence was switched OFF in the presence of Hg^{2+} (Figure 4.12). This loss in fluorescence indicated the possibility of binding of Hg^{2+} to the oxygen atom of squaric acid. All other metals except Cu^{2+} did not bring about any noticeable change in the fluorescence of the dye.

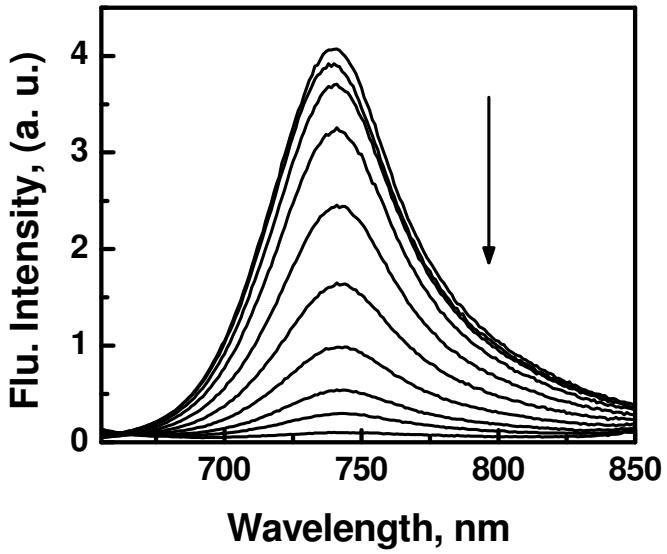

Figure 4.12. Change in emission spectrum of **Sq1** (30.2 μM) upon increase in addition of Hg^{2+} in 2:1 ethanol/water at pH 6.9.

Plot of I/I_0 against metal concentration clearly indicates the sensitivity of the dye to the presence of micromolar amounts of Hg^{2+} even in the presence of 1 mM concentration of other metals, with the exception of Cu^{2+} ions (Figure 4.13). I_o and I are the fluorescence intensities before and after the addition of the metal ions. It is well known in the literature that Cu^{2+} can bring about electron transfer induced quenching of fluorescence in amine containing systems.[17,18]

It has been reported in the literature that dyes containing 'S' and 'O' atoms in close proximity are ideally suited for binding Hg^{2+}.[19] In the present system, **Sq1** contains benzothiazolium species with Hg^{2+} coordinating element 'S'. To get a more insight to the binding site, we have optimized the structure of dye by using BLYP method[20,21] as implemented in the Gaussian 03 suite of programs (Figure

4.14).[22] It was observed that the distance between 'S' atom of benzothiazolium and 'O' atom of squaric acid were 3 Å, which matches well with the ionic radii of Hg^{2+} (2.2 Å).

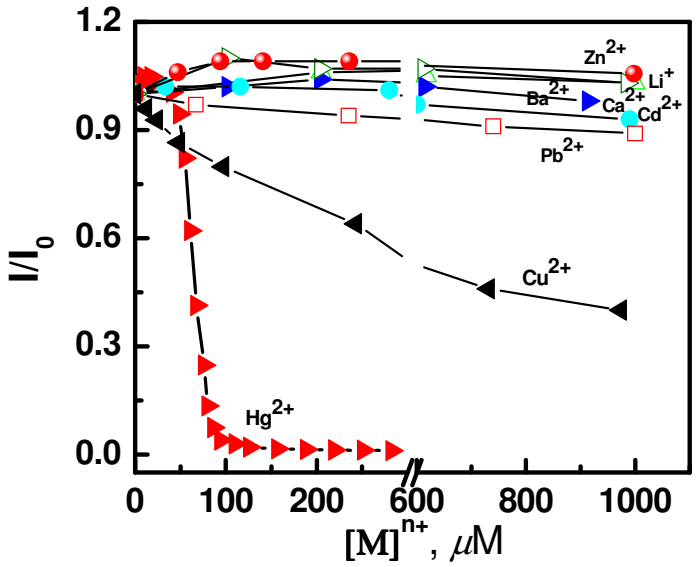

Figure 4.13. Plot of I/I_0 versus the metal concentration.

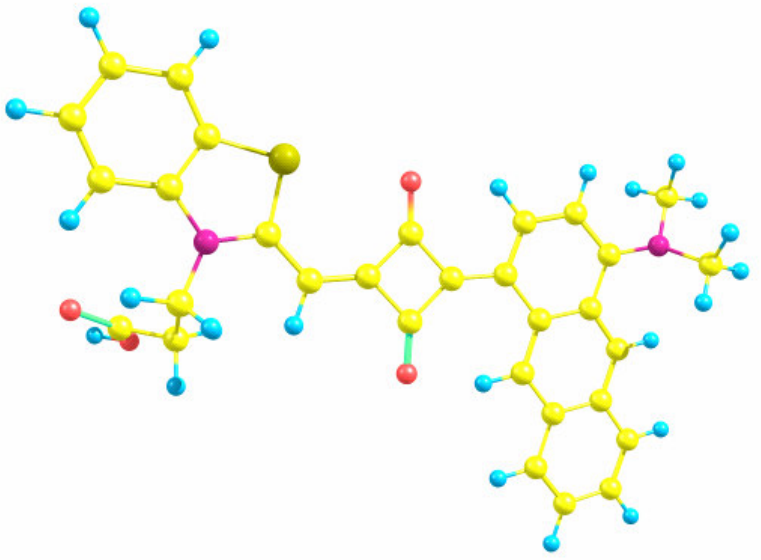

Figure 4.14. Optimized geometry of **Sq1** at BLYP/6-31G* level calculation.

4.3.4. Interaction with Proteins

It has been reported in the literature that several dyes in which the benzindolenium group is linked to a carboxylate group undergo noncovalent interactions with proteins.[23] In view of this and the large Stokes' shift in emission of **Sq2**, we investigated its interaction with proteins such as HSA and BSA.

Figure 4.15 shows changes in absorption spectrum of **Sq2** with increasing concentration of HSA in 4% ethanol/phosphate buffer at pH 7.4. In the absence of HSA, **Sq2** showed an absorption maximum at 588 nm. On addition of up to 2.6 μM of HSA, a broad red shifted band with two absorption maxima at 659 nm and 705 nm were observed and the changes were marked by the presence of an isosbestic point at 620 nm. These changes resulted in a clear visible colour change from blue to green as shown below.

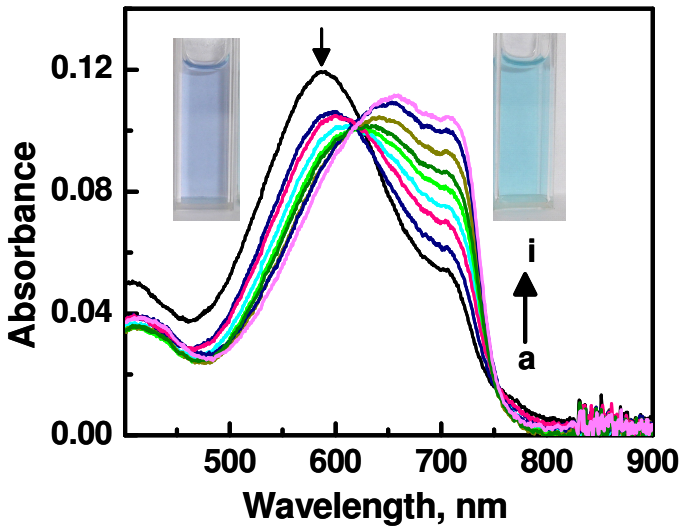

Figure 4.15. Change in absorbance of **Sq2** [7 μM] in 4% ethanol/phosphate buffer at pH 7.4, [HSA] a) 0, b) 0.5, c) 0.8, d) 1.1, e) 1.4, f) 1.6, g) 1.9, h) 2.3 and i) 2.6 μM.

Figure 4.16 shows the corresponding changes in the fluorescence properties of the solution. In 4% ethanol/phosphate buffer, the fluorescence quantum yield of **Sq2** was 0.004 which increased to 0.2 on addition of HSA. Inset in Figure 4.16 shows plot of fluorescence quantum yield versus HSA concentration. A 55-fold enhancement in fluorescence was observed on addition of 2.6 μM of HSA.

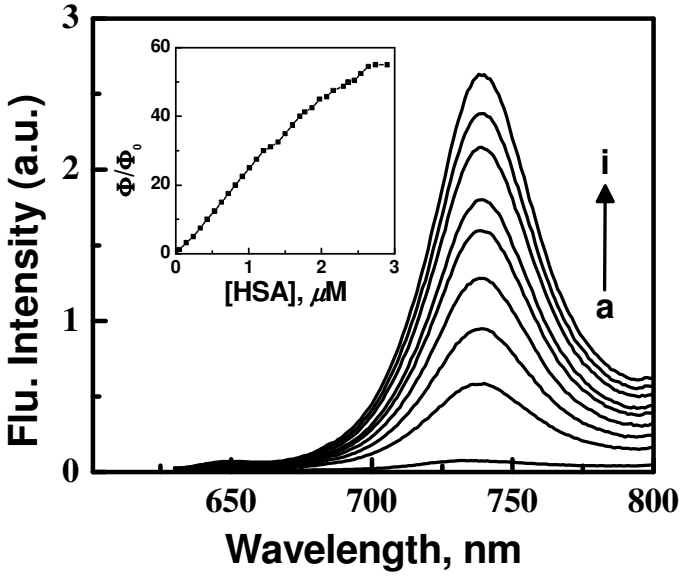

Figure 4.16. Change in fluorescence of **Sq2** [7 μM] in 4% ethanol/phosphate buffer at pH 7.4, [HSA] a) 0, b) 0.5, c) 0.8, d) 1.1, e) 1.4, f) 1.6, g) 1.9, h) 2.3 and i) 2.6 μM, Excitation wavelength λ_{ex}, 620 nm. Inset shows plot of fluorescence quantum yield *vs* HSA concentration.

Figure 4.17 shows the difference in absorption spectra on titration of **Sq2** with HSA in 4% ethanol/phosphate buffer at pH 7.4. The new peak at around 720 nm formed on addition of HSA was assigned to the dye-HSA complex. The stability constant of dye-HSA complex was calculated as reported earlier by Tarazi and coworkers.[24] The stability constant (K_S) of the complex is given by the

equation 4.3, where, the quantities in the square brackets represent molar concentrations at equilibrium.

$$K_S = \frac{[DM]}{[D][M]} \qquad 4.3$$

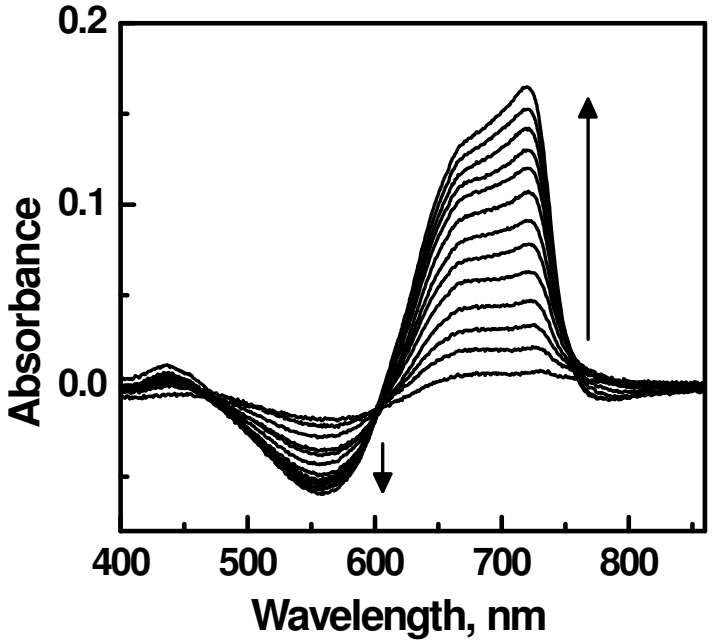

Figure 4.17. Difference absorbance spectra of **Sq2** [8.3 μM] with increase in addition of HSA in 4% ethanol/phosphate buffer at pH 7.4.

The stability constant K_S of the dye–protein complex was obtained from the fluorimetric titration of the dye with the protein by using equation 4.4, where k is a constant that depends on the quantum efficiency of the process and on instrumental parameters.

$$\frac{1}{F} = \frac{1}{kD_T} + \frac{1}{kD_T Ks} \times \frac{1}{[M]_T} \qquad 4.4$$

A plot of $1/F$ versus 1/[M] gave a straight line (Figure 4.18). The stability constant K_S (K_S = intercept/slope) was calculated to be 7×10^4 M^{-1}.

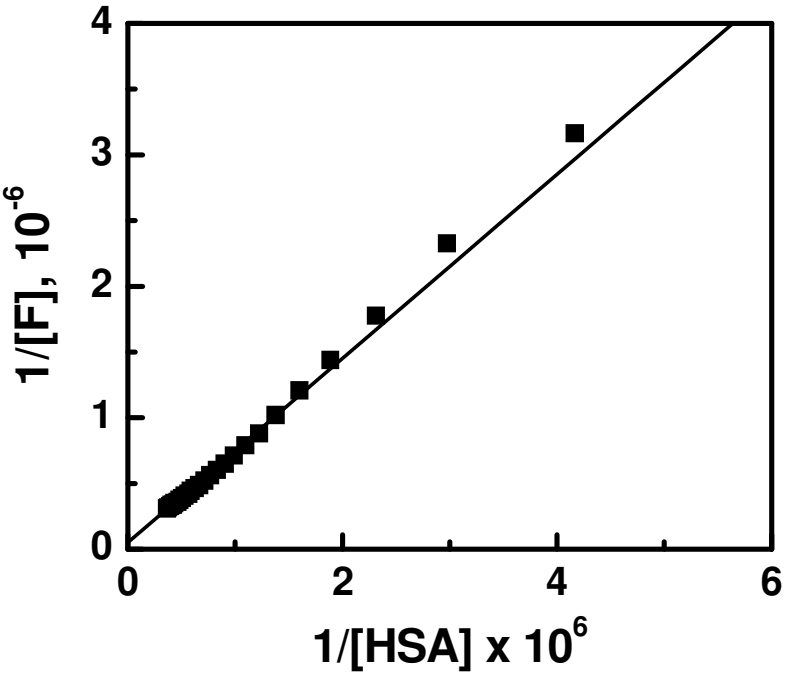

Figure 4.18. Plot of 1/F versus 1/[HSA].

One of the requirements for dyes to be useful in biological applications is good photostability. The photostability of **Sq2** in buffer was investigated by studying the change in intensity of the fluorescence on extended irradiation (>4 h) with the output of 450 W excitation lamp. Only less than 10% decay in fluorescence intensity of the dye was observed in the presence of HSA.

Figure 4.19 shows time-resolved fluorescence decay profile of **Sq2** in the absence and presence of HSA in 4% ethanol/phosphate buffer at pH 7.4, and the fluorescence data are summarized in Table 4.2.

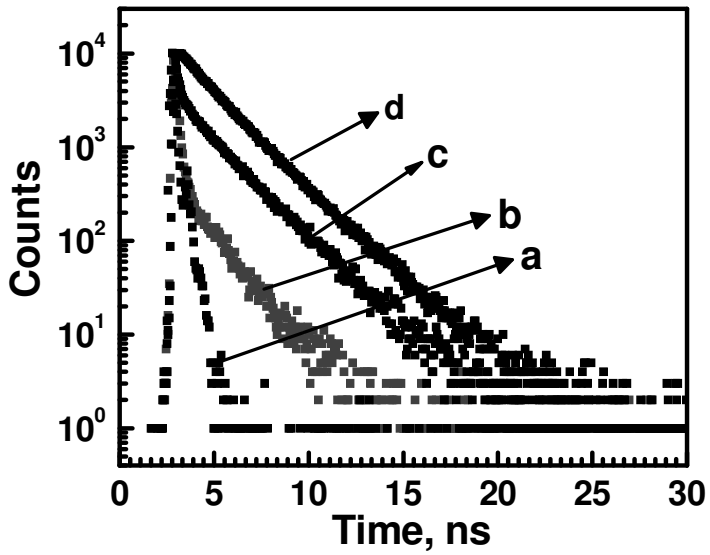

Figure 4.19. Time-resolved fluorescence decay of **Sq2** on the addition of HSA, [HSA] a) Lamp, b) 0, c) 0.1 and d) 2.6 μM. Excitation wavelength 635 nm, Emission monitored at 740 nm.

Table 4.2. Time-resolved fluorescence lifetime of **Sq2** on the addition of HSA. Excitation wavelength 635 nm, Emission monitored at 740 nm.

HSA, μM	Lifetime		χ^2
	τ_1, ns (Rel.ampl.)	τ_2, ns (Rel.ampl.)	
0	0.27 (85.09)	1.11 (14.91)	1.07
0.1	0.24 (13.55)	2.07 (86.45)	1.26
2.6		2.07	1.26

Sq2 showed a biexponential decay indicating a major species with a short lifetime of 0.27 ns (85.09%) and a minor one with a longer lifetime of 1.11 ns (14.91%) in 4% ethanol/phosphate buffer. On addition of up to 0.1 μM of HSA, a biexponential decay with the major species having a long lifetime of 2.07 ns

(86.25%) was observed. In the presence of 2.6 μM of HSA, **Sq2** showed a mono-exponential decay with lifetime of 2.07 ns. The biexponential decay in fluorescence in ethanol/buffer indicates the presence of two species probably due to aggregation of the dye in aqueous media. The mono-exponential decay obtained after addition of HSA indicates the breaking of aggregate followed by complexation of the monomer with the protein.

The interaction of **Sq2** with BSA also was investigated. On addition of BSA up to a concentration of 2.8 μM to a solution of **Sq2** in 4% ethanol/phosphate buffer led a decrease in absorbance at 588 nm and formation of a red shifted band with a maximum at around 637 nm. These changes were marked by the presence of an isosbestic point at 600 nm (Figure 4.20). The dye showed very weak fluorescence in ethanol/phosphate buffer, which increased substantially on addition of BSA.

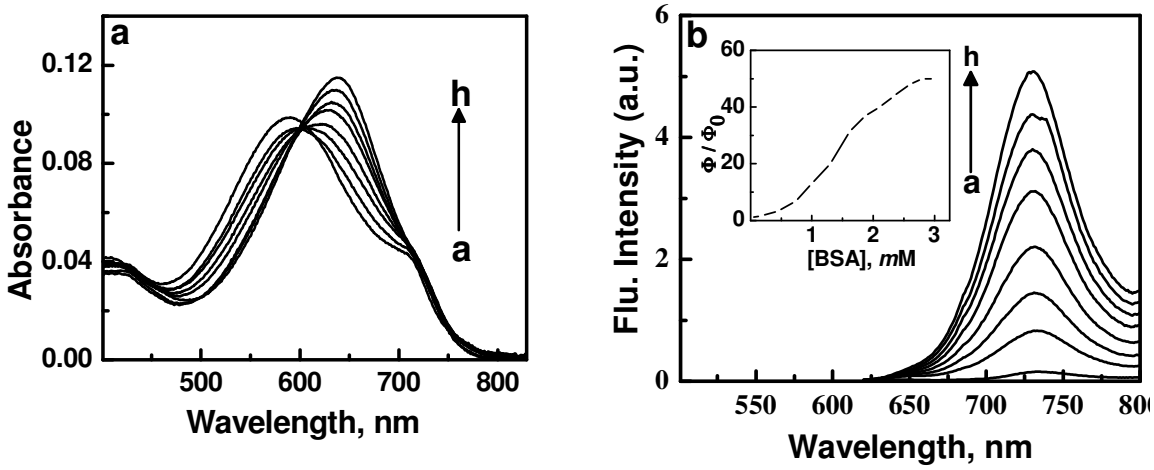

Figure 4.20. Change in a) absorbance and b) Fluorescence of **Sq2** [5.9 μM] in 4% ethanol/phosphate buffer, [BSA] a) 0, b) 0.73, c) 1, d) 1.3, e) 1.5, f) 1.8, g) 2.1 and h) 2.8 μM. Excitation wavelength, 600 nm.

The stability constant K_S (K_S = intercept/slope) was calculated from the plot of $1/F$ versus 1/[M], which gave a straight line. K_s was estimated as 8×10^4 M^{-1}. The dye was fairly photostable, and only less than 10% loss in fluorescence was observed on extended irradiation of the dye for >4h in the presence of BSA.

As in the case of addition of HSA, time-resolved fluorescence lifetime measurements indicated that addition of BSA led to break-up of the dye aggregate to the monomer form and the subsequent formation of a complex of the dye with BSA (Figure 4.21).

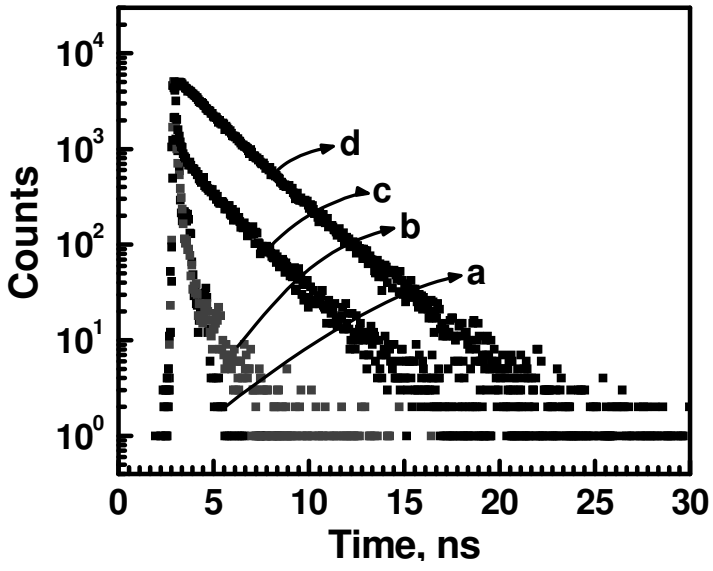

Figure 4.21. Time-resolved fluorescence decay of **Sq2** on the addition of BSA, [BSA] a) Lamp, b) 0, c) 0.13 and d) 2.8 μM. Excitation wavelength 635 nm, Emission monitored at 730 nm.

In buffer, the fluorescence lifetime profile of **Sq2** showed biexponential decay with a major species with a lifetime of 0.17 ns (86.6%) and a minor one

with a lifetime of 1.15 ns (13.4%). On addition of 2.8 μM of BSA, **Sq2** showed a mono-exponential decay with lifetime of 2.27 ns (Table 4.3).

Table 4.3. Time-resolved fluorescence lifetime of **Sq2** on the addition of BSA, Excitation wavelength 635 nm, Emission was monitored at 730 nm.

BSA, μM	Lifetime		χ^2
	τ_1, ns (Rel.ampl.)	τ_2, ns (Rel.ampl.)	
0	0.17 (86.6)	1.15 (13.4)	1.07
0.1	0.08 (35.7)	2.02 (64.3)	1.04
2.8	-	2.27	1.24

The ability of proteins such as BSA and HSA to bind hydrophobic compounds and dyes are reported in literature.[25,26] Electrostatic factors also play a role in the interaction of dyes with proteins.[27] In the present case, the observed interaction of **Sq2** with proteins may be due to the electrostatic interaction between carboxyl group of dye (Figure 4.22) and peptide group of protein as well as the hydrophobic nature of the squaraine chromophore.

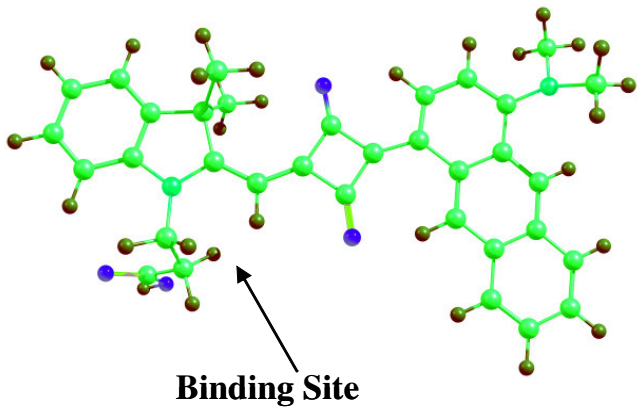

Figure 4.22. Binding site of **Sq2** with HSA or BSA.

These results suggest that the dye **Sq2** can be used as a noncovalent labeling agent for HSA and BSA. The main advantages of these dyes are that, they fluoresce in the NIR region and binding with HSA or BSA results in enhancement of their fluorescence.

4.3.5. Absorption and Emission Properties of Sq3–6

The absorption and emission spectra of **Sq3** and **Sq4** in methanol are shown in Figure 4.23. In methanol, **Sq3** showed absorption and emission maximum at 618 nm and 658 nm respectively, whereas **Sq4** possessed a broad absorption band in the 700-500 nm range and an emission maximum was centered at 748 nm.

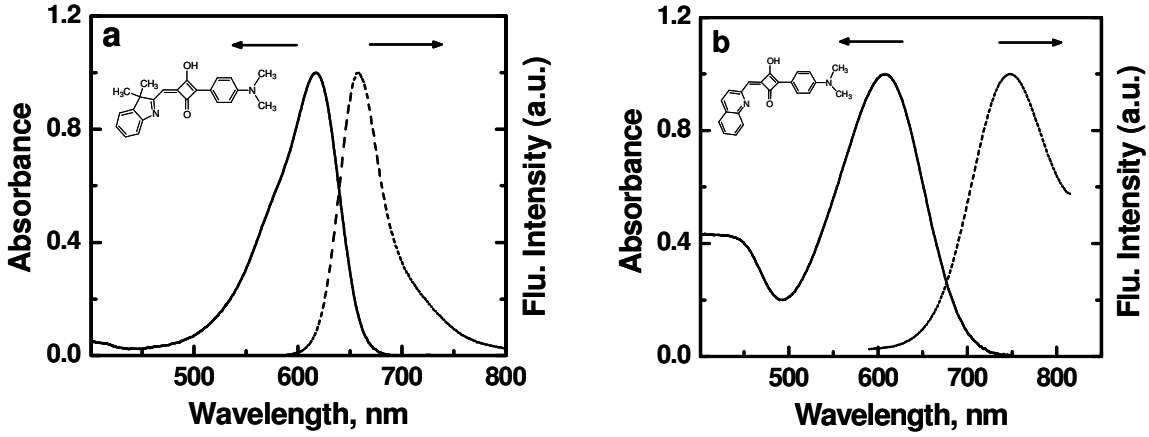

Figure 4.23. Normalized absorption (solid line) and emission spectra (dashed line) of a) **Sq3** and b) **Sq4** in methanol.

The photophysical properties of **Sq3** and **Sq4** in different solvents are summarized in Table 4.4. It is interesting to note that the benzindolenium-based dye showed an exceptionally high quantum yield of fluorescence (0.7 in DCM),

whereas the quinaldine based dye showed relatively low fluorescence quantum yields. These dyes possessed high extinction coefficients, which were in the range of 10^4.

Table 4.4. Photophysical properties of **Sq3** and **Sq4** in different solvents.

Solvents	Sq3			Sq4		
	λ_{max}		Φ_f	λ_{max}		Φ_f
	Abs	Ems		Abs	Ems	
MeOH	617	657	0.17	607	657	0.006
EtOH	622	661	0.25	612	661	0.007
ACN	613	661	0.44	611	661	0.005
DCM	623	656	0.68	637	656	0.007
Toluene	629	652	0.57	661	652	0.006

The absorption bands of **Sq5** and **Sq6** in DCM were in the 600–1000 nm range. In protic solvents the absorption bands were highly blue shifted. A large blue shift was also observed on adding trifluoroacetic acid (TFA) to the solutions of the dyes in DCM (Figure 4.24). The acridine-based dyes were found to be nonfluorescent.

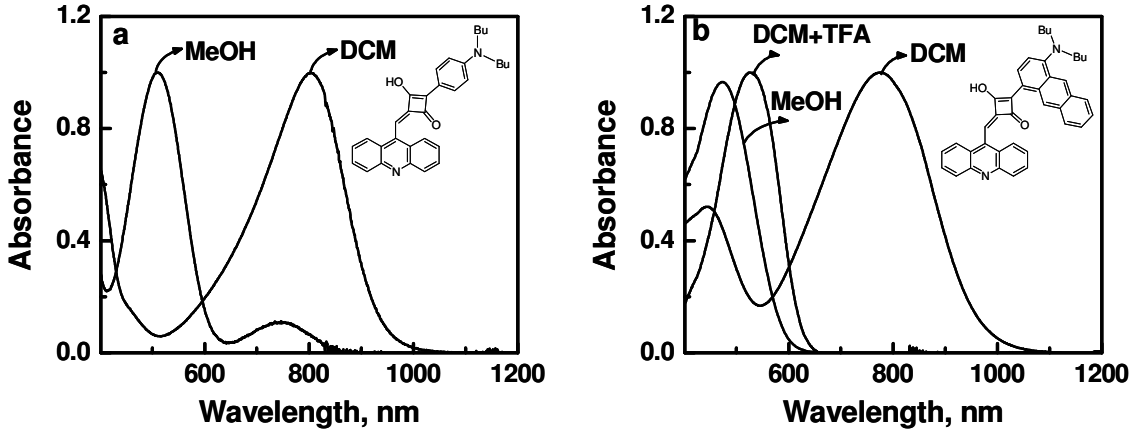

Figure 4.24. Normalized absorption spectra of a) **Sq5** and b) **Sq6**.

4.3.6. Effect of pH on Sq3

Due to the presence of a heteroaromatic ring with free nitrogen, these dyes were very sensitive to the pH of the medium. The absorption spectra of **Sq3** were measured in buffered solutions at various pH. Figure 4.25 shows the absorption changes of **Sq3** in pH range 7.4–1. In neutral pH, **Sq3** showed a broad absorption band in the range 700-500 with maximum centered on 623 nm. On lowering the pH, formation of a blue shifted absorption band with maximum centered at around 476 nm was observed. The inset in Figure 4.25 shows the photograph of different colours of the solution obtained at different ranges of pH.

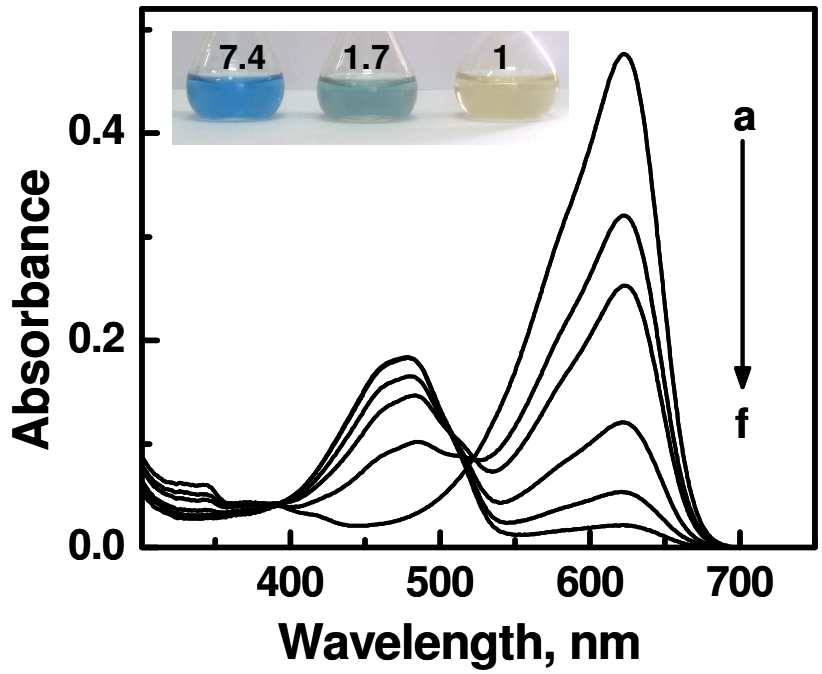

Figure 4.25. Effect of pH on absorption spectrum of **Sq3** in phosphate buffer at pH a) 7.4, b) 2, c) 1.7, d) 1.5, e) 1.2 and e) 1. Inset shows the photograph at different ranges of pH.

4.4. Conclusions

The photophysical properties of some unsymmetrical squaraine dyes have been investigated. The squaraine dyes, **Sq1** and **Sq2** exhibited very large Stokes' shift in emission in the NIR region. The absorption spectra of these dyes underwent a significant blue shift with increasing polarity of the solvents, whereas their emission spectra were hardly affected. The dyes were characterized by good quantum yields of fluorescence and high extinction coefficients as well as good photostability which makes them highly suitable as probes for various biological imaging applications. The benzothiazolium based dye **Sq1**, was shown to be useful as a ratiometric, colourimetric probe for selective detection of Hg^{2+} in the presence of other environmentally relevant metal ions in aqueous media. **Sq2** showed substantial enhancement in fluorescence efficiency and lifetime in the presence of proteins such as HSA and BSA. Some new unsymmetrical squaraine dyes containing N-heteroaromatic ring with free nitrogen were also synthesized and their photophysical properties have been studied. The absorption properties of these dyes were found to be very sensitive to the pH of the medium.

4.5. Experimental Section

4.5.1. Materials

HSA, BSA and all perchlorate salt of metal ions used for the metal binding studies were purchased from Sigma-Aldrich. The solutions of HSA and BSA were

prepared in doubly distilled water. All other materials and reagents were purchased from commercial suppliers and used without further purification. The solvents used were purified and dried by standard methods prior to use.

4.5.2. General Techniques

Melting points were determined with a Mel-Temp-II melting point apparatus and were uncorrected. FT-IR spectra were recorded on a Shimadzu IRPrestige-21 Fourier Transform Infrared Spectrophotometer. ^{1}H NMR spectra were measured on a 300 MHz Bruker Avance DPX NMR Spectrometer. High resolution mass spectral (HRMS) analysis was obtained from JEOL JMS600 instrument. Electronic absorption spectra were recorded on a Shimadzu UV-3101 PC NIR scanning spectrophotometer and the emission spectra were recorded on a SPEX-Fluorolog, F112X Spectrofluorimeter. Fluorescence quantum yields were measured by the relative method using optically matched dilute solutions. 1,1'-Diethyl-2,2'-dicarbocyanine iodide (**DDI**) having a quantum yield of 0.0028 in ethanol[28] was used as the standard.

Fluorescence lifetimes were measured using IBH (FluoroCube) Time-Correlated Picosecond Single Photon Counting (TCSPC) system using a 635 nm IBH NanoLED source and Hamamatsu C4878-02 MCP detector. The fluorescence decay profiles were deconvoluted using IBH data station software V2.1, fitted

with mono-exponential decay and minimizing the χ^2 values of the fit to 1 ± 0.3. The Gaussian 03 suite of programs was used for the calculations.

4.5.3. General Procedure for the Protein Binding Studies

Stock dye solution was made by dissolving the dye, **Sq2** in 4% ethanol/phosphate mixture. A 0.1 M phosphate buffer was used for controlling the pH of solutions at 7.4. Protein solutions were prepared in doubly distilled water and kept overnight for complete solublization. The concentration of stock solution of protein was determined based on their extinction coefficients at 280 nm (HSA = 36600 $mol^{-1}cm^{-1}$, BSA = 44720 $mol^{-1}cm^{-1}$). It was also determined on the basis of their molecular weight (HSA = 66000 *D*a, BSA = 65000 *D*a). Absorption measurements were carried out in a 4 mL quartz cuvette. Working solutions of the free dyes and dye-protein were prepared immediately before the experiments by mixing of an aliquot of dye stock solution and an aliquot of protein in a buffer.

4.5.4. Test of Photostability

The photostability of the dye was tested by irradiation of a working stock solution of free dye and dye-protein complex using a 450 W excitation lamp of the Spex fluorolog for >4h and monitoring the fluorescence intensity at the emission maxima.

4.5.5. Synthesis of Squaraine Dye, Sq1

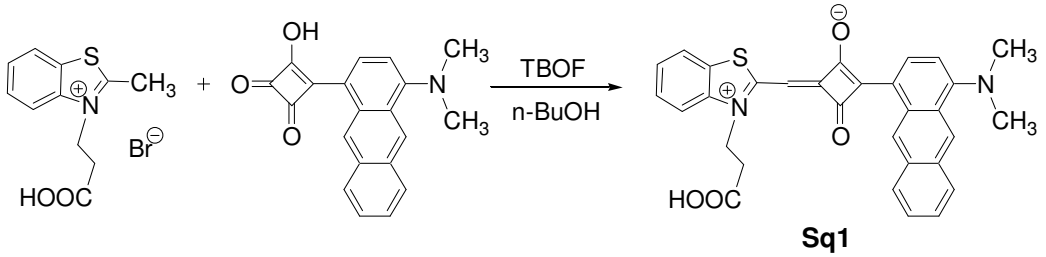

Sq1

Scheme 4.3

3-[4-(*N,N*-dimethylamino)anthracene]-4-hydroxycyclobutene-1,2-dione, (42 mg, 0.13 mmol) and 3-carboxyethyl-2-methylbenzothiazolium bromide (40 mg, 0.13 mmol) were reacted in a solvent mixture containing 10 mL of n-butanol and 1 mL of tributylorthoformate (TBOF) in a 100 mL RB flask and heated for 3 h at 60–70 °C (Scheme 4.3). The solvent was removed under reduced pressure and product was precipitated by adding hexane and it was purified by column chromatography over silica gel (100–200 mesh) using 10% MeOH/$CHCl_3$ mixtures as eluent to give solid product (25 mg, 37%). Mp 215-220 ºC (decomp.); (ε 12000 $M^{-1}cm^{-1}$ EtOH); FT-IR (KBr): ν_{max} 3415, 1730, 1554 cm^{-1}; ^1H NMR (300 MHz, $CD_3OD/CDCl_3$ (1:1)): δ 2.88 (2H, t, $-CH_2-CO-$), 3.06 (6H, s, $-NCH_3$), 3.19 (2H, t, $+NCH_2-$), 6.7-9.9 (13H, m, aromatic, vinylic); (HRMS-FAB) Mol. wt. calcd. for $C_{31}H_{24}N_2O_4S$ (MH^+) 520.59. Found 521.48.

4.5.6. Synthesis of Squaraine Dye, Sq2

Sq2 was synthesized from 3-[4-(*N,N*-dimethylamino)anthracene]-4-hydroxycyclobutene-1,2-dione and 1-carboxyethyl-2,3,3-trimethy-*3H*-indolium bromi-

de. The procedure followed for the preparation of the dye **Sq2** was same as that of **Sq1**.

Yield: 74%; mp 205-210 ºC (decomp.); (ε 24000 $M^{-1}cm^{-1}$ EtOH); FT-IR (KBr): ν_{max} 2960, 1730, 1587 cm^{-1}; ^1H NMR (300 MHz, CD_3OD,): δ 1.31 (3H, s, $-CCH_3$), 1.42 (3H, s, $-CCH_3$), 1.8 (6H, s, $-NCH_3$), 2.88 (2H, t, $-CH_2-CO-$), 3.3 (2H, t, $+NCH_2-$), 6.74-10.2 (13H, m, aromatic, vinylic); (HRMS-FAB) Mol. wt. calcd. for $C_{34}H_{30}N_2O_4$ (MH^+) 530.61. Found 531.50.

4.5.7. Synthesis of Squaraine Dye, Sq3

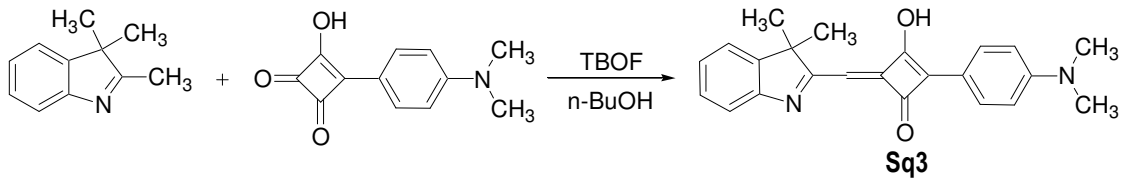

Scheme 4.4

A mixture of 3-[4-(*N,N*-dimethylamino)phenyl]-4-hydroxycyclobutene-1,2-dione, (272 mg, 1.26 mmol) and 2,3,3-trimethylindolenine (200 mg, 1.26 mmol) were heated in a solvent mixture containing n-butanol (10 mL) and TBOF (1 mL) for 3 h at 60–70 °C (Scheme 4.4). The solvent was removed under reduced pressure and product was precipitated by adding hexane, purified by column chromatography over silica gel (100–200 mesh) using chloroform as eluent to give solid product (40 mg, 9%). Mp 203-207 ºC (decomp.); (ε 40000 $M^{-1}cm^{-1}$ MeOH); FT-IR (KBr): ν_{max} 2964, 1734, 1570 cm^{-1}; ^1H NMR (300 MHz, $CDCl_3$): δ

1.63 (3H, s, -CCH_3), 2.10 (3H, s, -CCH_3), 3.03 (6H, s, -NCH_3), 5.79 (1H, s, vinylic -CH=), 6.65 (2H, d, *J* = 9 Hz, aromatic), 7.12 (1H, t, *J* = 7.2 Hz, aromatic), 7.22 (1H, t, *J* = 7.5 Hz, aromatic), 7.26 (1H, d, *J* = 6.6 Hz, aromatic), 7.46 (1H, d, *J* = 7.8 Hz, aromatic), 8.06 (2H, d, *J* = 7.2 Hz, aromatic), 14.66 (1H, s, -OH); (HRMS-FAB) Mol. wt. calcd. for $C_{23}H_{22}N_2O_2$ (MH^+) 358.43. Found 359.24.

4.5.8. Synthesis of Squaraine Dye, Sq4

Sq4 was synthesized from 3-[4-(*N,N*-dimethylamino)phenyl]-4-hydroxycyclobutene-1,2-dione and 2-methyl quinoline. The procedure followed for the preparation of the dye **Sq4** was same as that of **Sq3**.

Yield: 3%; mp 238-243 ºC (decomp.); (ε 27000 $M^{-1}cm^{-1}$ MeOH); FT-IR (KBr): ν_{max} 3072, 1732, 1595 cm^{-1}; ^1H NMR (300 MHz, $CDCl_3$): δ 3.06 (6H, s, -NCH_3), 5.99 (1H, s, vinylic -CH=), 6.73 (2H, d, *J* = 9 Hz, aromatic), 7.31 (1H, d, *J* = 9 Hz, aromatic), 7.53 (1H, t, *J* = 7.8 Hz, aromatic), 7.78 (1H, d, *J* = 8.1 Hz, aromatic), 7.8 (1H, t, *J* = 7.8 Hz, aromatic), 7.99 (1H, d, *J* = 8.1 Hz, aromatic), 8.04 (2H, d, *J* = 9 Hz, aromatic), 8.15 (1H, d, *J* = 8.7 Hz, aromatic), 17.52 (1H, s, -OH); (HRMS-FAB) Mol. wt. calcd. for $C_{22}H_{18}N_2O_2$ (MH^+) 342.39. Found 343.30.

4.5.9. Synthesis of Squaraine Dye, Sq5

Sq5 was synthesized from 3-[4-(*N,N*-dibutylamino)phenyl]-4-hydroxycyclobutene-1,2-dione and 9-methyl acridine. The procedure followed for the preparation of the dye **Sq5** was same as that of **Sq3**.

Yield: 47%; mp 258-262 ºC (decomp.); (ε 23000 $M^{-1}cm^{-1}$ DCM); FT-IR (KBr): ν_{max} 2974, 1728, 1573 cm^{-1}; ^1H NMR (300 MHz, $CDCl_3$): δ 0.97 (6H, t, $-CH_3$), 1.3-1.4 (4H, m, $-CH_2-$), 1.5-1.6 (4H, m, $-CH_2-$), 3.37 (4H, t, $-NCH_2-$), 6.74 (2H, d, J = 9 Hz, aromatic), 7.13 (1H, s, vinylic), 7.20 (2H, d, J = 7.2 Hz, aromatic), 7.26-7.33 (4H, m, aromatic), 8.22 (2H, d, J = 9 Hz, aromatic), 8.40 (2H, d, J = 8.4 Hz, aromatic), 14.98 (1H, s, -OH); (HRMS-FAB) Mol. wt. calcd. for $C_{32}H_{32}N_2O_2$ (MH^+) 476.60. Found 477.58.

4.5.10. Synthesis of Squaraine Dye, Sq6

Sq6 was synthesized from 3-[4-(*N,N*-dibutylamino)anthracene]-4-hydroxy-cyclobutene-1,2-dione and 9-methyl acridine. The procedure followed for the preparation of the dye **Sq6** was same as that of **Sq3**.

Yield: 56%; mp 254-260 ºC (decomp.); (ε 6000 $M^{-1}cm^{-1}$ DCM); FT-IR (KBr): ν_{max} 2953, 1726, 1564 cm^{-1}; ^1H NMR (300 MHz, $CDCl_3$): δ 0.97 (6H, t, $-CH_3$), 1.2-1.3 (4H, m, $-CH_2-$), 1.5-1.6 (4H, m, $-CH_2-$), 3.34 (4H, t, $-NCH_2-$), 7.21 (1H, d, J = 8.1 Hz, aromatic), 7.26 (1H, s, vinylic), 7.3-7.47 (6H, m, aromatic), 7.46 (2H, d, J = 8.4 Hz, aromatic), 8.07 (1H, d, J = 9 Hz, aromatic), 8.16 (1H, d, J = 6.9 Hz, aromatic), 8.60 (2H, d, J = 8.7 Hz, aromatic), 8.78 (1H, d, J = 7.8 Hz, aromatic), 8.85 (1H, s, aromatic), 10.20 (1H, s, aromatic), 15.46 (1H, s, -OH); (HRMS-FAB) Mol. wt. calcd. for $C_{40}H_{36}N_2O_2$ (MH^+) 576.72. Found 577.17.

4.6. References

1. Tolosa, L.; Nowaczyk, K.; Lakowicz, J. *An Introduction to Laser Spectroscopy*, 2nd ed.; Kluwer: New York, 2002.
2. Zhang, Z.; Achilefu, S. *Org. Lett.* **2004**, *6*, 2067-2070.
3. Haugland, R. P. *Handbook of Fluorescent Probes and Research Chemicals*, Sixth Ed., Molecular Probes: Eugene, OR, 1996.
4. Pham, W.; Lai, W. F.; Weissleder, R.; Tung, C. H. *Bioconjugate Chem.* **2003**, *14*, 1048-1051.
5. Soper, S. A.; Mattingly, Q. L. *J. Am. Chem. Soc.* **1994**, *116*, 3744-3752.
6. Reichardt, C. *Chem. Rev.* **1994**, *94*, 2319-2358.
7. Reichardt, C. *Chem. Soc. Rev.* **1992**, *21*, 147-153.
8. Reichardt, C.; Asharinfard, S.; Blum, A.; Eschner, M.; Mehranpour, A. M.; Milart, P.; Niem, T.; Schafer G.; Wilk, M. *Pure Appl. Chem.* **1993**, *65*, 2593-2601.
9. Dimroth, K.; Reichardt, C.; Siepmann, T.; Bohlmann, F. *Liebigs Ann. Chem.* **1963**, *661*, 1-37**.**
10. Mishra, A.; Behera, R. K.; Behera, P. K.; Mishra, B. K.; Behera, G. B. *Chem. Rev.* **2000**, *100*, 1973-2011.
11. Reichardt, C.; Harbusch-Görnert, E. *Liebigs Ann. Chem.* **1981**, 721.

12. Peng, X.; Song, F.; Lu, E.; Wang, Y.; Zhou, W.; Fan, J.; Gao, Y. *J. Am. Chem. Soc.* **2005**, *127*, 4170-4171.

13. Al-Ansari, I. Az. *Bull. Soc. Chim. Fr.* **1997**, *134*, 593-599.

14. Grabowski, Z. R.; Rotkiewicz, K.; Rettig, W. *Chem. Rev.* **2003**, *103,* 3899-4031.

15. Siemiarczuk, A.; Grabowski, Z. R.; Krówczyński, A.; Asher, M.; Ottolenghi, M. *Chem. Phys. Lett*. **1977**, *51*, 315-320.

16. Grabowski, Z. R.; Rotkiewicz K.; Siemiarczuk, A. *J. Lumin.* **1979**, *18/19*, 420-424.

17. Bodenant, B.; Weil, T.; Businelli-Pourcel, M.; Fages, F.; Barbe, B.; Pianet, I.; Laguerre, M. *J. Org. Chem.* **1999**, *64,* 7034-7039.

18. Zheng, Y.; Cao, X.; Orbulescu, J.; Konka, V.; Andreopoulos, F. M.; Pham, S. M.; Leblanc, R. M. *Anal. Chem.* **2003**, *75*, 1706-1712.

19. Tatay, S.; Gaviña, P.; Coronado, E.; Palomares, E. *Org. Lett.* **2006**, *8*, 3857-3860.

20. Becke, A. D. *J. Chem. Phys.* **1993**, *98*, 5648–5652.

21. Lee, C.; Yang, W.; Parr, R. G. *Phys. Rev. B: Condens. Matter Mater. Phys.* **1988**, *37*, 785-789.

22. Gaussian 03, Revision C.02, Frisch, M. J. *et al.*

23. Nizomov, N.; Ismailov, Z. F.; Nizamov, S. N.; Salakhitdinova, M. K.; Tatarets, A. L.; Patsenker, L. D.; Khodjayev, G. *J. Mol. Struct.* **2006**, *788*, 36-42.

24. Tarazi, L.; Narayanan, N.; Sowell, J.; Patonay, G.; Strekowski, L. *Spectrochim. Acta Part A* **2002**, *58*, 257-264.

25. Lakovicz, J. R. *Bases Florescent Spectroscpopy*, Premium: New York, 2002.

26. Yarmoluk, S. M.; Lukashov, S. S.; Losytskyy, M. Y.; Akerman, B.; Kornyushina, O. S. *Spectrochim. Acta Part A* **2002**, *58*, 3223-3232.

27. Blagoi, Y. P. *Soros Educ. J.* **1998**, *10*, 18-24.

28. Dempster, D. N.; Morrow, T.; Rankin, R.; Thompson, G. F. *J. Chem. Soc., Faraday Trans. 2* **1972**, *68*, 1479-1496.

List of Publications

1. A Squaraine-Based Chemosensor for Hg^{2+} and Pb^{2+}
   M. C. Basheer, S. Alex, K. G. Thomas, C. H. Suresh and Suresh Das *Tetrahedron* **2006**, *62,* 605–610.

2. Design and Synthesis of Squaraine Based Near Infrared Fluorescent Probes
   M. C. Basheer, U. Santhosh, S. Alex, K. G. Thomas, C. H. Suresh and Suresh Das *Tetrahedron* **2007**, *63*, 1617–1623.

3. Aggregation Properties of Heavy Atom Substituted Squaraine Dyes: Evidence for the Formation of J-Type Dimer Aggregates in Aprotic Solvents
   S. Alex, M. C. Basheer, K. T. Arun, D. Ramaiah and Suresh Das *J. Phys. Chem. A*, **2007**, *111,* 3226-3230.

Posters presented at conferences/conferences attended

1. Design and Synthesis of Novel Class of Cationic Squaraine Dyes and their use as Fluorescent Probes for Selective Detection of Metal Ions
   M. C. Basheer and Suresh Das
   3rd Trivandrum International Symposium on Recent Trends in Photochemical Sciences, held at RRL, Trivandrum, January 05–07, 2004.

2. A Squaraine-Based Chemosensors for Hg^{2+} and Pb^{2+}
   M. C. Basheer and Suresh Das
   7th National Symposium in Chemistry, held at Department of Organic Chemistry, Indian Association for Cultivation of Science, Kolkata, February 4–6, 2005 Conducted by Chemical Research Society of India.

3. Synthesis and Study of Squaraine Dye-Based Sensitizers and Probes
   M. C. Basheer, Saji Alex and Suresh Das
   JNC Research Conference on Chemistry of Materials, held at Aquaserene, Quilon, October 01–03, 2005.

4. Attended "*Fourth Technology Led Entrepreneurship Programme,* held at CLRI, Chennai, February 12–March 11, 2007 Conducted by CSIR New Delhi and coordinated by IIM, Bangalore.